FHWA Contract No. GS00F341CA

Task Order 693JJ318F000316

Jointed Concrete Pavement Faulting Collection and Analysis: TPF-5(299)

Final Report

Submitted to:

U.S. Department of Transportation

Federal Highway Administration

Office of Innovation Implementation – Resource Center

31 Hopkins Plaza, Suite 840

Baltimore, MD 21201

U.S. Department of Transportation

Federal Highway Administration

FOREWORD

The FHWA managed pooled fund study, TPF-5(299) Improving the Quality of Pavement Surface Distress and Transverse Profile Data Collection and Analysis, was established to assemble State Departments of Transportation (DOTs) and the Federal Highway Administration, alongside industry and academia to meet six main goals. (1) Identify pavement surface distress and transverse profile (PSDAT) data integrity and quality issues; (2) Suggest approaches to addressing identified issues and provide solutions; (3) Initiate and monitor pilot projects intended to address identified issues; (4) Disseminate results; (5) Assist in the deployment of research findings and recommendations; and (6) Support other efforts related to improving pavement surface distress and transverse profile data collection and analysis. This is the final report of a FHWA project, Jointed Concrete Pavement Faulting Collection and Analysis, managed within TPF-5(299). The main goal of the project was to develop standardized procedures for consistent measurement and analysis of faulting data within a jointed concrete pavement section, between different pavement sections, and between different state highway agencies.

This report will be useful for personnel involved in jointed concrete pavement surface condition data collection and analysis.

Shay K. Burrows, Resource Center Director, Office of Technical Services - Resource Center

TECHNICAL REPORT DOCUMENTATION PAGE

1. Report No. FHWA-RC-24-0007	2. Government Accession No.	3. Recipient's Catalog No.
4. Title and Subtitle Jointed Concrete Pavement Faulting Collection and Analysis: TPF-5(299) Final Report		5. Report Date September 2024 6. Performing Organization Code:
7. Author(s) Shreenath Rao, Ph.D., P.E., Hyung Lee, Ph.D., P.E., Ahmad Alhasan, Ph.D., and Hesham Abdualla, Ph.D.		8. Performing Organization Report No.
9. Performing Organization Name and Address Applied Research Associates, Inc. 100 Trade Centre Dr., Champaign, IL 61820		10. Work Unit No. 11. Contract or Grant No. GS00F341CA Task Order 693JJ318F000316
12. Sponsoring Agency Name and Address U.S. Department of Transportation Federal Highway Administration Office of Technical Services-Resource Center 31 Hopkins Plaza, Suite 840 Baltimore, MD 21201		13. Type of Report and Period Covered Final 14. Sponsoring Agency Code HIT-RC
15. Supplementary Notes The FHWA COR for this project was Andy Mergenmeier.		
16. Abstract This report summarizes work performed under TPF-5(299) towards developing standardized procedure for consistent measurement and analysis of faulting data within a pavement section, between different pavement sections, and between different state highway agencies (SHAs). The work was performed in two Phases. In Phase I, the research team proposed a framework for establishing jointed concrete pavement (JCP) faulting collection and analysis standards based on review of existing standards, definitions, and protocols, along with data standards needs based on SHAs use of faulting data. The framework included a new procedure for defining, measuring, and collecting faulting data using highway speed equipment. The framework also included procedures for verifying faulting data and certifying faulting equipment. In Phase II, the research team sought to evaluate and validate the proposed framework using data provided by SHAs. The final section of this report summarizes efforts conducted under Phase II.		
17. Key Words Jointed concrete pavement, faulting, performance metrics, performance standards, HPMS	18. Distribution Statement No restrictions. This document is available to the public through the National Technical Information Service, Springfield, VA 22161. http://www.ntis.gov	

19. Security Classif. (of this report) Unclassified	20. Security Classif. (of this page) Unclassified	21. No. of Pages 89	22. Price N/A

Form DOT F 1700.7 (8-72) Reproduction of completed page authorized.

SI* (MODERN METRIC) CONVERSION FACTORS

APPROXIMATE CONVERSIONS TO SI UNITS

Symbol	When You Know	Multiply By	To Find	Symbol
		LENGTH		
in	inches	25.4	millimeters	mm
ft	feet	0.305	meters	m
yd	yards	0.914	meters	m
mi	miles	1.61	kilometers	km
		AREA		
in^2	square inches	645.2	square millimeters	mm^2
ft^2	square feet	0.093	square meters	m^2
yd^2	square yard	0.836	square meters	m^2
ac	acres	0.405	hectares	ha
mi^2	square miles	2.59	square kilometers	km^2
		VOLUME		
fl oz	fluid ounces	29.57	milliliters	mL
gal	gallons	3.785	liters	L
ft^3	cubic feet	0.028	cubic meters	m^3
yd^3	cubic yards	0.765	cubic meters	m^3
		NOTE: volumes greater than 1,000 L shall be shown in m^3		
		MASS		
oz	ounces	28.35	grams	g
lb	pounds	0.454	kilograms	kg
T	short tons (2,000 lb)	0.907	megagrams (or "metric ton")	Mg (or "t")
		TEMPERATURE (exact degrees)		
°F	Fahrenheit	5 (F-32)/9 or (F-32)/1.8	Celsius	°C
		ILLUMINATION		
fc	foot-candles	10.76	lux	lx
fl	foot-Lamberts	3.426	$candela/m^2$	cd/m^2
		FORCE and PRESSURE or STRESS		
lbf	poundforce	4.45	newtons	N
lbf/in^2	poundforce per square inch	6.89	kilopascals	kPa

APPROXIMATE CONVERSIONS FROM SI UNITS

Symbol	When You Know	Multiply By	To Find	Symbol
		LENGTH		
mm	millimeters	0.039	inches	in
m	meters	3.28	feet	ft
m	meters	1.09	yards	yd
km	kilometers	0.621	miles	mi
		AREA		
mm^2	square millimeters	0.0016	square inches	in^2
m^2	square meters	10.764	square feet	ft^2
m^2	square meters	1.195	square yards	yd^2
ha	hectares	2.47	acres	ac
km^2	square kilometers	0.386	square miles	mi^2
		VOLUME		
mL	milliliters	0.034	fluid ounces	fl oz
L	liters	0.264	gallons	gal
m^3	cubic meters	35.314	cubic feet	ft^3
m^3	cubic meters	1.307	cubic yards	yd^3
		MASS		
g	grams	0.035	ounces	oz
kg	kilograms	2.202	pounds	lb
Mg (or "t")	megagrams (or "metric ton")	1.103	short tons (2,000 lb)	T
		TEMPERATURE (exact degrees)		
°C	Celsius	1.8C+32	Fahrenheit	°F
		ILLUMINATION		
lx	lux	0.0929	foot-candles	fc
cd/m^2	candela/m2	0.2919	foot-Lamberts	fl
		FORCE and PRESSURE or STRESS		
N	newtons	2.225	poundforce	lbf
kPa	kilopascals	0.145	poundforce per square inch	lbf/in^2

*SI is the symbol for International System of Units. Appropriate rounding should be made to comply with Section 4 of ASTM E380. (Revised March 2003)

TABLE OF CONTENTS

INTRODUCTION **1**
- **Background** **1**
- **Purpose of Study** **1**
- **Definition of Significant Data Quality Terms** **2**
- **Organization of Report** **3**

CURRENT PRACTICES IN FAULTING DATA COLLECTION AND ASSESSMENT **5**
- **Manual Fault Meters** **5**
- **Two-Dimensional (2D) Automated Fault Measurements** **5**
- **Three-Dimensional (3D) Automated Fault Measurements** **10**
- **Agency Practice for Faulting Measurement** **11**
- **Summary** **13**

LIMITATIONS OF CURRENT PRACTICES **14**
- **Need for Improved Definition for Faulting** **14**
  - Uncertainties Associated with Different Methods 14
  - Lack of a Standard Reporting Protocol 15
  - Lack of a Certification Process for Faulting 15
- **Summary** **15**

PROPOSED DEFINITION OF FAULTING **16**
- **Rationale for Changes from AASHTO R 36-17** **16**
- **Current Definition** **16**
- **Proposed Definition (Option 1)** **16**
  - Enhanced Cumulative Difference Approach (ECDA) 19
  - Examples of faulting calculation using ECDA 24
- **Proposed Definition (Option 2)** **28**
- **Proposed Definition (Option 3)** **31**
- **Comparison of Results from Different Options** **41**
- **Summary** **42**

AUTOMATED FAULTING DATA COLLECTION EQUIPMENT CERTIFICATION **43**
- **Relevant Standards** **44**
  - AASHTO PP 107-21: Standard Practice for Assessment of Body Motion Cancelation in Transverse Pavement Profiling Systems. 44
  - AASHTO PP 108-21: Standard Practice for Assessment of Drift Mitigation in Transverse Pavement Profiling Systems. 45
  - AASHTO PP 106-21: Standard Practice for Assessment of Static Performance in Transverse Pavement Profiling Systems. 45
  - AASHTO PP 109-21: Standard Practice for Assessment of Dynamic Performance in Transverse Pavement Profiling Systems. 45
  - AASHTO PP 110-21: Standard Practice for Assessment of Ground Reference Measurements for Transverse Pavement Profiling System Certification. 46
- **Proposed Certification Procedure** **47**
  - Basis for Faulting Certification 47

Average of Multiple Joints vs. Single Joint Standard 48
Faulting Certification under Controlled Environment (for Accuracy) 48
Faulting Certification under Field Environment (for Precision and Joint Detection) 49
Summary 52

PRELIMINARY DESIGN AND FEATURES OF FAULTING CERTIFICATION ARTIFACT 53
Conceptual Design of Faulting Artifact (Phase I) 53
Proposed Faulting Artifact (Phase II) 54
Components of Proposed Faulting Fixture 54
Assembly of Faulting Fixture 56
Summary 58

EVALUATION OF NEW FAULTING DEFINITIONS AND PROCEDURES 59
Summary of Proposed Work for Phase II 59
Analysis of 2D Data 60
Joint Detection from 2D Data 60
ECDA Example from 2D Data 63
Preliminary Faulting Comparison 64
Summary and Recommendations for 2D Data 66
Analysis of 3D Data 67
Joint Detection from 3D Images 68
ECDA Example from 3D Data 71
Effect of Other JCP Features on Joint Detection and Faulting Assessment 80

SUMMARY AND RECOMMENDATIONS 83

REFERENCES 85

LIST OF FIGURES

Figure 1. Flowchart. Framework for establishing jointed concrete pavement faulting collection and analysis standards. 4
Figure 2. Photo. Various versions of Georgia faultmeters 5
Figure 3. Photo. 2D Automated Fault Measurement (AFM) equipment based on High-Speed Inertial Profiler (HSIP). 6
Figure 4. Graph. Illustration of AASHTO R 36 Method A. 7
Figure 5. Graph. Illustration of AASHTO R 36 Method B. 8
Figure 6. Graph. Illustration of LTPP AFM Slope Method. 9
Figure 7. Photo and Illustration. 3D Automated Fault Measurement (AFM) equipment 11
Figure 8. Illustration. Current definition of transverse joint or crack faulting. 16
Figure 9. Illustration. Wheelpath for joint faulting calculation. 17
Figure 10. Illustration. Representative Longitudinal Profile. 18
Figure 11. Illustration. Representative Longitudinal Profile for skewed joints. 18
Figure 12. Equation. Cumulative area under the actual response values 19
Figure 13. Equation. Cumulative area under overall average. 19
Figure 14. Equation. Cumulative difference. 20
Figure 15. Illustrations. Cumulative Difference Approach (top) uniform response value, (middle) cumulative and average areas, and (bottom) cumulative area difference. 21
Figure 16. Chart. Artificial pavement response parameter. 22
Figure 17. Charts. (a) Cumulative difference plot and (b) delineated uniform pavement sections using the original CDA method. 23
Figure 18. Charts. (a) Cumulative difference plot and (b) delineated uniform pavement sections using the Enhanced CDA (ECDA) method. 24
Figure 19. Chart. Option 1 Faulting calculation. LTPP Section 04-0215. Joint at Station 8.5 ft. 25
Figure 20. Chart. Option 1 Faulting calculation. LTPP Section 04-0215. Joint at Station 324.6 ft. 26
Figure 21. Chart. Option 1 Faulting calculation. LTPP Section 04-0215. Joint at Station 204.3 ft. 26
Figure 22. Chart. Option 1 Faulting calculation. LTPP Section 27-4040. Joint at Station 30.3 ft. 27
Figure 23. Chart. Option 1 Faulting calculation. LTPP Section 27-4040. Joint at Station 301.8 ft. 27
Figure 24. Chart. Option 1 Faulting calculation. LTPP Section 27-4040. Joint at Station 439.0 ft. 28
Figure 25. Chart. Option 2 Faulting calculation. LTPP Section 04-0215. Joint at Station 8.5 ft. 29
Figure 26. Chart. Option 2 Faulting calculation. LTPP Section 04-0215. Joint at Station 324.6 ft. 29
Figure 27. Chart. Option 2 Faulting calculation. LTPP Section 04-0215. Joint at Station 204.3 ft. 30
Figure 28. Chart. Option 2 Faulting calculation. LTPP Section 27-4040. Joint at Station 30.3 ft. 30
Figure 29. Chart. Option 2 Faulting calculation. LTPP Section 27-4040. Joint at Station 301.8 ft. 31

Figure 30. Chart. Option 2 Faulting calculation. LTPP Section 27-4040. Joint at Station 439.0 ft. 31
Figure 31. Illustration. Positive and negative faults with no grade. 32
Figure 32. Illustration. Measurement of positive fault with no grade. 33
Figure 33. Illustration. Measurement of negative fault with no grade..... 33
Figure 34. Illustration. Measurement of positive fault with down grade..... 34
Figure 35. Illustration. Measurement of negative fault with down grade..... 34
Figure 36. Artifact of curling and warping on fault measurement when using extrapolation. 35
Figure 37. Chart. Option 3 faulting calculation. Planes projected using points ±1.0 ft. from joint. LTPP Section 04-0215. Joint at Station 8.5 ft. 35
Figure 38. Chart. Option 3 faulting calculation. Planes projected using points ±1.0 ft. from joint. LTPP Section 04-0215. Joint at Station 324.6 ft. 36
Figure 39. Chart. Option 3 faulting calculation. Planes projected using points ±1.0 ft. from joint. LTPP Section 04-0215. Joint at Station 204.3 ft. 36
Figure 40. Chart. Option 3 faulting calculation. Planes projected using points ±1.0 ft. from joint. LTPP Section 27-4040. Joint at Station 30.3 ft. 37
Figure 41. Chart. Option 3 faulting calculation. Planes projected using points ±1.0 ft. from joint. LTPP Section 27-4040. Joint at Station 301.8 ft. 37
Figure 42. Chart. Option 3 faulting calculation. Planes projected using points ±1.0 ft. from joint. LTPP Section 27-4040. Joint at Station 439.0 ft. 38
Figure 43. Chart. Option 3 faulting calculation. Planes projected using points ±2.0 ft. from joint. LTPP Section 04-0215. Joint at Station 8.5 ft. 38
Figure 44. Chart. Option 3 faulting calculation. Planes projected using points ±2.0 ft. from joint. LTPP Section 04-0215. Joint at Station 324.6 ft. 39
Figure 45. Chart. Option 3 faulting calculation. Planes projected using points ±2.0 ft. from joint. LTPP Section 04-0215. Joint at Station 204.3 ft. 39
Figure 46. Chart. Option 3 faulting calculation. Planes projected using points ±2.0 ft. from joint. LTPP Section 27-4040. Joint at Station 30.3 ft. 40
Figure 47. Chart. Option 3 faulting calculation. Planes projected using points ±2.0 ft. from joint. LTPP Section 27-4040. Joint at Station 301.8 ft. 40
Figure 48. Chart. Option 3 faulting calculation. Planes projected using points ±2.0 ft. from joint. LTPP Section 27-4040. Joint at Station 439.0 ft. 41
Figure 49. Diagram. Process of faulting certification. 43
Figure 50. Photo. Creaform Metrascan 3DTM used to collect ground reference measurement data in the TPP study. 47
Figure 51. Equation. Pooled standard deviation. 51
Figure 52. Equation. Difference standard deviation. 51
Figure 53. Equation. Absolute difference between two measurements. 51
Figure 54. Diagram. Joint faulting artifact proposed in Phase I of this study. 53
Figure 55. Diagram. Proposed base plate for (left, flipped upside down) and connection beam (right). 55
Figure 56. Diagram. Proposed macrotexture surface (left) and spacer for fault height (right). ... 56
Figure 57. Diagram. Assembling the base plate, spacer, and macrotexture surface..... 56
Figure 58. Diagram. Top view (top) and side view (bottom) of assembled fixture with no faulting. 57
Figure 59. Diagram. Side view of assembled fixture with shallow joint depth and no faulting... 57

Figure 60. Diagram. Side view of assembled fixture with faulting. 57
Figure 61. Diagram. Assembly of faulting fixture with positive faulting and spalling. 58
Figure 62. Chart. Joints detected from 2D data using ProVAL. 61
Figure 63. Chart. Joints detected from 2D data using downward spike method. 61
Figure 64. Chart. High-pass filtered 2D pavement profile and joints detected using downward spike method. 62
Figure 65. Charts. 2D ECDA faulting using (top) original profile and (bottom) high-pass filtered profile at joint location 1,248 ft. 63
Figure 66. Charts. 2D ECDA faulting using (top) original profile and (bottom) high-pass filtered profile at joint location 1,263 ft. 64
Figure 67. Charts. Comparison of 2D ECDA faulting magnitudes from non-filtered and high-pass filtered profiles for left wheelpath (top) and right wheelpath (bottom). 65
Figure 68. Charts. Comparison of faulting magnitudes from 2D ECDA with high-pass filter and ProVAL AFM for left wheelpath (top) and right wheelpath (bottom). 66
Figure 69. Chart. Joints detected using downward spike method from 3D data. 68
Figure 70. Image. Sample 3D elevation image. 68
Figure 71. Image. 3D image processed through Canny Edge Detector. 69
Figure 72. Image. Joint detected using Hough Transform. 69
Figure 73. Chart. Joints detected from 3D image and downward spike methods. 70
Figure 74. Chart. Joints detected from 3D image using the proposed method. 70
Figure 75. Charts. Comparison of 2D and 3D representative profiles from SHA A (top) and SHA B (bottom) data. 72
Figure 76. Charts. Example of faulting obtained from SHA A's 2D data using Option 1 (top), Option 2 (middle), and Option 3 (bottom). 73
Figure 77. Charts. Example of faulting obtained from SHA B's 2D data using Option 1 (top), Option 2 (middle), and Option 3 (bottom). 74
Figure 78. Chart. Comparison of faulting calculation options from SHA A's 2D data. 75
Figure 79. Chart. Comparison of faulting calculation options from SHA B's 2D data. 75
Figure 80. Charts. Example of faulting obtained from SHA A's 3D data using Option 1 (top), Option 2 (middle), and Option 3 (bottom). 77
Figure 81. Charts. Example of faulting obtained from SHA B's 3D data using Option 1 (top), Option 2 (middle), and Option 3 (bottom). 78
Figure 82. Chart. Comparison of faulting calculation options from SHA A's 3D data. 79
Figure 83. Chart. Comparison of faulting calculation options from SHA B's 3D data. 79
Figure 84. Illustration. 3-D surface and 2-D profiles (longitudinal and transverse). 80
Figure 85. Illustration. Representative longitudinal profiles from different devices. 81
Figure 86. Schematic illustration of differential curling and consequent faulting. 81
Figure 87. Illustration. Schematics of enhanced 2GCI procedure. 82
Figure 88. Illustration. Faulting due to differential curling. 82

LIST OF TABLES

Table 1. Comparison of joint detection rates. 10
Table 2. Summary of agency practices for faulting data collection. 12
Table 3. Statistics for the artificial pavement response parameter. 22
Table 4. Faulting calculations from different options. 41
Table 5. Body motion requirement statements for faulting. 44
Table 6. Static sensor system requirement statements for faulting. 45
Table 7. Dynamic sensor system requirement statements for faulting. 46
Table 8. Controlled test requirement statements for faulting. 49
Table 9. Number of joints detected from different methods. 62

ACKNOWLEDGEMENTS

The following State Highway Agencies provided information regarding their practices and/or provided data for analyses – Alabama, California, Florida, Illinois, Kansas, Mississippi, Missouri, North Dakota, Ohio, South Dakota, Texas, Utah, and Washington. The following vendors provided information regarding their equipment and data collection procedures – Ames Engineering Inc., Dynatest North America, Inc., International Cybernetics Corp. (ICC), Pathway Services Inc., and Pavemetrics.

INTRODUCTION

BACKGROUND

Faulting in rigid pavements is defined as the difference in elevation across a transverse joint or crack as described in AASHTO R 36. It is one of the key distresses for jointed concrete pavements (JCP) as it affects both the functional and structural performance of pavement and impacts pavement life-cycle-costs, vehicle operating costs, safety, and ride quality. Recognizing the significance of faulting in JCPs, Federal programs use faulting as one of the performance metrics for evaluating progress toward the National Highway Performance Program (NHPP) goals (§ 1106; 23 U.S.C. 119) set forth in Fixing America's Surface Transportation (FAST) Act (FHWA, 2016).

Traditionally, State Highway Agencies (SHAs) have used manual, site-specific methods for measuring fault magnitudes of JCP joints. These manual methods range from simple straight-edge type equipment to those designed and manufactured specifically for faulting such as the Georgia Fault Meter (GFM). Many SHAs have moved away from manual methods and have adopted high-speed, automated methods for faulting data collection. As a result, a variety of data collection equipment has been used for this purpose [e.g., 2-Dimensional (2D) point or line lasers used typically for roughness assessment, 3-Dimensional (3D) technologies that are becoming more popular for automated crack assessment, etc.]. Accordingly, a variety of algorithms have been used to calculate faulting magnitude from these high-speed devices.

Due to the diversity in technology for faulting data collection and analysis, quality assessment of measured faulting data has been difficult. Other surface distresses (e.g., joint and crack spalling) and pavement features (e.g., sealed vs unsealed joints) have caused added challenges in obtaining harmonized, consistent results from different fault measuring technologies. Furthermore, although 3D technologies show potential for overcoming some of the limitations of 2D and manual devices, the data collection and analysis of 3D technologies have not been properly incorporated in the current standard for faulting assessment. As such, there is a need for developing a standardized procedure for faulting that can be used with currently available technologies. Such standardized procedure will allow for consistent measurement and analysis of faulting data within a pavement section, between different pavement sections, and between different SHAs.

PURPOSE OF STUDY

The purpose of this study is to improve the faulting data collection and analysis methods and help develop certification and verification procedures to evaluate the precision and accuracy. Collecting accurate fault data is important to assess pavement conditions and to determine maintenance and rehabilitation needs.

The objectives of this study are to assist SHAs with the following:

1. Information and procedures necessary to collect, monitor, and evaluate faulting of JCPs,
2. Ability to quantify faulting at each joint or crack according to a standard definition, and

3. Ability to determine the precision and accuracy of high-speed faulting measurement. This includes identification of the joints and cracks and assessment of the precision and accuracy of the measurement compared to the recommended guidelines and practical operating conditions.

DEFINITION OF SIGNIFICANT DATA QUALITY TERMS

The following definitions were taken from "Guidelines for Development and Approval of State Data Quality Management Programs" (FHWA, 2018) and AASHTO R 10.

Acceptance – The process or set of criteria used by the agency (i.e., sampling, testing, and inspection) to determine if the results of the data collection and processing meets the level of accuracy set by the agency. Also referred to as verification when used to validate the collected data.

Accuracy – The degree to which a measurement, or the mean of a distribution of measurements, tends to coincide with the true population mean. When the true population mean is not known, as is the case with pavement data collection, the degree of agreement between the observed measurements and an accepted reference standard (ground reference) is typically used to quantify the accuracy of the measurements.

Bias – An error, constant in direction, that causes a measurement, or the mean of a distribution of measurements, to be offset from the true population mean.

Calibration – Process used to standardize (something, such as a measuring instrument) by determining the deviation from a standard to ascertain the proper correction factors. Calibrating a measuring equipment or person assure that a piece of equipment or person is producing measurements or observations as intended. The processes may include adjustments to the device and rechecking outcomes where necessary. Calibration is normally done by qualified persons at qualified facilities on a periodic basis.

Certification – The process of assuring that persons understand and equipment involved in the data collection and processing use the correct methods to collect, process and analyze data.

Data – Numerical outcomes from the collection and processing of measurements of pavement conditions or conditions of other assets. The term usually refers to electronic records of these outcomes although it could include manually recorded paper copies of measurements.

Data Collection – Measurement of some characteristics of pavement condition, converting the measurements into numerical values, and electronically storing the values.

Data Collector – Vendor or state staff responsible for collecting pavement condition data.

Data Processing – Extracting, manipulating, and recording results of data collection using a defined process or algorithm. This could include processes that analyze data such as derivation of International Roughness Index from pavement profile and accelerometer measurements.

Precision – The degree of agreement among a randomly selected series of measurements; or the degree to which tests or measurements on identical samples tend to produce the same results.

Quality – The degree of excellence of a product or service; the degree to which a product or service satisfies the needs of a specific customer; or the degree to which a product or service conforms with a given requirement.

Quality control (QC) – The system used by the Data Collector to monitor, assess, and adjust its production or placement processes to ensure that the final product will meet the specified level of quality. Quality control includes sampling, testing, inspection and corrective action (where required) to maintain continuous control of a production or placement process.

Reference value – A value that serves as an agreed-upon reference for comparison, and which is derived as a theoretical or established value, based on scientific principles, an assigned or certified value, based on experimental work of some national or international organization, or a consensus or certified value, based on collaborative experimental work under the auspices of a scientific or engineering group (AASHTO 2011). Reference value is also known as ground reference.

Repeatability – Degree of variation among the results obtained by the same operator repeating a test on the same material. The term repeatability is therefore used to designate test precision under a single operator.

Reproducibility – Degree of variation among the test results obtained by different operators performing the same test on the same material.

Resolution – The smallest change in a quantity being measured that causes a perceptible change in the corresponding indication.

Sample – A portion of the data used for reviewing and examining the quality of the data collection and processing process. This is usually done with a statistically significant sample size that corresponds to a defined level of confidence and confidence interval.

Validation – The mathematical comparison of two independently obtained sets of data (e.g., agency acceptance data vs. contractor data) to determine whether it can be assumed they came from the same population.

ORGANIZATION OF REPORT

Figure 1 shows an overall framework for establishing JCP faulting collection and analysis standards. This report is organized along the lines of this framework developed in Phase I of this project. The last section of this report documents the research team's efforts to use data provided by SHAs to evaluate and validate the definitions and standards proposed in Phase I.

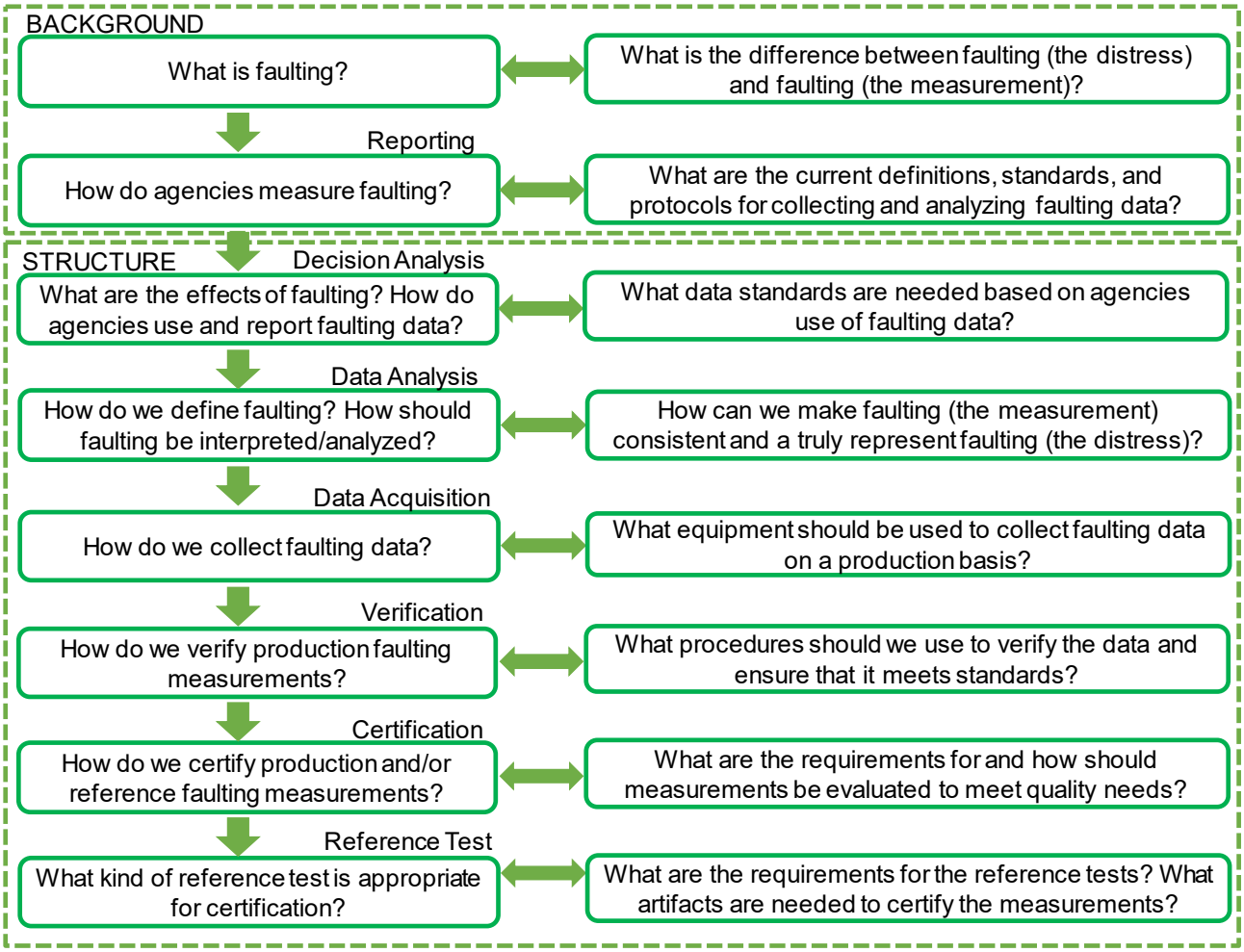

Source: FHWA

Figure 1. Flowchart. Framework for establishing jointed concrete pavement faulting collection and analysis standards.

CURRENT PRACTICES IN FAULTING DATA COLLECTION AND ASSESSMENT

A variety of devices including manual fault meters and laser (2D and 3D) technologies are currently being used for faulting data collection and analysis.

MANUAL FAULT METERS

Manual fault meters refer to the handheld, site-specific, stationary devices capable of measuring the fault at a given location. Historically, these devices ranged from simple straight-edge type of devices to those that are custom made for faulting. The most well-known and frequently used device of this type is the Georgia Faultmeter (GFM) shown in Figure 2 which is still being used by the Long-Term Pavement Performance (LTPP) program and various SHAs as a reference fault meter.

Although these manual fault meters are still being used frequently, they are generally not efficient for network level surveys. For this reason, manual fault meters are typically used to collect faulting data from a small subset of all joints within a section (most recent AASHTO R 36 standard recommends surveying only 10 percent of all joints). Furthermore, manual measurements expose testing personnel to potential traffic safety hazards even with lane closures. Mississippi DOT also discovered that GFM produced inaccurate measurements on pavements with grade (Chang, 2012).

Current version of AASHTO R 36 provides the basic theory behind the manual fault meter and the relevant fault calculation. However, the standard does not stipulate any specific requirements for a manual fault meter, and only provides recommendations and an example design of a manual fault meter.

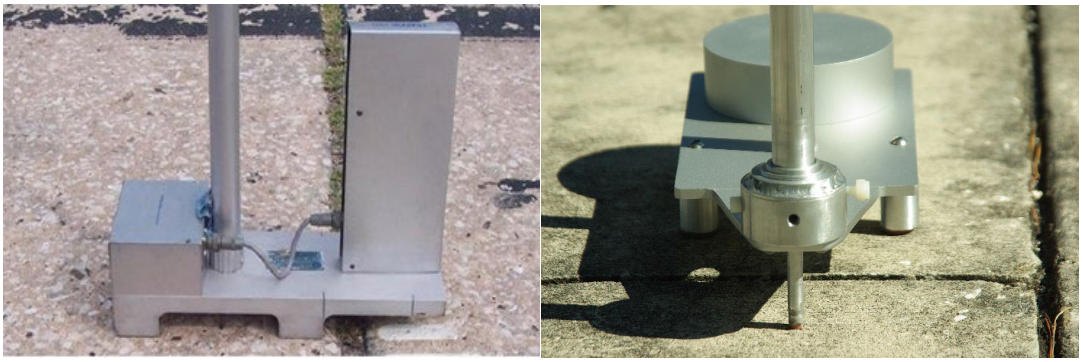

Source: FHWA

Figure 2. Photo. Various versions of Georgia faultmeters.

TWO-DIMENSIONAL (2D) AUTOMATED FAULT MEASUREMENTS

The limitations of the manual fault meters mentioned above were the primary motivations to develop the Automated Fault Measurement (AFM) methods based on High-Speed Inertial Profiler (HSIP) data (Figure 3) which is collected primarily for pavement roughness evaluation in terms of the International Roughness Index (IRI). AASHTO R 36 provides the current standards for evaluating JCP faulting from the HSIP data.

Source: ARA

Figure 3. Photo. 2D Automated Fault Measurement (AFM) equipment based on High-Speed Inertial Profiler (HSIP).

Currently, AASHTO R 36 specifies that the HSIP equipment should comply with AASHTO M 328 and its operation in accordance with AASHTO R 56. More specifically, this means that any HSIP with a sampling interval of 1.5 inches or less can be used for AFM as long as the cross-correlation repeatability and accuracy scores based on AASHTO R 56 are greater than or equal to 92 percent and 90 percent, respectively (for pavements with IRI less than 150 in/mi).

For calculation of fault magnitude from the pavement profiles, AASHTO R 36 provides two different AFM methods, namely Method A and Method B. Method A was developed by Chang et. al. (2008) and Chang et. al. (2012) and has been implemented in the AFM module of ProVAL, hence also known as the "ProVAL method."

Method A uses a two-step approach. The first step involves detecting the joint locations from the pavement profiles using one of the following three methods:

- Downward spike method: This method is partly based on FHWA's JCP curling/warping analysis methodology using pavement profiles (Karamihas and Senn, 2012). The method is essentially based on anti-smoothing the pavement profile and normalizing it with its Root Mean Square (RMS) to produce downward spikes at the joint locations (Chang et. al., 2008).
- Step detection method: The step detection method was originally developed by Mississippi DOT (Chang et. al., 2008) and also referred to as the "MDOT method" of joint detection. The method is based on identifying the locations where the elevation difference between adjacent profile samples is greater than 0.08 in.
- Curled edge detection method: This method utilizes a bandpass filter (with cutoff thresholds of 9.84 in. and 150 ft.) and simulates the response of a 9.8 ft. rolling straightedge through the filtered profile. The joints are detected as the locations where the simulated rolling straightedge responses are greater than 0.12 in.

Chang et. al. (2008) indicated that all three of the above methods have advantages and disadvantages. The downward spike method generally works well with profiles collected at shorter intervals while the step detection method works well for profiles with apparent joint faults. The curled edge detection method works well when both above methods fail (i.e., when there are no downward spikes or apparent faulting), provided that the JCP slabs exhibit curling or warping. Once the joint and/or crack is detected, Method A continues with the second step in which the fault magnitude is calculated. In general, this involves the following.

1. Extract the pavement profile for a length of 8.0 ft. with the identified joint at the center of the extracted profile.
2. Conduct linear regression through the elevation points of the approach and leave slabs separately (Figure 4) and extend the regression line of the approach slab up to 9.0 inches into the departure slab.
3. The fault magnitude is obtained as the average of the elevation differences between the two regression lines calculated at points 3 in. to 9 in. away from the joint in the departure slab.

The two-step approach implemented in Method A may allow for advanced technologies to replace either the first step and/or the second step. For example, 3D technologies superior in joint identification can provide accurate joint locations for Step 1 and proceed with Step 2 computation of joint fault using the data from high resolution HSIP.

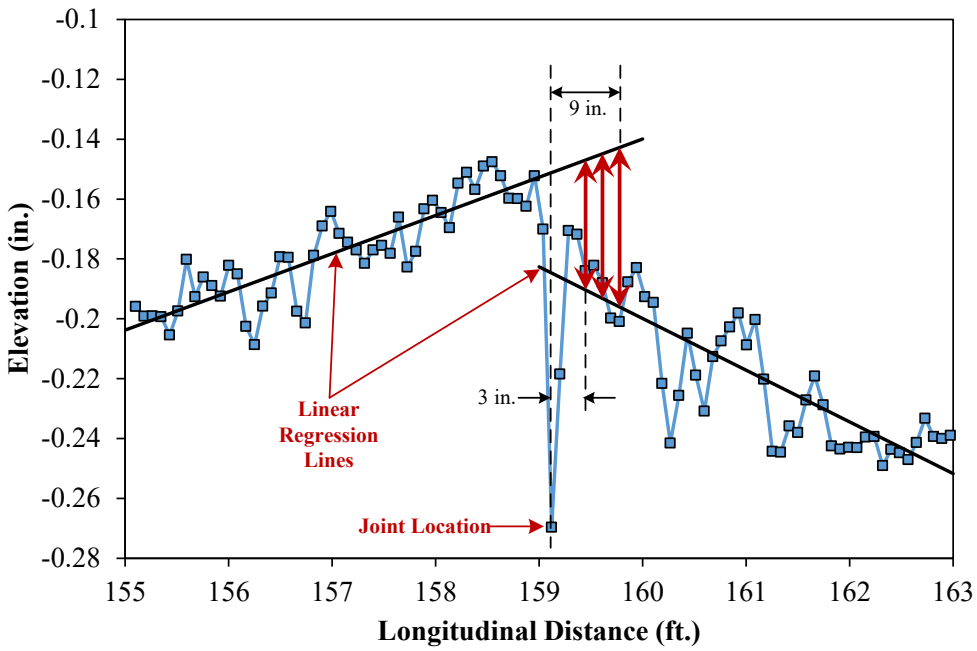

Source: FHWA

Figure 4. Graph. Illustration of AASHTO R 36 Method A.

Method B was developed by Florida DOT (hence also known as the "Florida method" or "FDOT method") and implemented in an Excel spreadsheet (Nazef 2009; Nazef 2010). Unlike Method A, this method combines the joint/crack identification and fault quantification into a single

procedure. As such, it is difficult to adapt new technologies such as 3D measurement into this method without separating the code. The general procedure is illustrated in Figure 5 and involves the following.

1. The method starts by defining a sensitivity factor (SF) for the slope between two consecutive profile points used for identifying the joint locations. The default SF is set to 0.01 multiplied by the sampling interval of the HSIP data. The user also has to input the joint spacing for the analysis.
2. The JCP joints are identified by finding valleys (i.e., negative slope) and peaks (i.e., positive slope) along the profile where the slope is greater than the SF. If the slope is greater than the SF, the location is identified as a joint.
3. The fault magnitude is obtained as the average of the elevation differences of the points separated by 11.8 in. (with the joint located in between the two points). Only the points between 3.0 in. and 8.8 in. from the joint location are considered for this analysis.
4. The above procedure is repeated (up to 9 times) by changing the SF value until the number of detected joints matches or is close to the theoretical number of joints (calculated based on user-supplied joint spacing and length of the pavement section). The joint location and faulting magnitudes are recalculated based on the optimum SF.

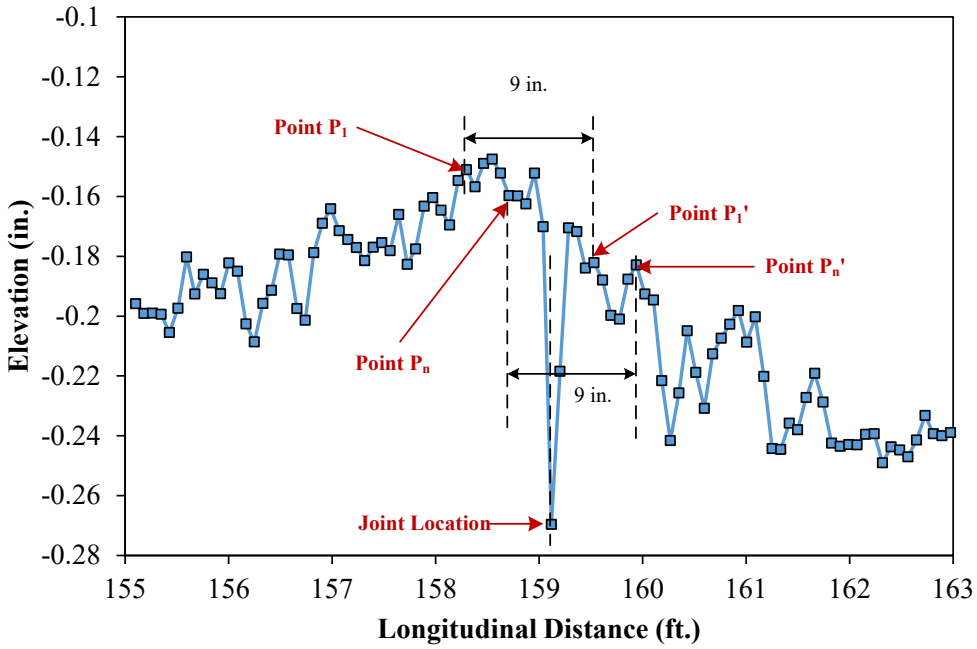

Source: FHWA

Figure 5. Graph. Illustration of AASHTO R 36 Method B.

Since the inclusion of Methods A and B in AASHTO R 36 in the year 2012, Agurla and Lin (2015) developed the LTPP AFM method which can also be used with HSIP profiles. Similar to Method A of AASHTO R 36, the LTPP AFM separates the analysis into two steps, i.e., joint detection and fault calculation.

The joint detection procedure of the LTPP AFM method starts by anti-smoothing the pavement profile which is similar to the downward spike method. Then, the filtered profile is inputted into MATLAB's Peakdet algorithm to find the joints. In addition, joints are detected by analyzing all three profiles (left and right wheelpaths and center of a lane) for a given pavement.

For calculating the fault magnitude, two methods are implemented in LTPP AFM. The first method corresponds to AASHTO R 36 Method A. The second method is known as the "Slope Method" which is illustrated in Figure 6. This method involves the following.

1. Starting at the joint location, the profile slope is calculated for two consecutive points. The first point at which the absolute value of the slope falls below 0.12 in./ft. (10 mm/m) is identified for both the approach and leave slabs.
2. The fault magnitude is calculated as the elevation difference between the two points identified from the previous step.

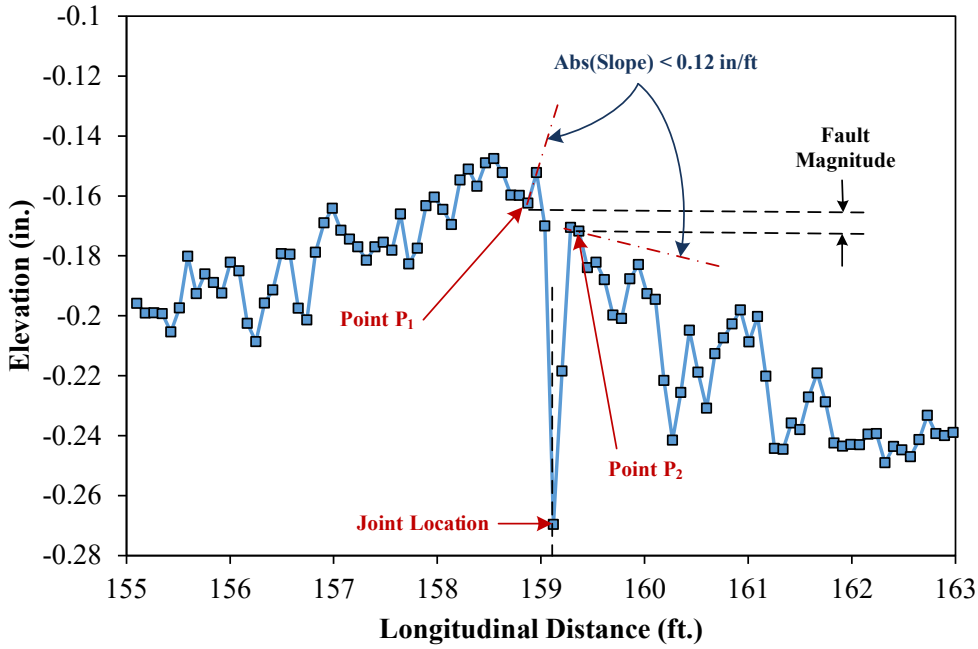

Source: FHWA

Figure 6. Graph. Illustration of LTPP AFM Slope Method.

Chang et. al. (2012) indicated that the joint detection algorithms for 2D HSIP profiles have difficulties in detecting joints that are sealed, spalled, and/or skewed, and none of these existing algorithms can always ensure the 100 percent successful Joint Detection Rate (JDR). Agurla and Lin (2015) compared the LTPP AFM against the two methods in AASHTO R 36 for joint/crack detection and fault measurements. The JDRs reported by this study are summarized in Table 1 (Agurla and Lin, 2015).

Table 1. Comparison of joint detection rates.

AFM algorithm	Joint detection rate (JDR)
LTPP AFM	95 to 100 % using LTPP profiles
ProVAL AFM	58 to 99.4 % using LTPP profiles
FDOT AFM	96% using FDOT profiles

THREE-DIMENSIONAL (3D) AUTOMATED FAULT MEASUREMENTS

Three-dimensional (3D) technologies have become more widely used to collect faulting data (Tsai et. al., 2012; Wang et. al., 2014; Geary et. al., 2018). Modern-day high-speed devices with laser/camera technologies (Figure 7) and software are mature enough to collect dense data for characterization of transverse profiles. The 3D technologies have the potential to overcome the joint detection issues encountered with 2D HSIP data.

According to information obtained from SHAs, equipment manufacturers, and service providers, a variety of 3D devices are currently being used for network level faulting assessment. The longitudinal sampling interval of these 3D equipment ranged approximately from 0.04 in. (1.0 mm) to 0.3 in. (8.0 mm) assuming a vehicle speed of 60 mph while the transverse sampling interval ranged approximately from 0.04 in. (1.0 mm) to 0.07 in. (1.89 mm) assuming a lane width of 12.0 ft. These sampling intervals meet the AASHTO R 36 requirement of 2 in. or less stipulated for the 2D HSIP data. However, one vendor indicated that the automated joint detection algorithm for 3D data may also struggle at higher vehicle speeds or with increased longitudinal sampling interval. This is in agreement with the findings of Nazef et. al. (2009) who reported that a JDR of 95 percent can be achieved with an HSIP sampling interval of 0.68 in. based on AASHTO R 36 Method B and the JDR reduces with increasing sampling interval. Nonetheless, manual inspection of the 3D data may allow for all the joints identified within the data.

Note that most of the algorithms for calculating faulting from 3D equipment are proprietary. In addition, the equipment vendors frequently modify the algorithm to meet the specific needs or protocol required by the agency.

An important consideration is that 3D technologies (with wide-field lasers/cameras with overlap and vehicle motions removed by inertial measurement units) are generally able to collect data across the entire pavement width, while HSIP generally only collects two longitudinal profiles in the wheelpaths. Therefore, measurements may not be at the same location across a transverse joint/crack, resulting in different values for faulting. Furthermore, in-lane wander of survey vehicles creates further challenges for the correlation between HSIP and 3D devices. A field experimental study conducted by Wang and Lin (2014) compared the fault values obtained from 3D pavement texture using a template-matching algorithm to those from ProVAL. They found that fault values across the transverse joint were fluctuating/non-uniform and the presence of joint spalling may increase the difference between the fault magnitudes obtained from 2D and 3D systems.

Source: ARA (left photo) and Pavemetrics (right illustration)

Figure 7. Photo and Illustration. 3D Automated Fault Measurement (AFM) equipment.

AGENCY PRACTICE FOR FAULTING MEASUREMENT

During Phase I of this study, the research team obtained information from several SHAs on their current practice regarding fault data collection and analysis and how fault data is used in their pavement management system. Table 2 provides a brief summary of the current technologies used by the SHAs. An overview summary of information is as follows:

- The majority of SHAs are using 3D system to collect faulting data. The 3D system was mainly used for collecting various pavement distress data for both asphalt and concrete surfaces on the entire network, such as rutting, roughness, cracking, and faulting for Highway Performance Monitoring System (HPMS) purposes.
- A few State DOTs are still using the 2D systems, however, they are moving to collect fault data from 2D to 3D system in the near future. The primary challenge with 2D systems was found to be the joint detection, especially when line lasers are used with HSIPs. Although the line lasers are becoming more popular for roughness assessment due to their effectiveness on aggressive surface textures (e.g., tined concrete surface), the averaging filter associated with the line laser makes it difficult to detect the joints using the automated algorithms.
- The GFM is commonly used as a device for reference measurements by several states. A few states developed their own reference measurement devices. For example, Florida DOT recently developed a device known as the "laser-based straightedge" based on the concept of transverse profiler. AASHTO R 36 Method B is used for calculating the reference faulting value from the elevation collected using the laser-based straightedge technology.
- In lieu of a manual fault meter as a device for reference measurements, Alabama DOT extracts a 2D profile from the 3D data. The fault magnitude obtained from the extracted 2D profile using AASHTO R 36 Method A (step detection) is used as the reference for the 3D system.

- Most SHAs are less concerned about the effect of curling/warping, spalled joints, and/or sealed joints on fault measurements and do not make special accommodations to account for these effects.
- With the exception of North Dakota DOT, the SHAs indicated that they are not concerned with the differences between positive and negative faults (i.e., a step down and a step up in the profile, respectively), and are taking absolute average of the fault magnitudes from the joints detected by the AFM algorithm.

Table 2. Summary of agency practices for faulting data collection.

Agency	Practice for Collection of Faulting Data
Alabama DOT	• Outsourcing faulting data collection. • Uses 3D technology for network level faulting assessment. • 2D profile extracted from 3D data and used with AASHTO R 36 Method A (step detection) as a reference.
Florida DOT	• Uses 2D system (in-house) with AASHTO R 36 Method B for network level PMS survey. • Outsourcing faulting data collection for HPMS reporting (3D equipment). • Developed an in-house device for reference measurements based on transvers profiler known as “laser-based straightedge”
Kansas DOT	• Used GFM (before 1990) • 2D HSIP data (1990 - 2013) • Using 3D system as implemented by the contractor
Mississippi DOT	• Outsourcing faulting data collection. • Uses 3D technology for network level faulting assessment. • GFM is used as a device for reference measurements.
Missouri DOT	• Recently switched from 2D to 3D system for faulting assessment.
North Dakota DOT	• Using in-house 2D system since 1991. • Faulting is calculated using vendor software which is based on AASHTO R 36 Method A (downward spike).
Ohio DOT	• Using 3D equipment and automated data processing for faulting assessment. • 3D equipment showed better correlation with GFM than 2D equipment (AASHTO R 36 Method A).
South Dakota DOT	• In-house 3D equipment for data collection and manufacturer software for calculating faulting. • GFM is used as a device for reference measurements.
Utah DOT	• Using 3D equipment and automated data processing for faulting assessment.
Washington State DOT	• 2D equipment with manufacturer software (1998 – 2014). • Moved to 3D equipment since 2014.

SUMMARY

While faulting (the distress) is established by all agencies as the difference in elevation across a joint or crack, the specifics of faulting (the measurement) in terms of defining, collecting, analyzing, referencing, and reporting faulting data varies from one agency to another. A consequence of this difference is that there could be differences in reported values even for the same stretch of roadway making comparisons between agencies inappropriate or difficult.

LIMITATIONS OF CURRENT PRACTICES

NEED FOR IMPROVED DEFINITION FOR FAULTING

Joints (specifically contraction joints that are most common) in rigid pavements are, by definition, purposefully placed discontinuities to control the location of cracking caused by dimensional changes of the PCC material. The LTPP distress survey manual defines transverse cracks as those that are "predominantly perpendicular to the pavement centerline" and faulting as "difference in elevation across a joint or a crack" (FHWA, 2014). Similar definitions are also used by State DOTs for distress data collection and pavement management purposes (FDOT, 2018; Bandini et. al., 2012).

While the above definitions for joints/cracks and faulting are simple and may have been sufficient for the individuals in the field conducting a manual distress survey, additional consideration needs to be given for faulting, especially when new methodologies are available for collection of faulting data (automated and 3D technologies).

In addition, the issue pertaining to the lateral location of faulting measurement needs to be considered. Recent 3D technologies have the capability of measuring faulting almost continuously along transverse length of the joint/crack. Wang and Lin (2014) have also reported that the faulting profile extracted from the 3D data along the joint may vary substantially. However, it is impractical and may be even impossible to measure the faulting along the entire length of a joint or crack with traditional 2D AFM.

Uncertainties Associated with Different Methods

There are a number of devices being used for faulting assessment (ranging from manual fault meters to 3D equipment) and the differences arising from these different devices have been known for a long time. Some of the issues relating to these different devices include the following.

- Manual fault meters and 2D HSIP technologies are limited in the location of faulting assessment (i.e., wheelpaths or a set distance from the lane-shoulder edge).
- The profile trace from the HSIP is also affected by the lateral wander of the profiler.
- Skewed joints, corner cracks, spalling, and transverse cracks not extending to full width of the pavement may cause additional challenges with joint detection algorithm of the AFM.
- Different lasers used in HSIPs (point vs. line laser) may cause additional variability in the measured faulting. Faulting, as compared to IRI, is evaluated in a more localized manner (i.e., at joints and cracks) and may be affected more by these laser types used to identify the transverse joint locations and compute faulting.

Unlike the IRI which is always calculated based on Golden Car simulation, there are many different AFM methods for calculating faulting. The difference in these methods may result in different number of joints detected and different faulting values from the same joint. This issue is

elevated further with the development of numerous 3D technologies using proprietary algorithms that are not well documented.

Lack of a Standard Reporting Protocol

Guidance and information on how the faulting data should be recorded and reported is limited and not complete. As such, some SHAs indicated that only the average fault value is recorded for pavement management purposes, while some others indicated that average and maximum values are recorded.

According to the information obtained during Phase I, it was also found that most agencies do not distinguish between positive and negative faults. Furthermore, while most agencies reported that they are taking absolute averages of faulting data, it is possible that some agencies are taking a straight average of all the faults for each section. For example, if there were only two joints with +1.0 mm and -1.0 mm faults, the reported faulting for this section is zero. This approach is also used by the LTPP program.

There is no guidance on JDR and the joints undetected from the AFM. As an example, consider a pavement segment which includes a total of 10 joints with 5 of them exhibiting 0.5 in. faulting and the other 5 joints with no faulting. If the AFM only detected 5 joints that showed faulting and assuming that the fault magnitude was accurately determined, the analyst may only see these detected joints from the data and may conclude that the average faulting in this pavement segment is (5 joints X 0.5 in.) / (5 detected joints) = 0.5 in. However, if the other 5 joints having zero fault are to be included in the calculation, the average fault would be (5 joints X 0.5 in.) / (10 total joints) = 0.25 in. Some agencies reported that they are not overly concerned about accounting for the missed or undetected joints that may potentially have zero faulting as it does not impact their decision making in terms of maintenance and rehabilitation.

Lack of a Certification Process for Faulting

There is a certification procedure for inertial profilers based on AASHTO R 56, with an emphasis on IRI, but there is no certification procedure that is specific to faulting. AASHTO R 36 recommends that the profiling equipment be verified per AASHTO R 56 and that the SHAs be responsible for training and certification.

SUMMARY

The objective of this project (Phase I and Phase II) is to address the shortcomings of current faulting practices and help establish standards to quantify the accuracy and precision requirements for faulting data collection and analysis to meet SHA requirements.

PROPOSED DEFINITION OF FAULTING

RATIONALE FOR CHANGES FROM AASHTO R 36-17

The definition and measurement requirements of faulting need to be connected (data collection and processing requirements) and clarified, so that any current and future technologies can be used as long as they can meet the requirements.

CURRENT DEFINITION

Currently, faulting is defined as the difference in elevation across a transverse joint or crack as illustrated in Figure 8.

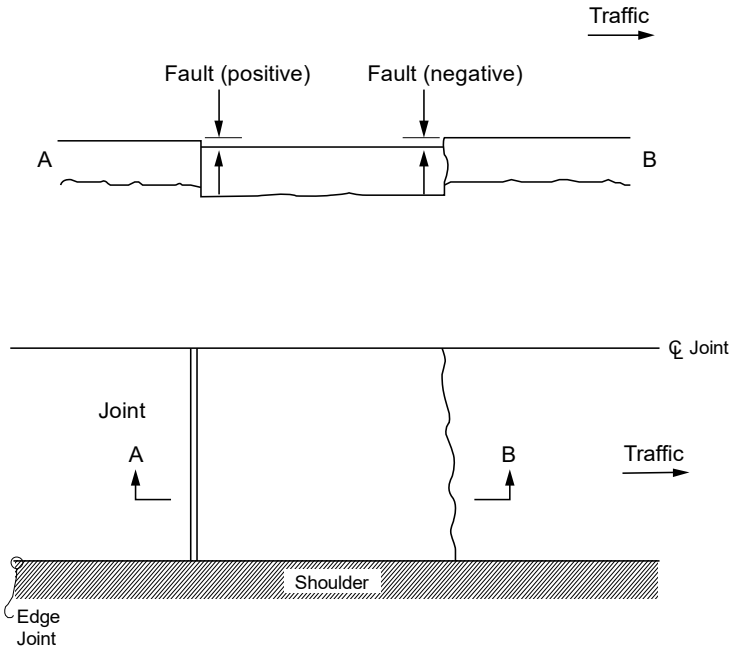

Source: FHWA

Figure 8. Illustration. Current definition of transverse joint or crack faulting.

In the following, the definition of faulting developed from this study is provided along with three options for calculating the fault magnitude. Note that the definition and faulting calculation methods were developed such that they are equipment neutral (i.e., can be used for both 2D HSIP data and 3D data).

PROPOSED DEFINITION (OPTION 1)

Faulting is defined as the difference in average elevations across a transverse joint, measured within the outer wheelpath, in accordance with the following items.

The outer wheelpath for faulting is defined as the area within 15 in. to 45 in. from the lane center (i.e., center of wheelpath is 30 in. from the lane center and the width of wheelpath is 30 in.), regardless of the lane width. Figure 9 shows a schematic of the outer wheelpath for faulting.

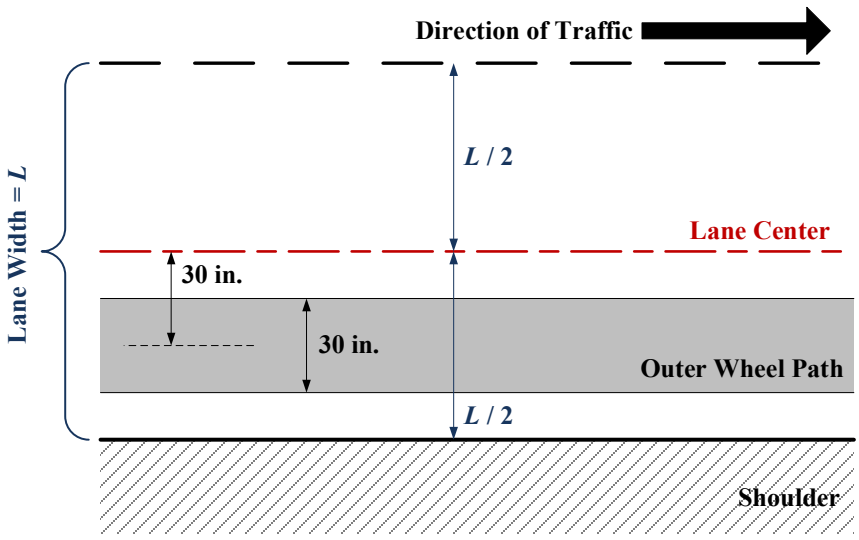

Figure 9. Illustration. Wheelpath for joint faulting calculation.

The above numbers were determined assuming a track width (distance between the two tires in the same axle) of 60 in., which is typical for most passenger vehicles in the U.S. Using a typical tire contact width of 8 in., the wheelpath width of 30 in. correspond approximately to ± (2 × width of tire). Assessed differently, the wheelpath width of 30 in. correspond to where 95 percent of the tires will be located assuming a vehicle wander in terms of standard deviation of 7.7 in.

Faulting is calculated from a "Representative Longitudinal Profile" of the outer wheelpath. The concept of representative longitudinal profile is schematically shown in Figure 10.

a. In case of 3D data where elevations are measured longitudinally and transversely, the representative longitudinal profile is obtained by averaging the elevations within the wheelpath in the transverse direction. The averaging is done in the transverse direction regardless of the joint skew (Figure 11). This is in recognition of the direction of traffic being independent of the joint skew and the tire contact area occupying both the approach and leave slabs when travelling over the skewed joint.
b. For 2D profile data, the representative longitudinal profile is simply the longitudinal profile collected by the HSIPs. It is noted that the 2D representative longitudinal profile may be subject to wander and increased level of noise, and thus lower precision.

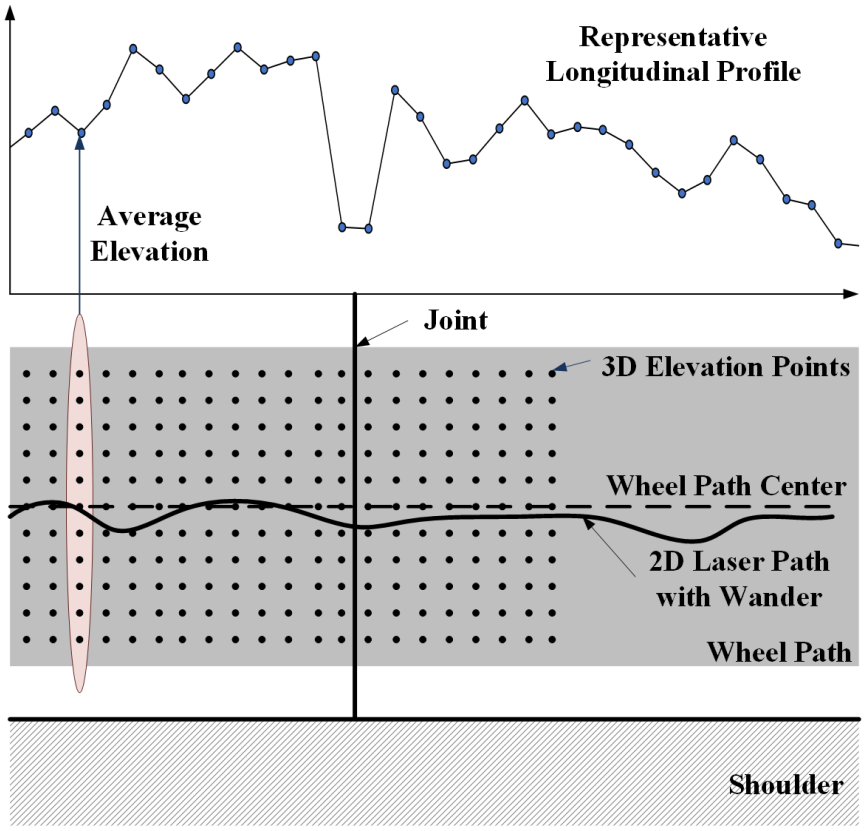

Source: FHWA

Figure 10. Illustration. Representative Longitudinal Profile.

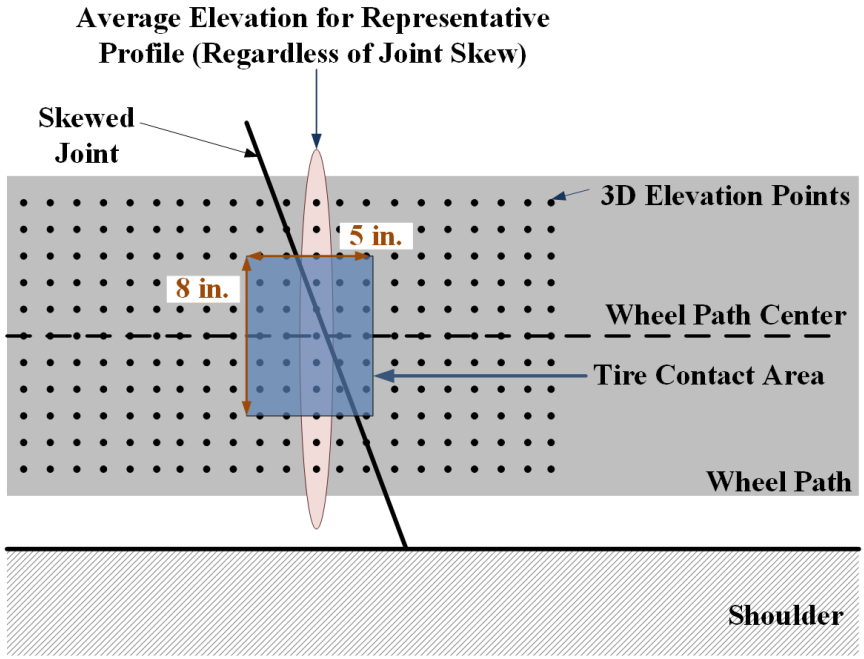

Source: FHWA

Figure 11. Illustration. Representative Longitudinal Profile for skewed joints.

From the representative longitudinal profile, the average elevations before and after the joint are calculated using an Enhanced Cumulative Difference Approach (ECDA). Since the tire contact length (in the direction of traffic) of 5 in. is typical for a passenger car, the minimum longitudinal distance for calculating the average elevations before and after the joint is 5 in. Furthermore, the potential effect of spalling and/or wide joint opening detected by the ECDA algorithm is to be excluded from faulting calculation.

Faulting is calculated with the following sign convention.

a. Positive (+) faulting: Average elevation in the approach slab is greater than that of the leave slab.
b. Negative (-) faulting: Average elevation in the approach slab is less than that of the leave slab.

The ECDA method is explained in the following section.

Enhanced Cumulative Difference Approach (ECDA)

The original Cumulative Difference Approach (CDA) was introduced in 1993 AASHTO Pavement Design Guide, for delineating statistically homogeneous sections from a variety of pavement response values including deflections, serviceability, friction numbers, pavement distress or severity indices, etc. (AASHTO, 1993).

The overall approach of the CDA method is illustrated in Figure 15. The simplified scenario in Figure 15 (top) shows three uniform sections with response values of r_1, r_2, and r_3, respectively. The overall average from all three sections are shown as r in the figure. The cumulative area under the actual response values can be calculated from the following equation (Figure 12).

$$A_x = \int_0^{x_1} r_1 dx + \int_{x_1}^{x_2} r_2 dx + \int_{x_2}^{x} r_3 dx$$

Figure 12. Equation. Cumulative area under the actual response values.

Where:

A_x = cumulative area under response values for $x_2 \leq x \leq x_3$.
$r_{1, 2, 3}$ = responses such as deflections, serviceability, friction numbers, pavement distress or severity indices, etc.
$x_{1, 2}$ = distance corresponding to responses r_1 and r_2, respectively.
x = distance (independent variable).

On the other hand, the cumulative area under the overall average is obtained as calculated from the following equation (Figure 13):

$$\bar{A}_x = \int_0^{x} r dx$$

Figure 13. Equation. Cumulative area under overall average.

Where:

$\bar{A}_x$ = cumulative area under overall average response value.

r = overall average response.

Given the cumulative areas, A_x and $\bar{A}_x$, the cumulative difference is simply obtained as the following.

$$Z_x = A_x - \bar{A}_x$$

Figure 14. Equation. Cumulative difference.

Where:

Z_x = cumulative difference.

Figure 15 (middle) shows the plot of cumulative areas while Figure 15 (bottom) shows the cumulative difference plot. The original CDA method identifies the section boundaries as the locations where the slope of the cumulative difference (Z_x) changes algebraic signs (from positive slope to negative slope, or vice versa).

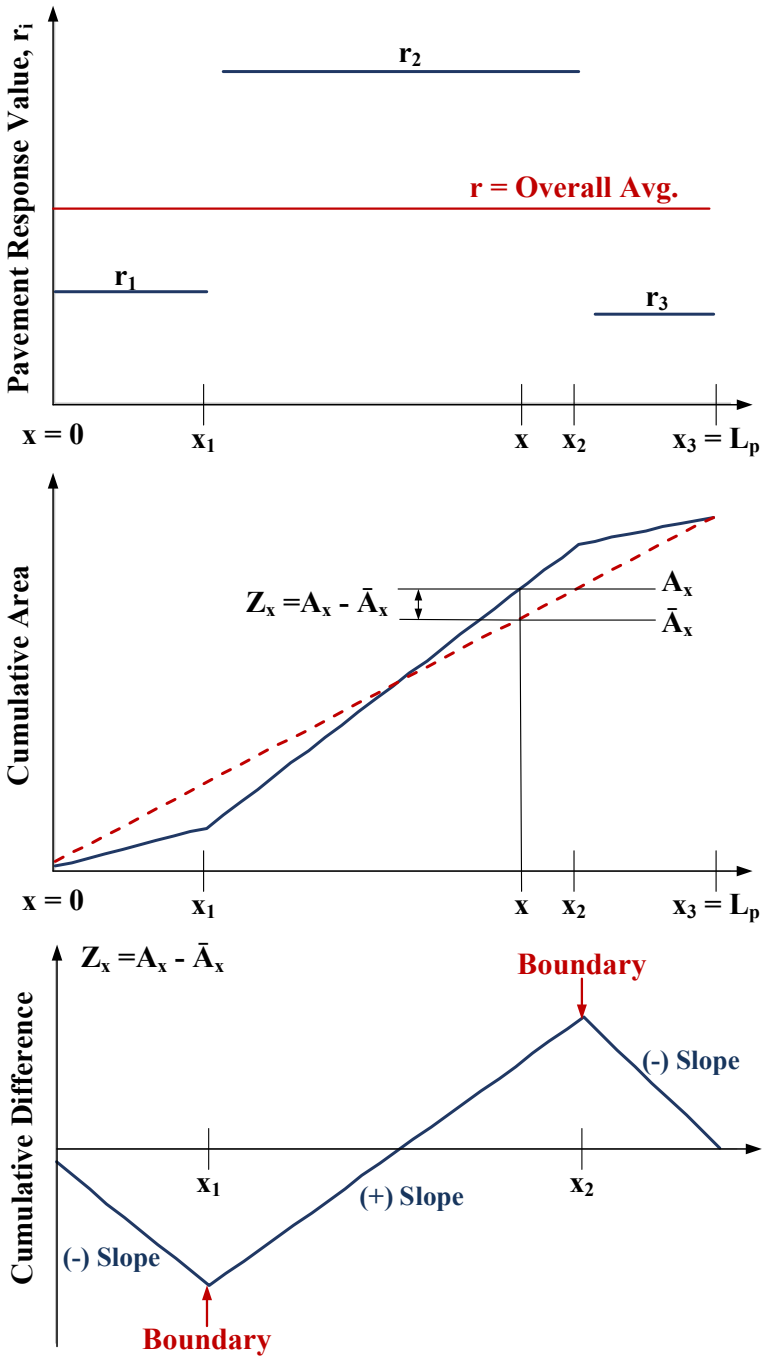

Source: FHWA

Figure 15. Illustrations. Cumulative Difference Approach (top) uniform response value, (middle) cumulative and average areas, and (bottom) cumulative area difference.

Although the original CDA method is relatively powerful and readily implementable into a computer algorithm, it is not free of limitations. To demonstrate the limitation of the original CDA, an artificial pavement response has been constructed using the statistics shown in Table 3. The table shows that there are five uniform sections with different mean values, all with a Coefficient of Variation (COV) of 15 percent. Figure 16 shows a plot of the artificial profile.

Table 3. Statistics for the artificial pavement response parameter.

Section Number	Section Begin Point	Section End Point	Response Parameter Mean	Response Parameter Standard Deviation	Response Parameter Coefficient of Variation (%)
1	0	50	10	1.5	15.0
2	50	100	15	2.25	15.0
3	100	150	22	3.3	15.0
4	150	200	28	4.2	15.0
5	200	250	13	1.95	15.0

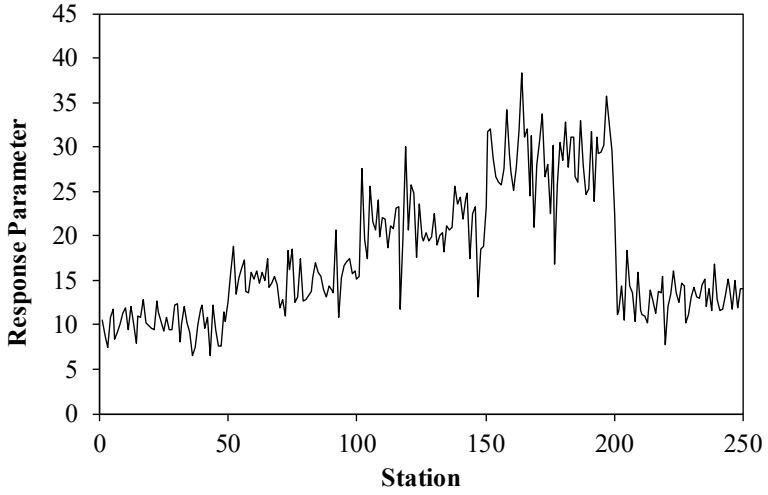

Source: FHWA

Figure 16. Chart. Artificial pavement response parameter.

Figure 17 (top) shows the corresponding cumulative difference plot and the locations where the slope of the cumulative difference changed signs – i.e., the boundaries of the uniform sections. Figure 17 (bottom) shows the corresponding mean values for the delineated sections. It is seen from these figures that the original CDA method was not able to delineate the boundaries between sections 1 and 2, and sections 3 and 4.

It is seen from Figure 17 (top) that although the cumulative difference did not change its arithmetic sign, its slope has changed at the boundaries between sections 1 and 2, and sections 3 and 4. To overcome such limitation of the original CDA method, Haider and Varma (2015) developed the Enhanced Cumulative Difference Approach (ECDA) which is capable of identifying the boundaries based on the changes in slope of the cumulative difference. Figure 18 (top) shows the cumulative difference plot and the boundaries identified from ECDA while Figure 18 (bottom) shows the means obtained from the delineated sections that are in agreement with the true values shown in Table 3.

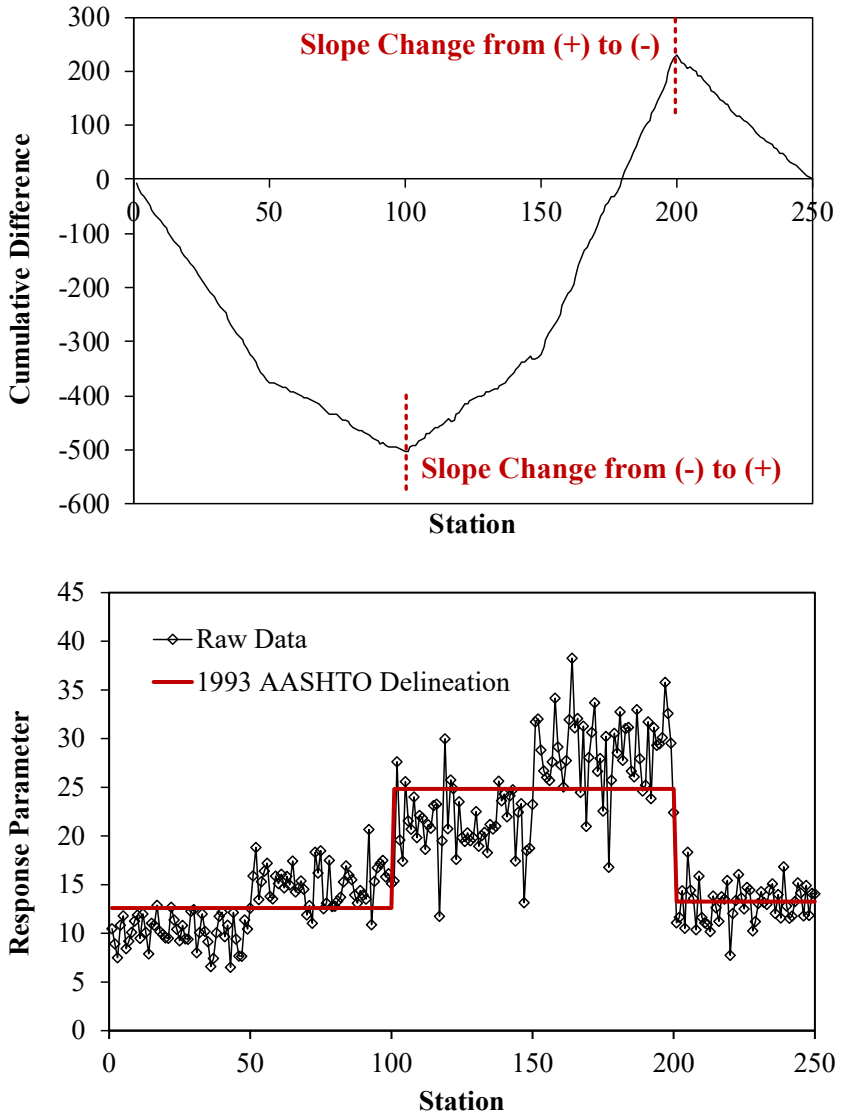

Source: FHWA

Figure 17. Charts. (a) Cumulative difference plot and (b) delineated uniform pavement sections using the original CDA method.

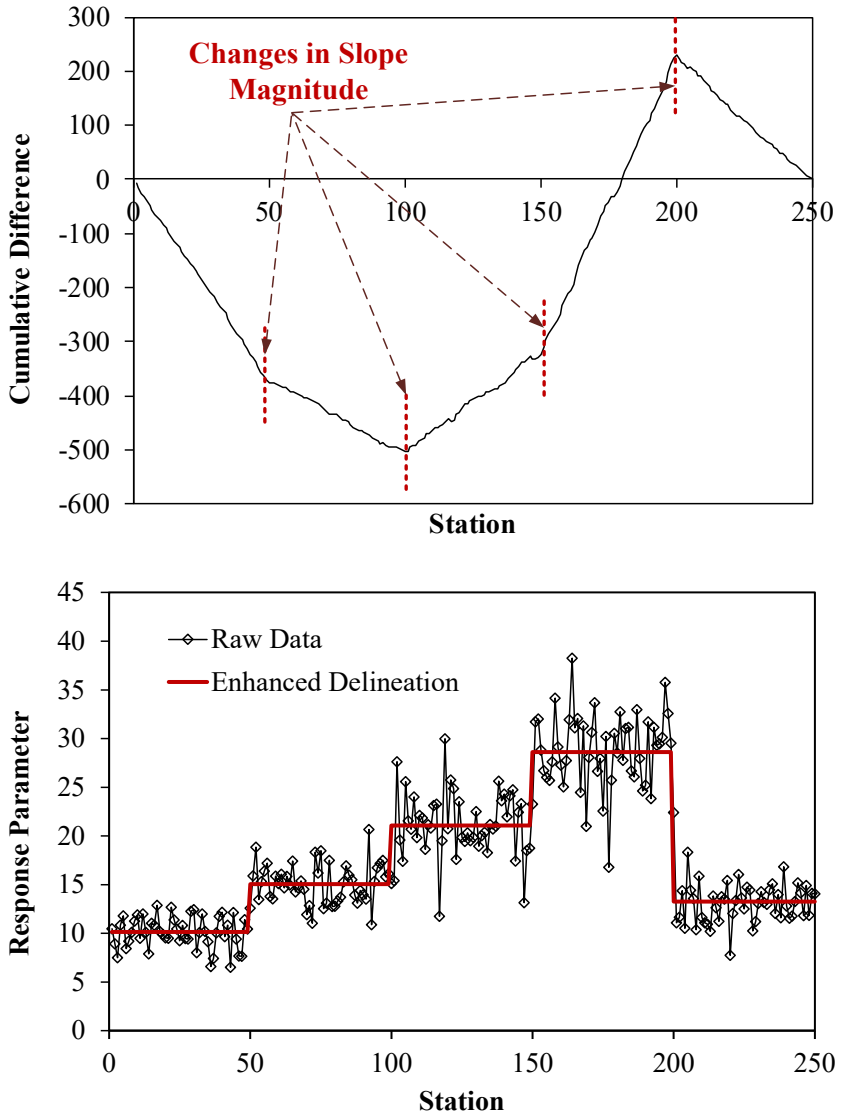

Source: FHWA

Figure 18. Charts. (a) Cumulative difference plot and (b) delineated uniform pavement sections using the Enhanced CDA (ECDA) method.

Examples of faulting calculation using ECDA

To demonstrate the use of ECDA for faulting calculation, a couple of pavement profiles were extracted from LTPP database. The first profile was collected in 2002 from section 04-0215 in Arizona. This section primarily showed upward curling of the slabs but no major spalling at the joints. The other profile was collected in 1999 from section 27-4040 in Minnesota. All the slabs in this section showed downward curling. In addition, approximately 5 to 10 percent of the joints suffered severe joint spalling and few joints showed severe faulting.

Figure 19 through Figure 21 show the raw elevation data from selected joints of section 04-0215 along with the ECDA average elevations. Figure 19 simply shows that +0.02 in. faulting was obtained from the joint located at 8.5 ft.

On the other hand, Figure 20 shows that the ECDA method delineated the joint location as a separate segment, i.e., the joint is wide enough and its elevation is deep enough to be separated from the slab elevations. It is hypothesized that this may be an indication of other joint issues such as spalling and/or wide joint opening. If this joint elevation is excluded from the analysis, no faulting is observed from this joint based on average elevations before and after the joint. Figure 21 shows another situation where the joint may have other issues (spalling or wide opening) with minimal faulting (0.004 in.).

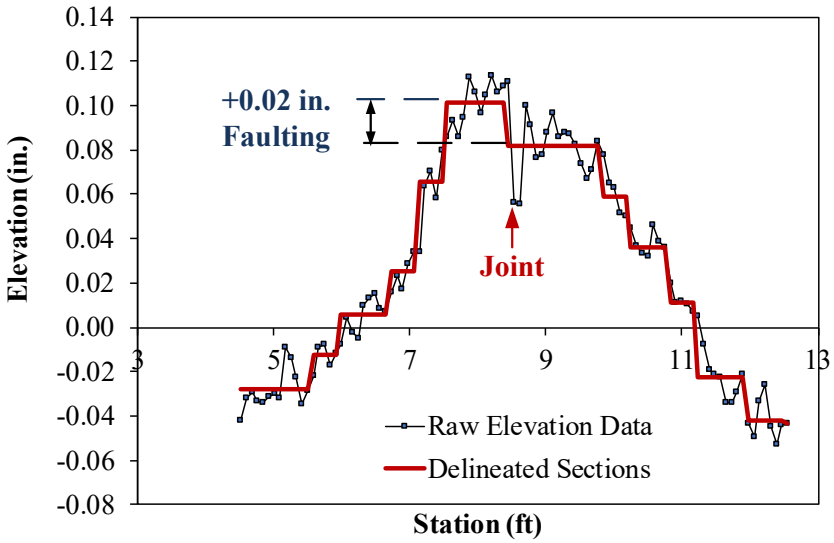

Source: FHWA

Figure 19. Chart. Option 1 Faulting calculation. LTPP Section 04-0215. Joint at Station 8.5 ft.

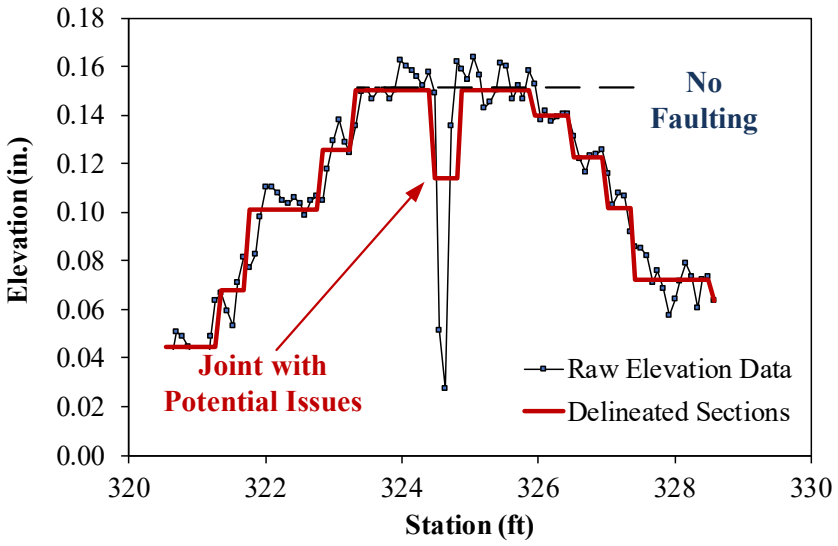

Source: FHWA

Figure 20. Chart. Option 1 Faulting calculation. LTPP Section 04-0215. Joint at Station 324.6 ft.

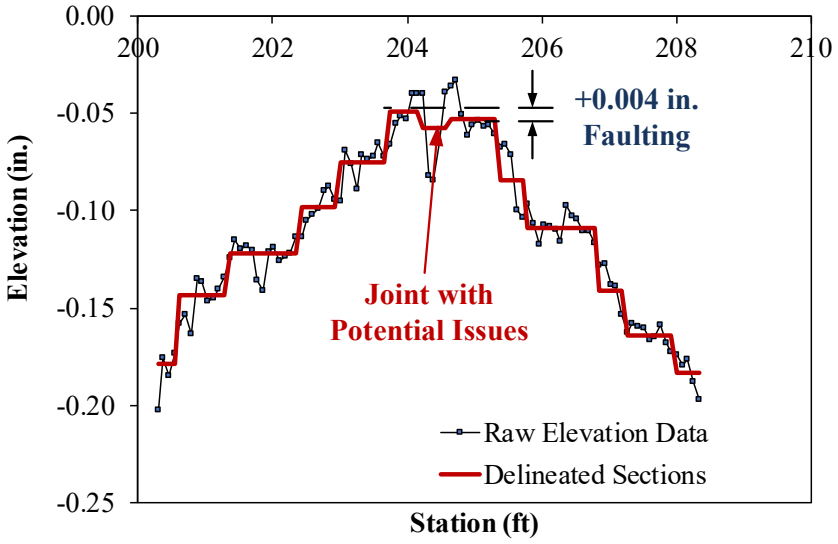

Source: FHWA

Figure 21. Chart. Option 1 Faulting calculation. LTPP Section 04-0215. Joint at Station 204.3 ft.

Figure 22 through Figure 24 show the ECDA faulting calculation from section 27-4040. Figure 22 shows the example where the joint only showed minor faulting and possibly free of other issues. Figure 23 and Figure 24 are examples of relatively higher levels of faulting (> 0.1 in.) with potential joint issues as well.

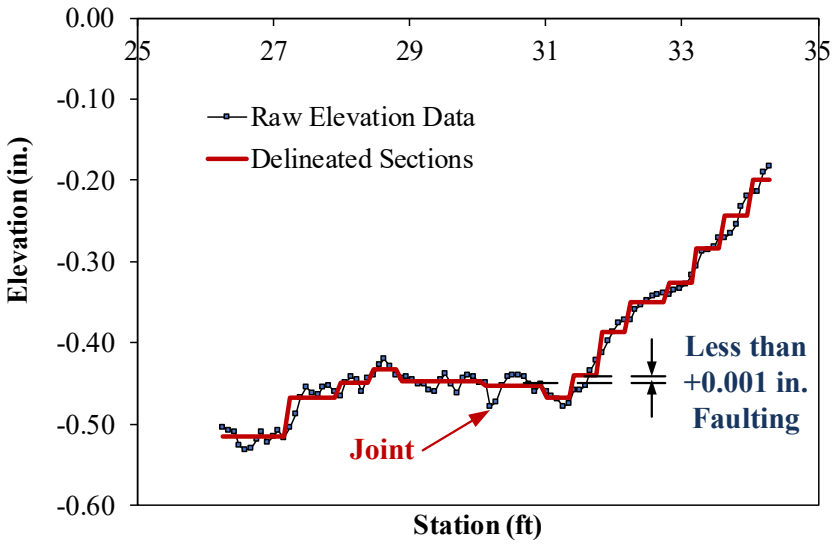

Source: FHWA

Figure 22. Chart. Option 1 Faulting calculation. LTPP Section 27-4040. Joint at Station 30.3 ft.

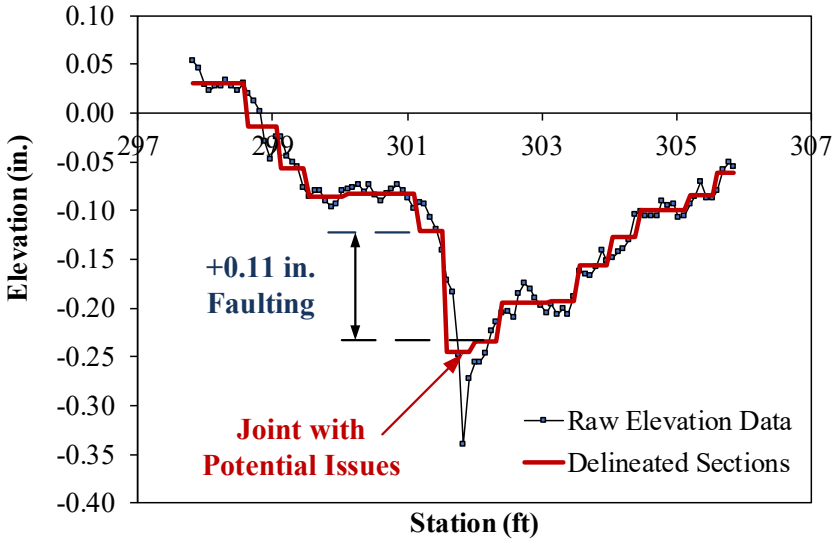

Source: FHWA

Figure 23. Chart. Option 1 Faulting calculation. LTPP Section 27-4040. Joint at Station 301.8 ft.

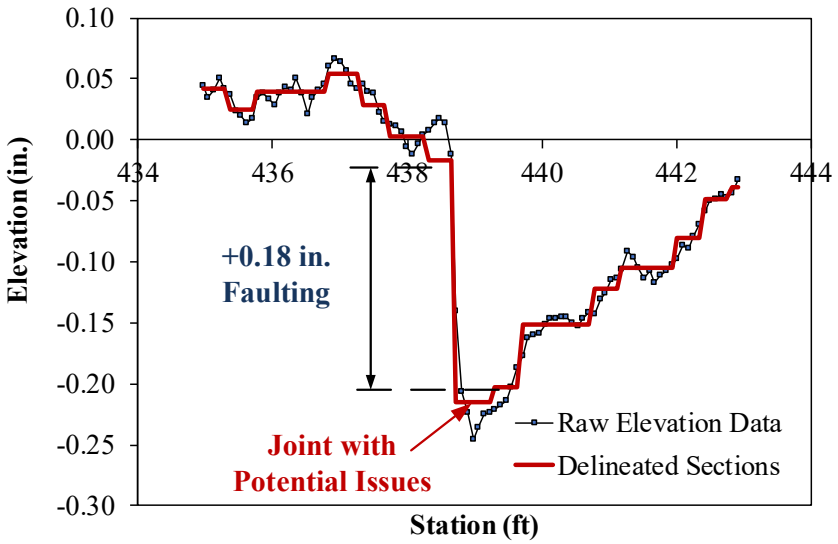

Source: FHWA

Figure 24. Chart. Option 1 Faulting calculation. LTPP Section 27-4040. Joint at Station 439.0 ft.

Note that Option 1 eliminates certain issues with current methods (Figure 4). More specifically, the proposed definition and method eliminates the need to project planes of approach and leave slabs, the need to identify how many points are needed for this projection, and once projected, the need to specify the location or locations (when averaging) to measure the elevation difference between the projected surfaces.

Option 1 also removes any artifacts from curling and warping that arise when using projected planes, which could result in an improper measure of faulting at the joint. Option 1 is a rational statistical-based methodology for optimizing the number of points and distance from a joint without going too far away from the joint where non-faulting-related factors may affect the faulting measurement.

PROPOSED DEFINITION (OPTION 2)

Option 2 is a simplified version of Option 1. Rather than use ECDA from the representative longitudinal profile, the average elevations before and after the joint are calculated using all elevations between the joint and 5 in. from the joint. Since the tire contact length (in the direction of traffic) of 5 in. is typical for a passenger car, the minimum longitudinal distance for calculating the average elevations before and after the joint is 5 in. The vendor or equipment manufacturer will be responsible to demonstrate the ability to remove elevations corresponding to spalls and wide joint openings, which shall be excluded from faulting calculation.

Note that it still eliminates certain issues with current methods (Figure 4). For example, this proposed Option 2 definition and method eliminates the need to project planes of approach and leave slabs, the need to identify how many points are needed for this projection, and once projected, the need to specify the location or locations (when averaging) to measure the elevation difference between the projected surfaces. It also removes any artifacts from curling and warping

that arise when using projected planes, which could result in an improper measure of faulting at the joint. However, it may reduce the number of elevation points available for faulting measurement, thus reducing accuracy of faulting measurements at some joints.

Figure 25 through Figure 30 show examples of Option 2 faulting calculation for the same LTPP joints previously shown in Figure 19 to Figure 24.

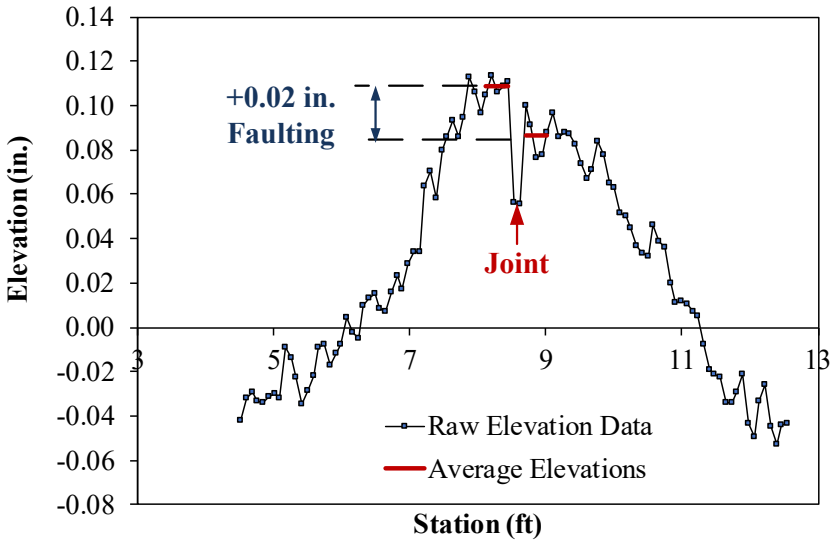

Source: FHWA

Figure 25. Chart. Option 2 Faulting calculation. LTPP Section 04-0215. Joint at Station 8.5 ft.

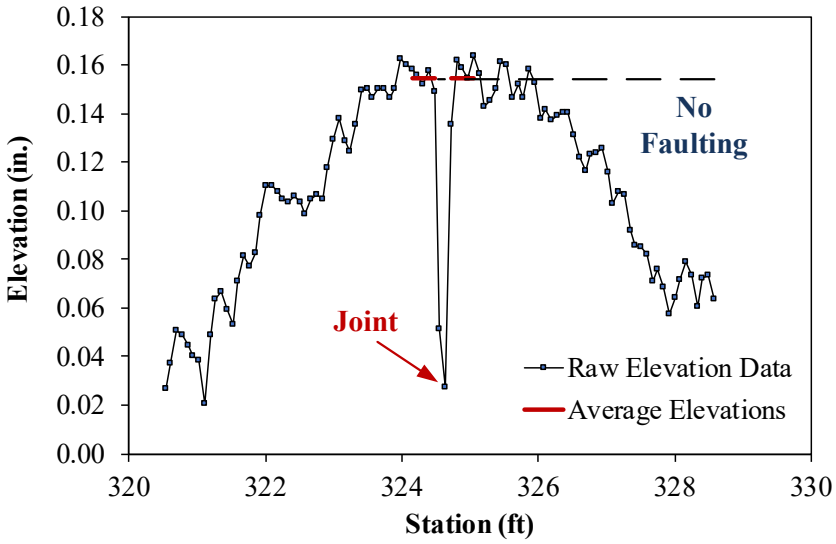

Source: FHWA

Figure 26. Chart. Option 2 Faulting calculation. LTPP Section 04-0215. Joint at Station 324.6 ft.

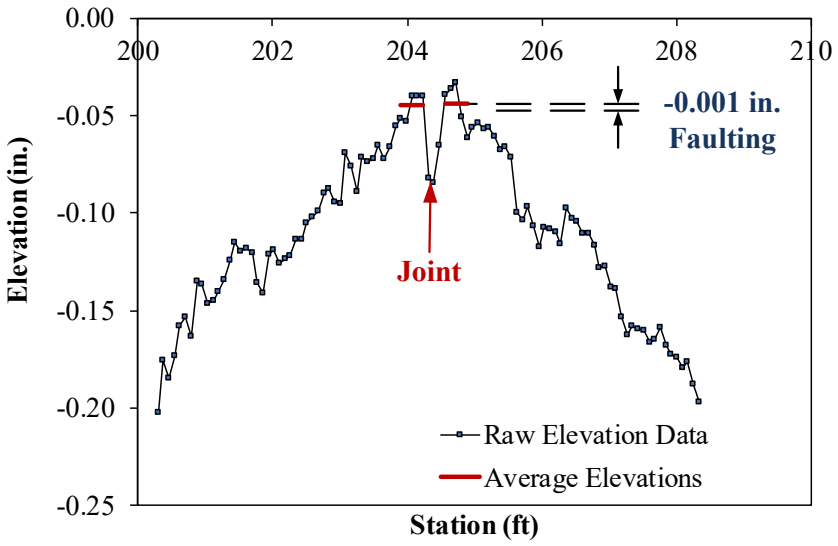

Source: FHWA

Figure 27. Chart. Option 2 Faulting calculation. LTPP Section 04-0215. Joint at Station 204.3 ft.

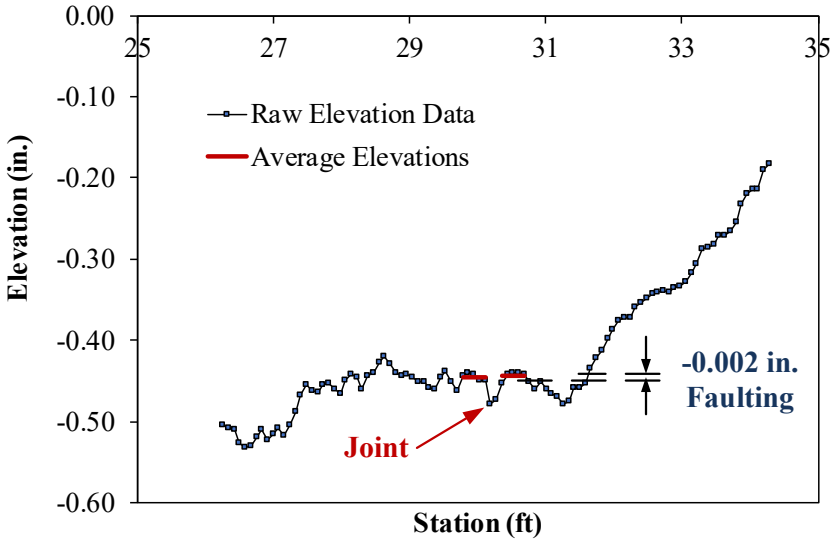

Source: FHWA

Figure 28. Chart. Option 2 Faulting calculation. LTPP Section 27-4040. Joint at Station 30.3 ft.

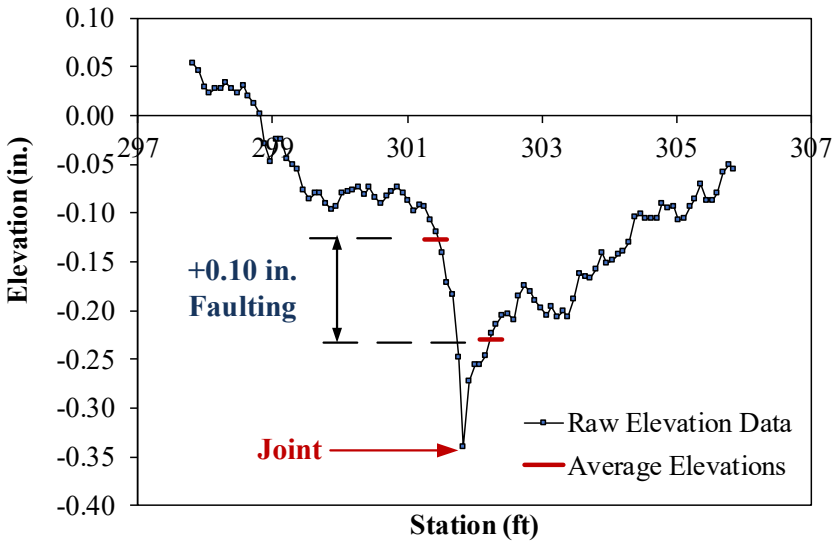

Source: FHWA

Figure 29. Chart. Option 2 Faulting calculation. LTPP Section 27-4040. Joint at Station 301.8 ft.

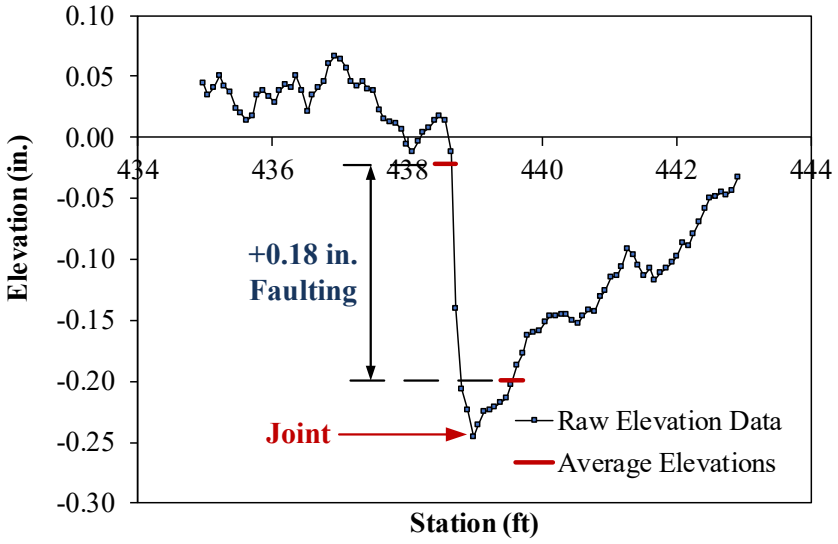

Source: FHWA

Figure 30. Chart. Option 2 Faulting calculation. LTPP Section 27-4040. Joint at Station 439.0 ft.

PROPOSED DEFINITION (OPTION 3)

For this option, faulting is defined as the difference in elevations of projected/existing planes of approach slab and departure slab surfaces across a transverse joint or crack along the outside wheelpath. The representative longitudinal profile shall be used for this projection. Faulting shall be measured as the difference (or the mean value of the differences) between the above mentioned, projected planes. Conceptual examples of this concept with faulting calculation from

the projected planes, between 0 in. to 9 in. offset from the center of a joint/crack in the traffic direction, are shown in Figure 31 to Figure 35.

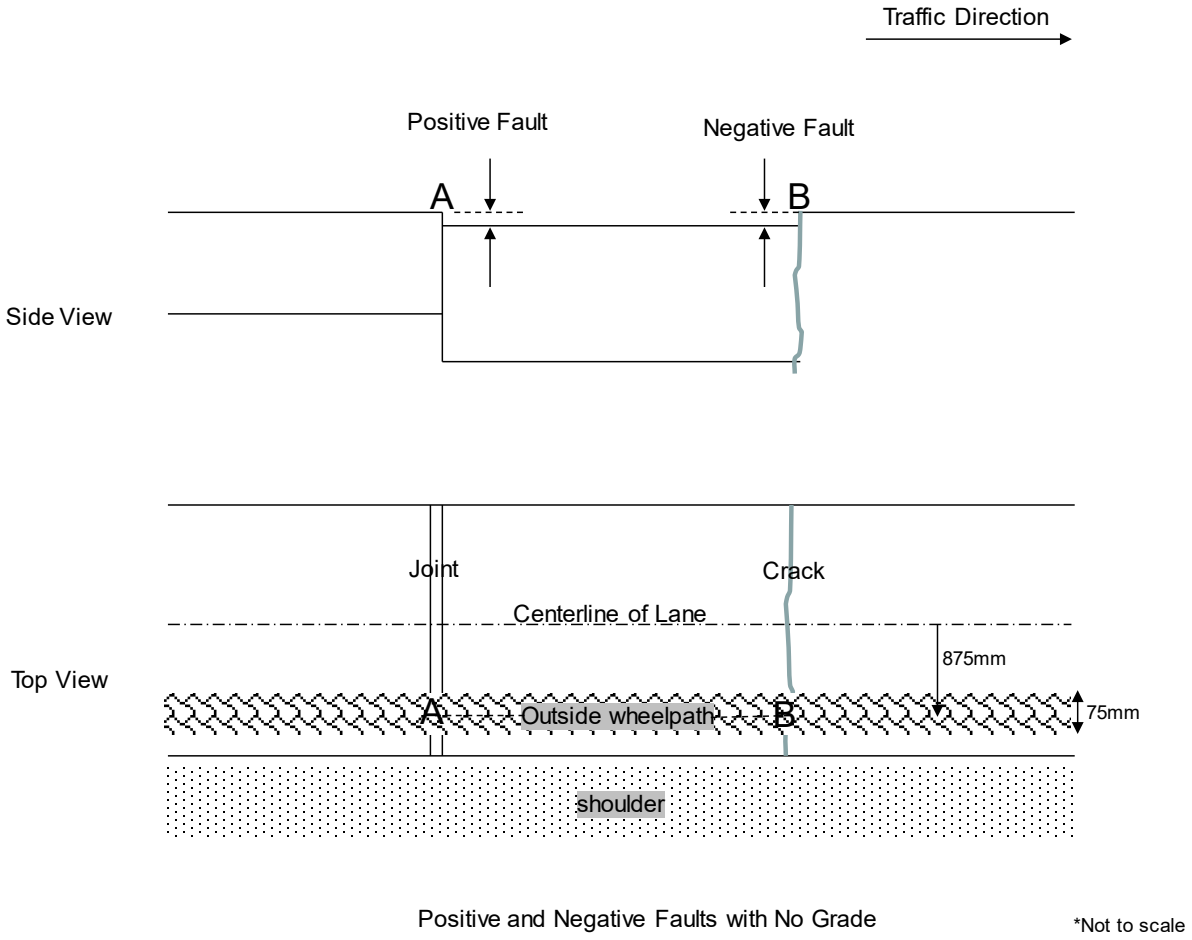

Source: FHWA

Figure 31. Illustration. Positive and negative faults with no grade.

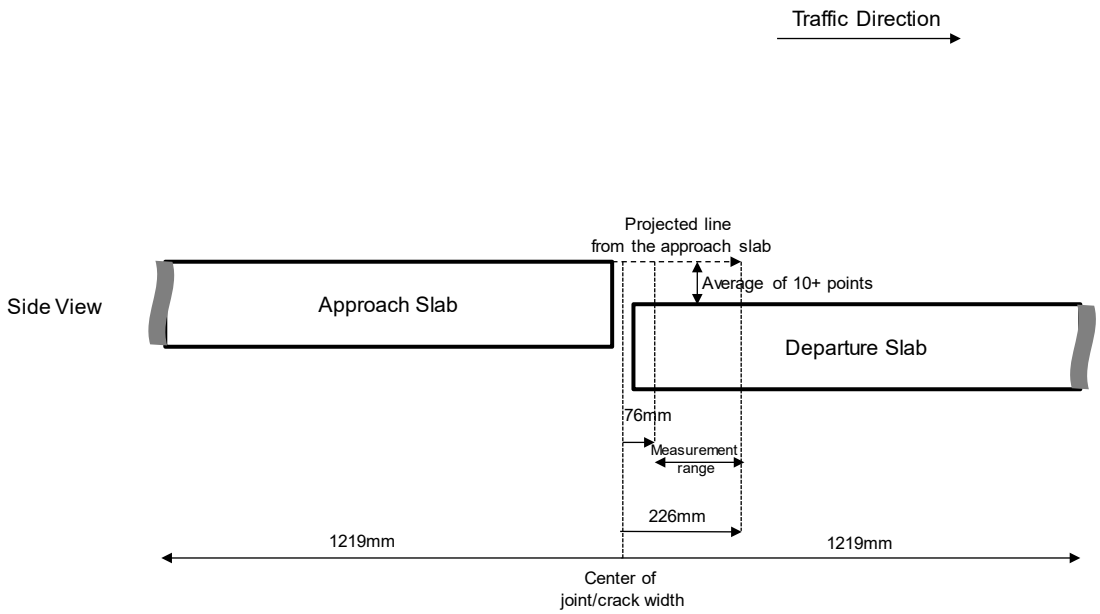

Source: FHWA

Figure 32. Illustration. Measurement of positive fault with no grade.

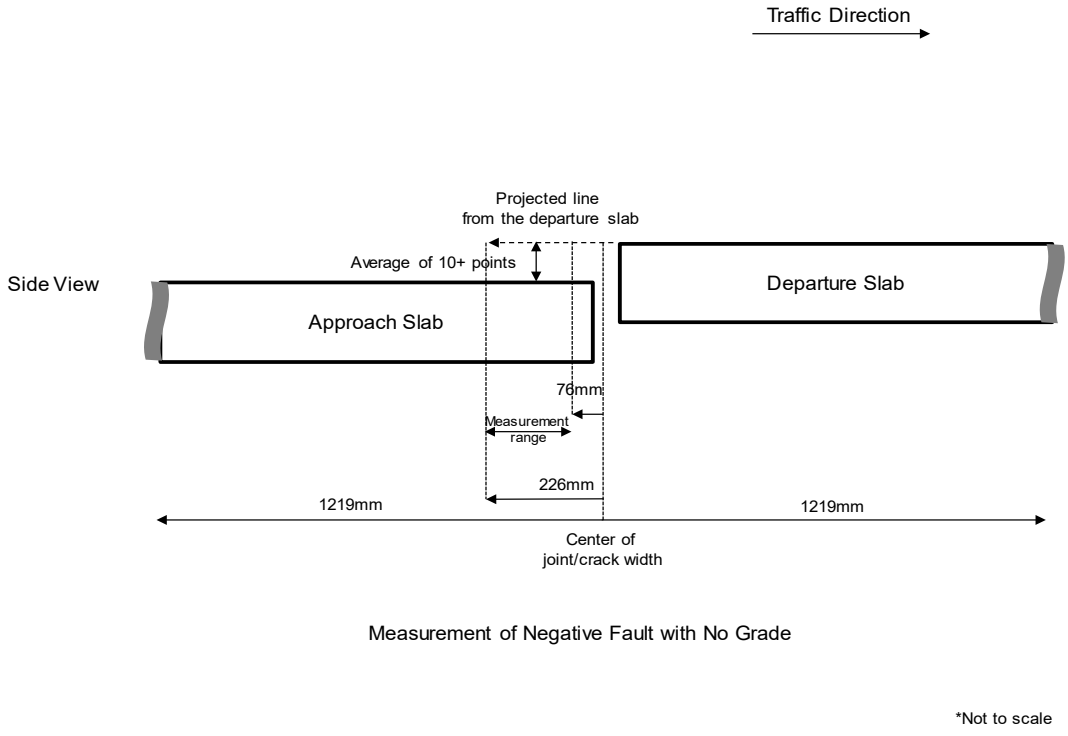

Source: FHWA

Figure 33. Illustration. Measurement of negative fault with no grade.

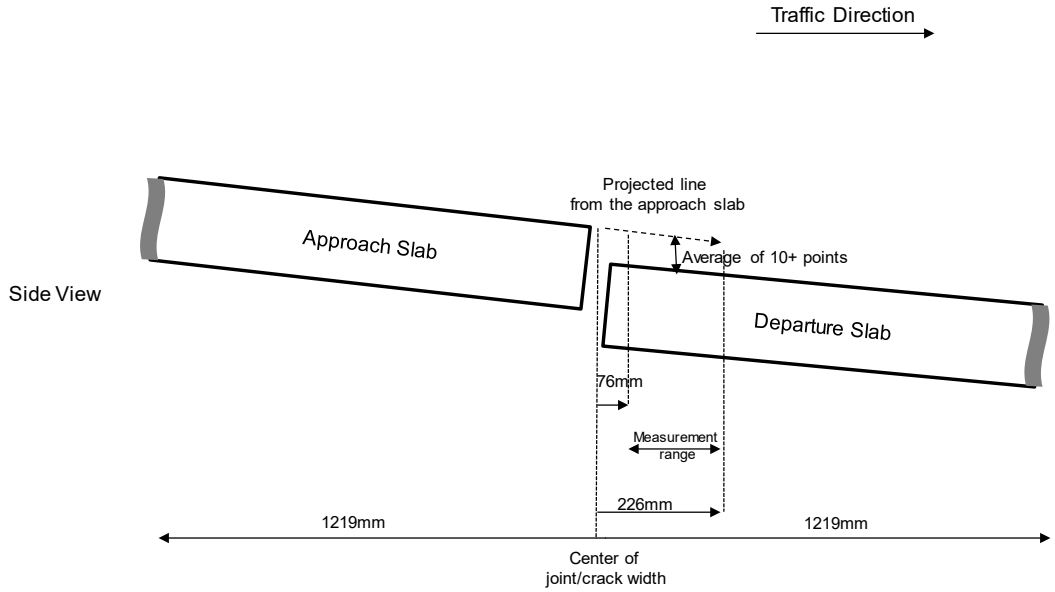

Measurement of Positive Fault with Down Grade

*Not to scale

Source: FHWA

Figure 34. Illustration. Measurement of positive fault with down grade.

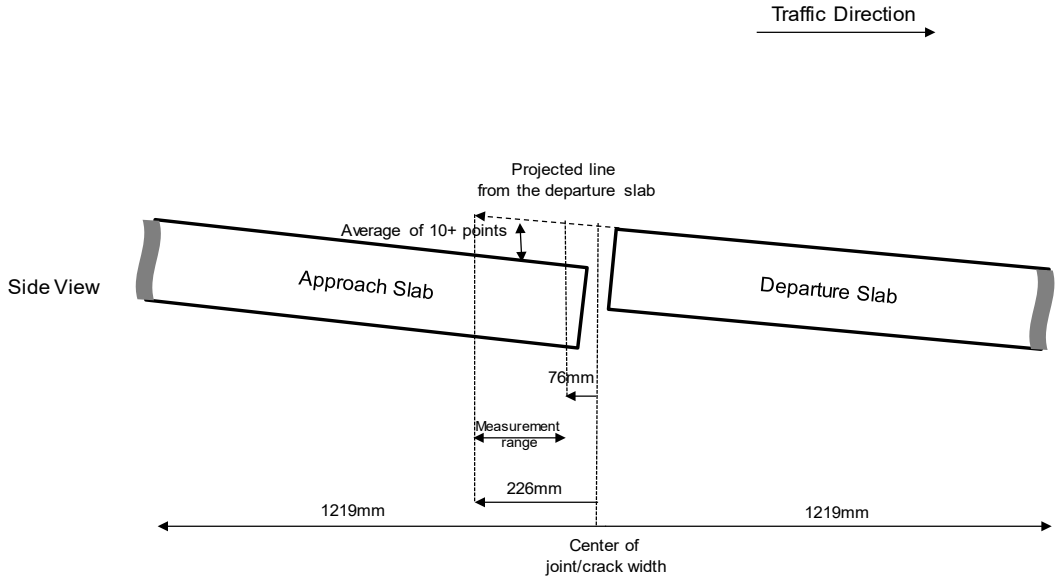

Measurement of Negative Fault with Down Grade

*Not to scale

Source: FHWA

Figure 35. Illustration. Measurement of negative fault with down grade.

Note that there are some issues with this option as we will need to identify how many points are needed to consider this projection a good measure of faulting (the distress) at the joint, and once projected, specify the location or locations (when averaging) to measure the elevation difference between the projected surfaces (which are virtual and not real data points). Also, when there is curling and warping, the projected lines may actually compute a non-zero faulting (the measurement) value (the difference in elevation between the projected surfaces) even when there is zero difference in elevation across the joint, thus measuring an artifact of curling/warping rather than faulting (the distress) at the joint (Figure 36).

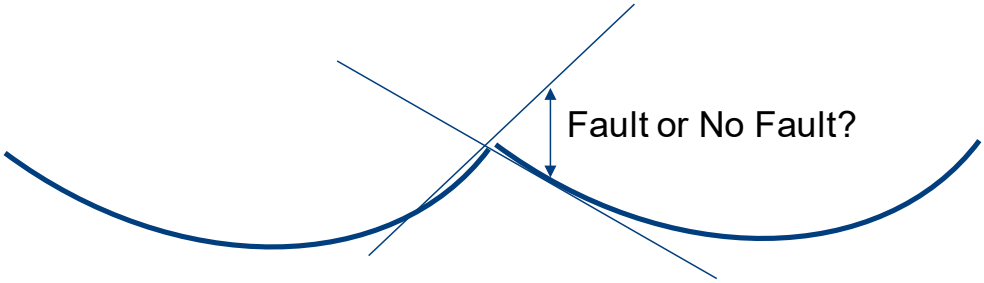

Source: FHWA

Figure 36. Artifact of curling and warping on fault measurement when using extrapolation.

As a preliminary examination of the above issues, Figure 37 through Figure 42 show examples of Option 3 faulting calculation using the planes projected from the points within ±1.0 ft. from the joint. Figure 43 through Figure 48 show examples of Option 3 calculation using the planes produced from points within ±2.0 ft. from the joint. Faulting was calculated as the difference in elevation of these projected lines at the joint location.

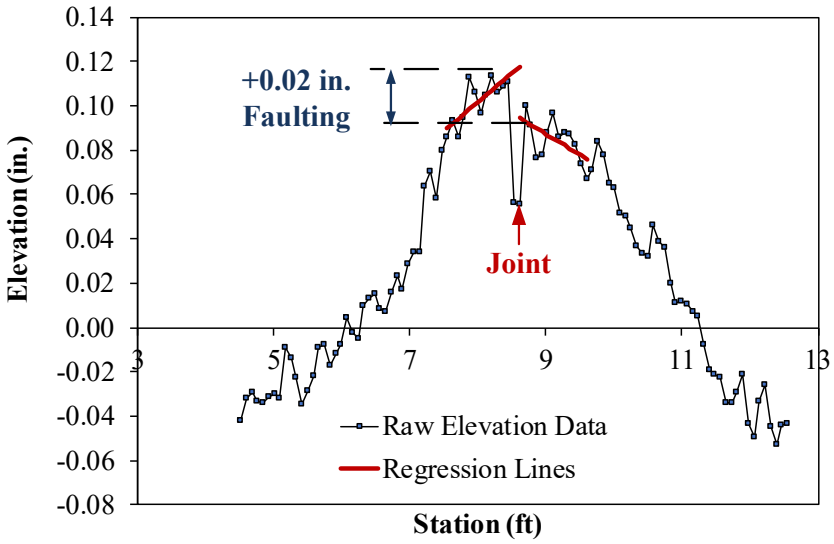

Source: FHWA

Figure 37. Chart. Option 3 faulting calculation. Planes projected using points ±1.0 ft. from joint. LTPP Section 04-0215. Joint at Station 8.5 ft.

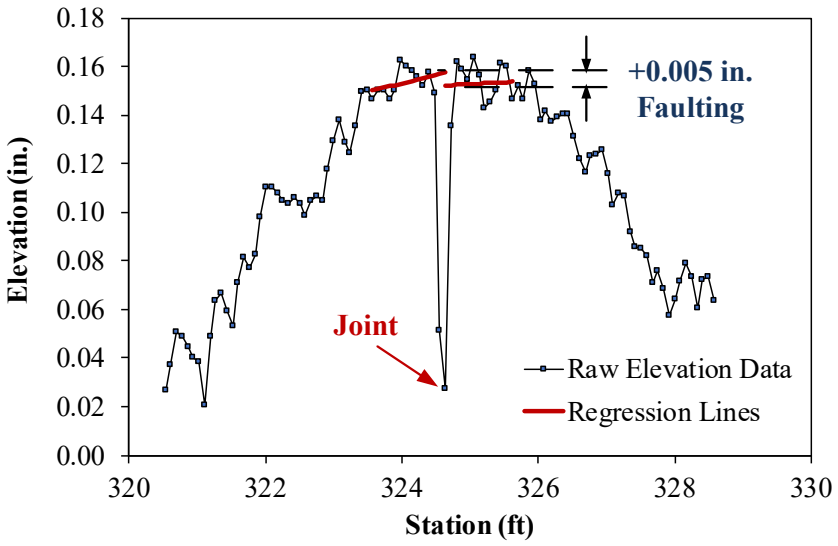

Source: FHWA

Figure 38. Chart. Option 3 faulting calculation. Planes projected using points ±1.0 ft. from joint. LTPP Section 04-0215. Joint at Station 324.6 ft.

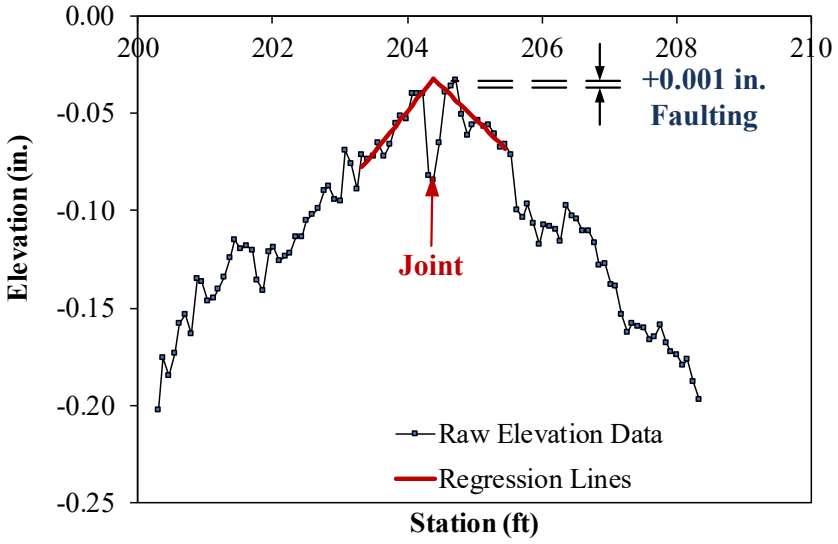

Source: FHWA

Figure 39. Chart. Option 3 faulting calculation. Planes projected using points ±1.0 ft. from joint. LTPP Section 04-0215. Joint at Station 204.3 ft.

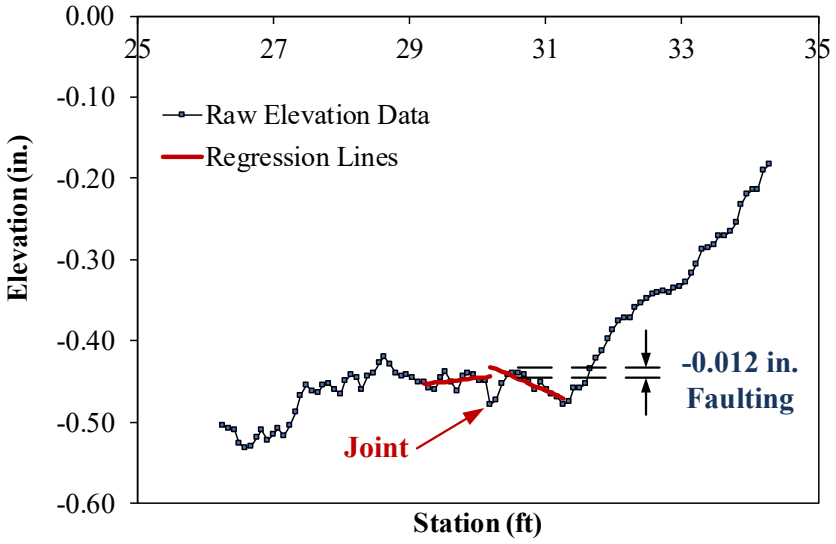

Source: FHWA

Figure 40. Chart. Option 3 faulting calculation. Planes projected using points ±1.0 ft. from joint. LTPP Section 27-4040. Joint at Station 30.3 ft.

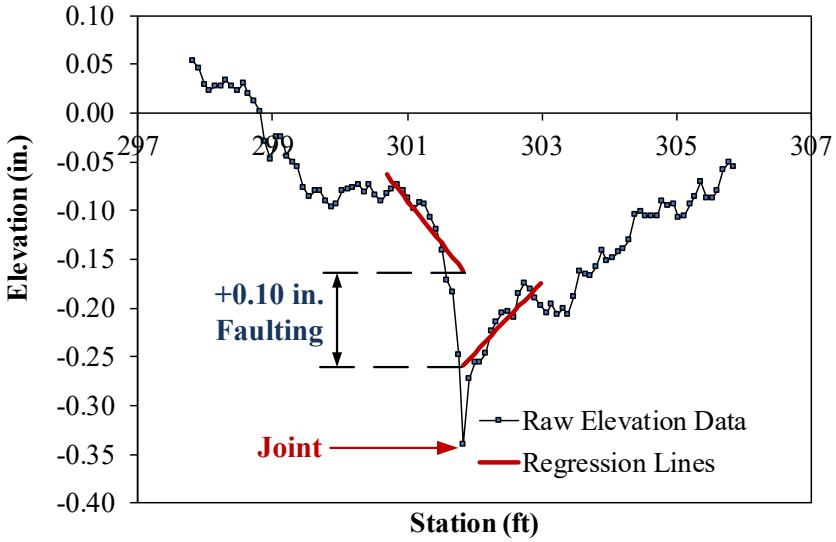

Source: FHWA

Figure 41. Chart. Option 3 faulting calculation. Planes projected using points ±1.0 ft. from joint. LTPP Section 27-4040. Joint at Station 301.8 ft.

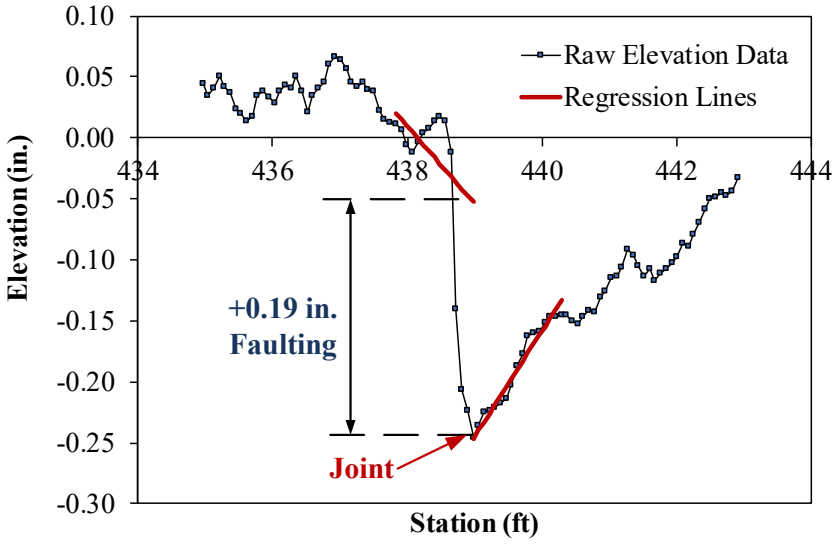

Source: FHWA

Figure 42. Chart. Option 3 faulting calculation. Planes projected using points ±1.0 ft. from joint. LTPP Section 27-4040. Joint at Station 439.0 ft.

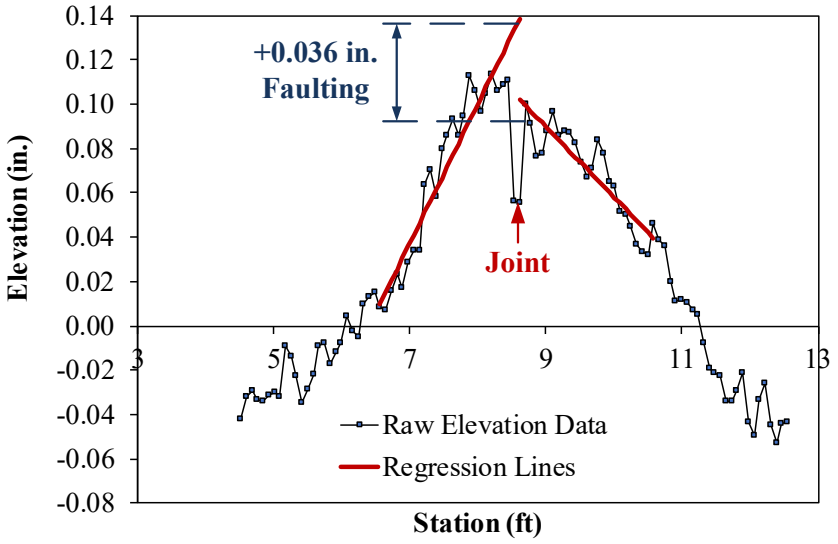

Source: FHWA

Figure 43. Chart. Option 3 faulting calculation. Planes projected using points ±2.0 ft. from joint. LTPP Section 04-0215. Joint at Station 8.5 ft.

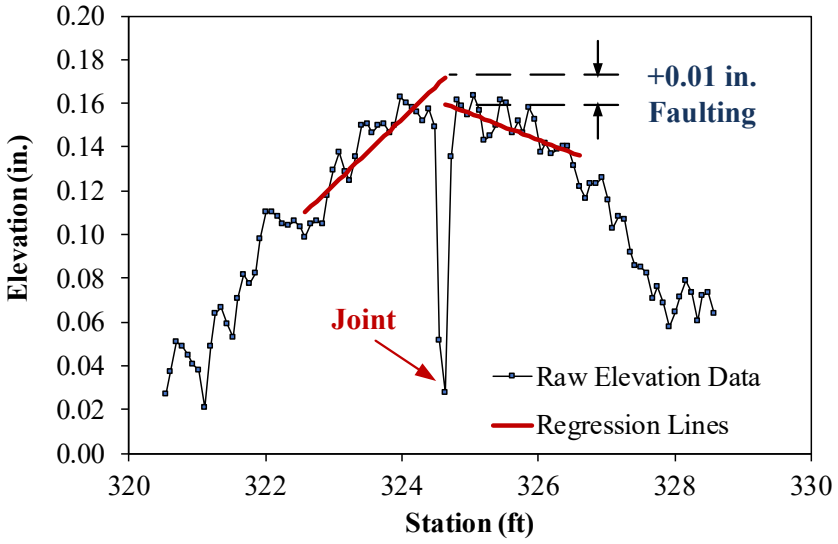

Source: FHWA

Figure 44. Chart. Option 3 faulting calculation. Planes projected using points ±2.0 ft. from joint. LTPP Section 04-0215. Joint at Station 324.6 ft.

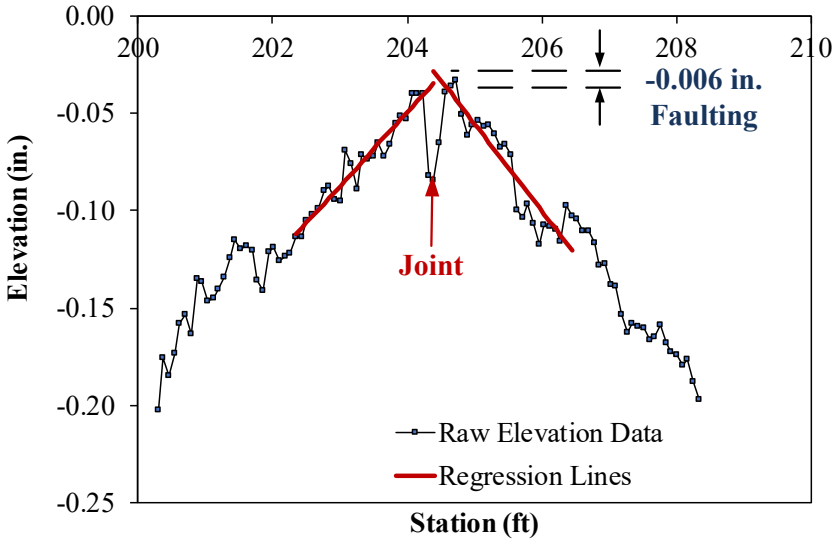

Source: FHWA

Figure 45. Chart. Option 3 faulting calculation. Planes projected using points ±2.0 ft. from joint. LTPP Section 04-0215. Joint at Station 204.3 ft.

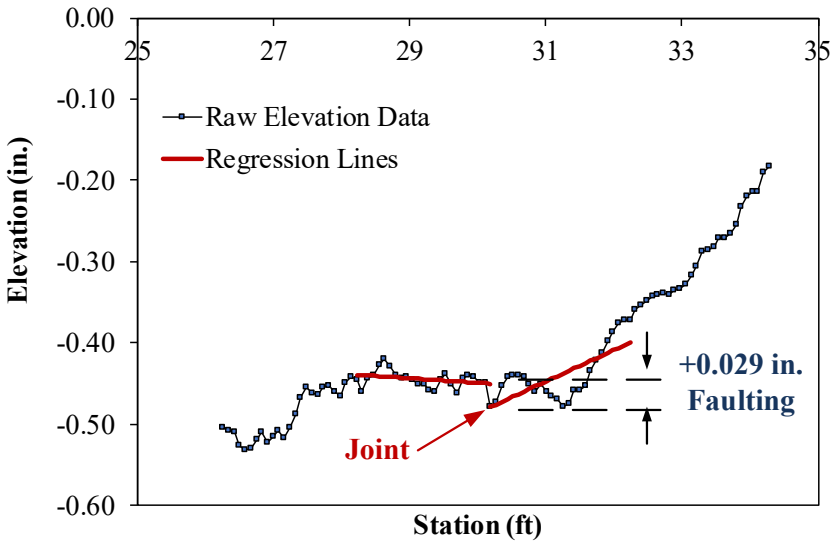

Source: FHWA

Figure 46. Chart. Option 3 faulting calculation. Planes projected using points ±2.0 ft. from joint. LTPP Section 27-4040. Joint at Station 30.3 ft.

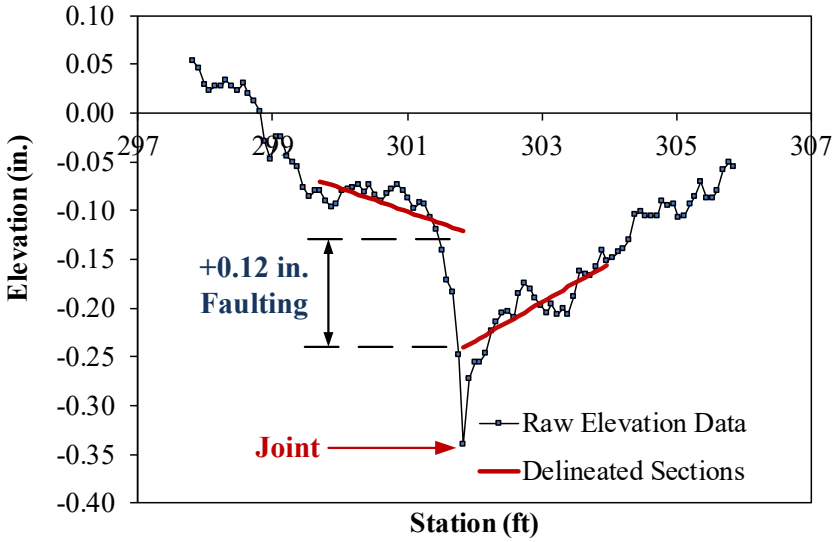

Source: FHWA

Figure 47. Chart. Option 3 faulting calculation. Planes projected using points ±2.0 ft. from joint. LTPP Section 27-4040. Joint at Station 301.8 ft.

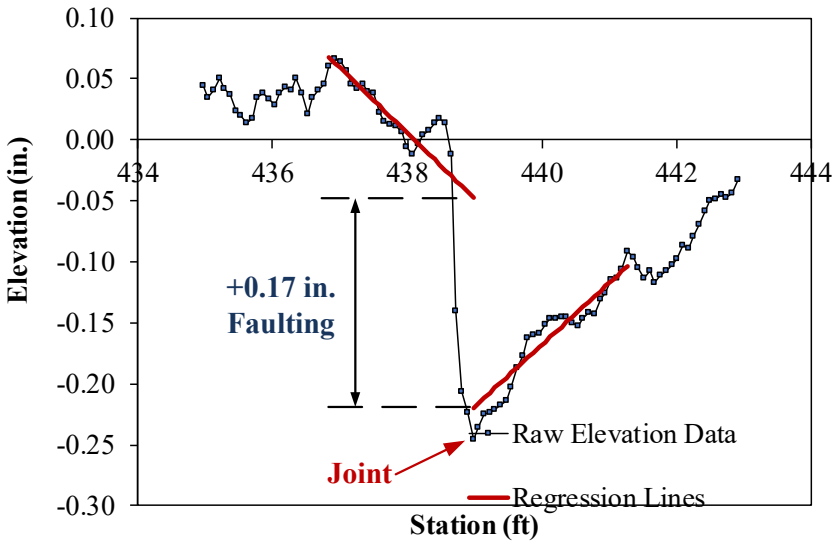

Source: FHWA

Figure 48. Chart. Option 3 faulting calculation. Planes projected using points ±2.0 ft. from joint. LTPP Section 27-4040. Joint at Station 439.0 ft.

COMPARISON OF RESULTS FROM DIFFERENT OPTIONS

Table 4 summarizes the fault values calculated from all Options discussed above, for the LTPP joints shown previously. While the fault values from Options 1 and 2, and Option 3 with ±1.0 ft. projection are reasonably comparable, results from Option 3 with ±2.0 ft. projection are significantly different from the other results. As seen from Figure 43 through Figure 48, this is clearly due to the projection lines being influenced more by slab elevations and/or curvatures that are not related to faulting.

In addition, Option 3 with ±2.0 ft. projection was further evaluated by calculating the elevation difference between the extrapolated lines at 6.0 in. away from the joint (i.e., in the leave slab, 6.0 in. from joint). This methodology is clearly affected by the artificial projection that may be amplified by extrapolation (see Figure 36).

Table 4. Faulting calculations from different options.

LTPP Section	Joint Location (ft)	Option 1	Option 2	Option 3 (±1.0 ft Projection)	Option 3 (±2.0 ft Projection)	Option 3 (±2.0 ft Projection, 6 in. Offset)
04-0215	8.5	0.020	0.020	0.020	0.036	0.083
04-0215	324.6	0.000	0.000	0.005	0.010	0.033
04-0215	204.3	0.004	-0.001	0.001	-0.006	0.034
27-4040	30.3	< 0.001	-0.002	-0.012	0.029	0.007
27-4040	301.8	0.110	0.100	0.100	0.120	0.088
27-4040	439	0.180	0.180	0.190	0.170	0.122

SUMMARY

All three options discussed herein for defining and measuring faulting were developed during Phase I of this study and were planned to be investigated further to arrive at a final recommendation. A key factor for evaluation is the impact of concrete pavement surface texture on computing the Representative Longitudinal Profile, its impacts on each of the three faulting definition Options, and specifically on the ECDA computations (Option 1).

The methodology for projecting planes based on AFM data will be based on that included in AASHTO R 36 (Option 3). The distance in the current faulting standard AASHTO R36 Method A—3 to 9 inches from the joint—likely arises from having to reconcile AFM faulting measurement with faulting measurement using handheld devices such as the GFM. However, with all three proposed definition options, it is recommended that the handheld devices not be considered further. As such, with Option 3, projected lines can be used down to a distance as small as zero inches from the joint, which is expected to eliminate the curling and warping artifact described above.

It is recommended that the wheelpath be specified relative to the lane longitudinal centerline because of differences in lane widths, widening, striping locations, etc., from one location to another. The centerline will need to be established from a measurable reference such as lane markings or longitudinal joints. 3D equipment can easily use the lane markings or longitudinal joints, but 2D HSIPs may need to be retrofitted with a device to detect lane markings or longitudinal joints.

AUTOMATED FAULTING DATA COLLECTION EQUIPMENT CERTIFICATION

With the development of high-speed AFM equipment (2D and 3D) for faulting, the manual fault meters are quickly becoming outdated for efficiency and safety purposes. Furthermore, the manual fault meters are not capable of producing the representative longitudinal profile, which is required for calculation of faulting based on the new definitions (Options 1, 2, and 3) and procedures presented earlier. Therefore, manual fault meters are inadequate for the proposed methodology and will not be considered further in this report.

Since the representative longitudinal profile is the key component of the new faulting definitions developed herein, all devices for faulting assessment (production equipment as well as those for reference measurements) must be capable of producing the representative profile which, in turn, can be used for calculating faulting in an automated fashion (e.g., ECDA for Option 1). The production devices include, but are not limited to, 2D HSIPs used for IRI measurements and 3D technologies used for Transverse Pavement Profile (TPP) measurements and crack detection. The goal of faulting certification is to ensure that the results obtained from the available 2D/3D devices (as well as those that may become available in the future) are not influenced or biased due to the inherent technological differences in representative longitudinal profile measurement. In other words, any device certified for faulting should be able to produce consistent and comparable faulting results.

Figure 49 conceptually outlines the certification procedure for faulting. Similar to the certification process developed under TPF-5(299) for TPP, the fundamental concept behind the faulting certification is to ensure that the production devices can produce the required data for reasonable and realistic faulting results (within the specified accuracy level) when compared to those from a more advanced (i.e., higher accuracy and precision) reference measurement.

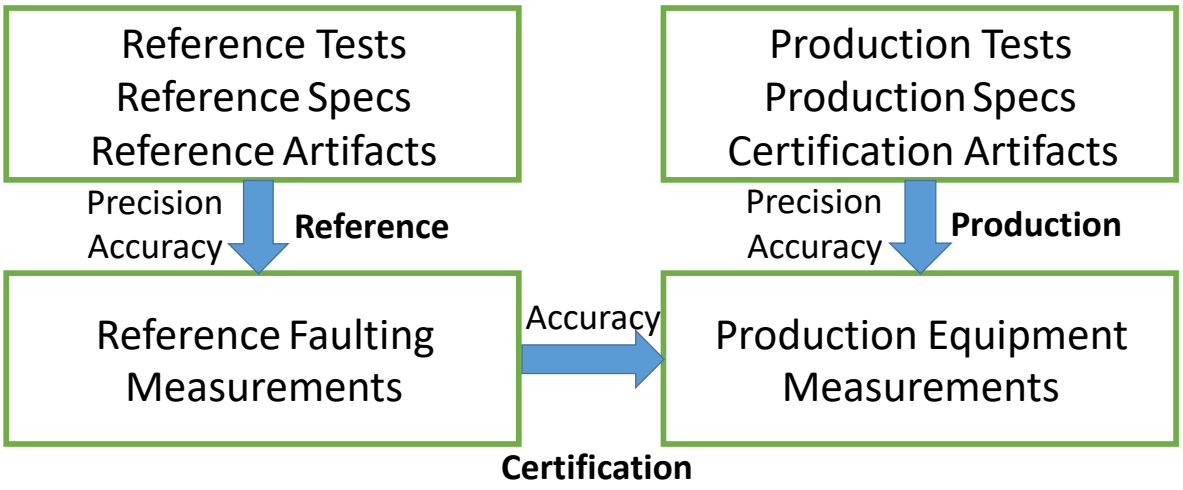

Source: FHWA

Figure 49. Diagram. Process of faulting certification.

RELEVANT STANDARDS

Since the 2D and 3D technologies available for faulting are also being used for other purposes such as IRI and transverse profiles, a number of relevant standards and certification procedures are already available or currently being developed for these technologies. As such, the proposed faulting certification procedure was developed such that these existing (or currently being developed) standards were used to the greatest extent possible.

For 2D HSIP equipment, the relevant standards include the following:

- AASHTO M 328, Standard Specification for Inertial Profiler.
- AASHTO R 56, Standard Practice for Certification of Inertial Profiling Systems.
- AASHTO R 57. Standard Practice for Operating Inertial Profiling Systems.

The above standards have been established nearly a decade ago and are widely adopted by SHAs for pavement roughness evaluation. As such, the 2D HSIPs must meet the requirements of AASHTO M 328 and AASHTO R 57, and certified in accordance with AASHTO R 56, prior to being used for faulting assessment. The additional, faulting-specific requirements for 2D HSIPs will be discussed in a subsequent section of the report.

Under TPF-5(299) for TPP measurements, 5 standards (AASHTO PP 106, PP 107, PP 108, PP 109, PP110) were developed for 3D systems. Although these standards are not developed specifically for AFM purposes, the generic requirements specified for the equipment are applicable to faulting measurements for 3D systems and may also be applicable and will be evaluated for 2D systems. As such, these standards will be discussed in the following.

AASHTO PP 107-21: Standard Practice for Assessment of Body Motion Cancelation in Transverse Pavement Profiling Systems.

This standard is proposed to assess the TPP measurement error due to the vehicle body motion. The extent of a typical vehicle body motion is greater than typical range of faulting by orders of magnitude. As such, the faulting equipment should not present any bias resulting from the vehicle motion. It is proposed that the certification procedure in the above standard also be adopted for faulting, with the requirement statement shown in Table 5.

The numbers in Table 5 were determined based on the low severity threshold for faulting to be between 0.1 in. and 0.2 in. for most SHAs, and requiring a standard error of less than 0.03 in. for the vehicle body motion.

Table 5. Body motion requirement statements for faulting.

Output Test Statistic	Accuracy and Precision Defined as Bias and Confidence Interval, inch				
	Lower Bounds (%-tiles)		Bias	Upper Bounds (%-tiles)	
	90% (5%)	50% (25%)		50% (75%)	90% (95%)
Vehicle Body Motion Error	-0.05	-0.02	0	0.02	0.05

AASHTO PP 108-21: Standard Practice for Assessment of Drift Mitigation in Transverse Pavement Profiling Systems.

This standard is proposed to assess the amount of drift error present in localization systems used with TPPs. For the purpose of faulting, the location sensors become the primary source of information for joint location. Since the typical JCP joint spacing (e.g., 15 ft.) is much larger than the spacing between TPP measurements, any device meeting the TPP requirements are deemed appropriate for faulting. As such, it is proposed that the certification procedure and the requirements in the above standard be directly adopted for faulting. Note that any drift error is expected to impact all longitudinal measurements equally, and not relative to each other; and since faulting measurement is computed relative to the joint, the impact of drift error on joint faulting computation is expected to be negligible, and the only impact is expected to be in terms of identifying the joint location.

AASHTO PP 106-21: Standard Practice for Assessment of Static Performance in Transverse Pavement Profiling Systems.

This standard is proposed to assess the accuracy and precision of TPPs under static operating conditions. These sensor characteristics are also important for faulting and need to be certified. Therefore, it is proposed that the certification procedure in the above standard also be adopted for faulting, with the requirement statement shown in Table 6.

Note that AASHTO M 328 requires that the 2D HSIPs have a vertical resolution of 0.002 in. and AASHTO R57 requires that the 2D HSIPs have an absolute error of less than 0.01 in. from the block test. Therefore, the 2D HSIPs are under a more stringent requirement than shown in Table 6.

Table 6. Static sensor system requirement statements for faulting.

Output Test Statistic	Accuracy and Precision Defined as Bias and Confidence Intervals, inch				
	Lower Bounds (%-tiles)		Bias	Upper Bounds (%-tiles)	
	90% (5%)	50% (25%)		50% (75%)	90% (95%)
Transverse Measurement Resolution	N/A	N/A	N/A	N/A	0.75
Transverse Measurement Accuracy and Precision	-0.6	-0.5	N/A	0.5	0.6
Straightness Error	0.10	-0.06	N/A	0.06	0.10
Vertical Measurement Resolution	N/A	N/A	N/A	N/A	0.004
Vertical Measurement Accuracy and Precision	-0.06	-0.04	N/A	0.04	0.06

AASHTO PP 109-21: Standard Practice for Assessment of Dynamic Performance in Transverse Pavement Profiling Systems.

This standard is proposed to assess the accuracy and precision of TPPs and to evaluate the resulting rut depth, cross-slope, and edge/curb drop off values under typical dynamic operating conditions. The accuracy and precision requirements are applicable to faulting, and Table 7 shows the relevant requirement statements. However, the requirements for rut depth, cross-slope,

and edge/curb in this standard are not adopted for faulting. Instead, it is proposed that the faulting-specific tests to be described in subsequent sections of this report, be used.

Note that AASHTO M 328 requires that the 2D HSIPs have a minimum longitudinal measurement spacing of 2.0 in. Therefore, requirement in Table 7 is more stringent and applies to 2D HSIPs as well.

Current AASHTO R 36 specifies that the longitudinal sampling shall be less than 0.75 in. for project level surveys and less than 1.5 in. for network level surveys. The new sampling interval requirement for AFM (both longitudinal and transverse), as indicated in Table 7, is 0.75 in. or less, regardless of the survey (project vs network level) and type of high-speed equipment (2D vs. 3D). The basis for such a more stringent requirement is provided below:

- Faulting is a highly localized feature, which needs to be calculated based on sufficient amount of data points before and after the joint, regardless of the type of survey (project vs. network level).
- Since the typical width of a joint saw-cut is between 0.75 in. and 1.00 in. (for saw cuts with a sealant reservoir), the above longitudinal spacing allows for at least one representative profile measurement within the joint.
- The longitudinal spacing of 0.75 in. allows for collecting at least 6 measurements on each side of the joint along the representative longitudinal profile within the specified 5 in minimum longitudinal distance for calculating the average elevations included in the Option 1 and Option 2 definitions. Six (6) measurements are deemed minimally sufficient to establish average elevations before and after the joint.
- The minimum transverse spacing of 0.75 in. allows for obtaining at least 40 transverse elevation points within the 30 in. wheelpath at a given longitudinal location (or 10 points within a typical tire width of 8 in.). This is sufficient to provide a statistical mean, which essentially becomes a single point in the representative longitudinal profile.

Table 7. Dynamic sensor system requirement statements for faulting.

Output Test Statistic	Accuracy and Precision Defined as Bias and Confidence Intervals, inch				
	Lower Bounds (%-tiles)		Bias	Upper Bounds (%-tiles)	
	90% (5%)	50% (25%)		50% (75%)	90% (95%)
Transverse Measurement Resolution	N/A	N/A	N/A	N/A	0.75
Vertical Measurement Resolution	N/A	N/A	N/A	N/A	0.004
Longitudinal Measurement Spacing*	N/A	N/A	N/A	N/A	0.75
TPP Data Vertical Error	-0.06	N/A	N/A	N/A	0.06

AASHTO PP 110-21: Standard Practice for Assessment of Ground Reference Measurements for Transverse Pavement Profiling System Certification.

This standard is proposed to assess if the accuracy and precision of a Ground Reference Measurements are suitable for ground reference data. The accuracy and precision of the Ground Reference Measurements are evaluated using 4 different surfaces that include, a certified straight

edge, a straight edge with gauge blocks, a road surface, and a manufactured macrotexture surface. The evaluated parameters include measurement spacing and error in all three directions (longitudinal, transverse, and vertical), planar flatness, and macrotexture surface error. The certification procedure and the requirements in the above standard are deemed appropriate for faulting and it is proposed that the above standard is directly adopted. In other words, any equipment that can collect and process data meeting the ground reference measurements required for transverse profile assessment purposes will also meet the requirements for ground reference faulting data.

A potential device that can be used for ground reference measurements is the Creaform Metrascan 3D™ used in the TPP study (Figure 50). The Metrascan is a scanner with reported 3D measurement accuracy of up to 0.0012 in., resolution of up to 0.0020 in., with high repeatability.

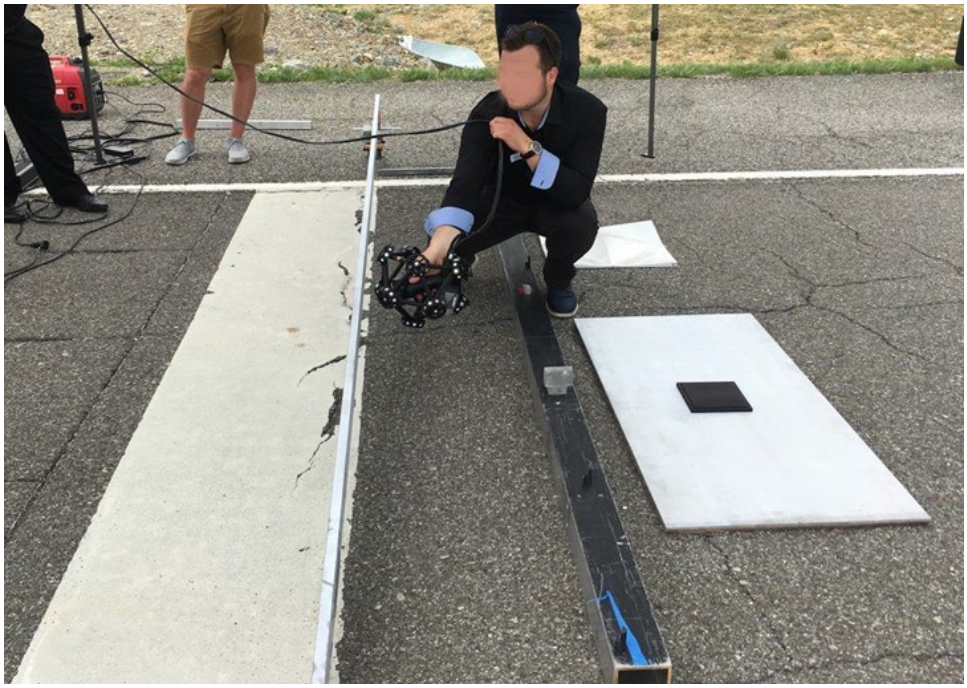

Source: FHWA

Figure 50. Photo. Creaform Metrascan 3DTM used to collect ground reference measurement data in the TPP study.

PROPOSED CERTIFICATION PROCEDURE

Basis for Faulting Certification

AASHTO R 56 provides a detailed certification procedure for HSIPs and is well-accepted by the SHAs. AASHTO R 56 certification allows for a more repeatable and consistent surface elevation measurements for 2D HSIPs, which is essential for reliable faulting calculation from surface profiles. However, it should be noted that AASHTO R 56 procedure was developed specifically for the purpose of obtaining consistent IRI measurements, rather than faulting. As such, AASHTO R 56 certification is not sufficient to account for the differences between the nature of

IRI and faulting measurements. Furthermore, AASHTO R 56 does not apply to 3D systems that can also be used for faulting.

On the other hand, the proposed certification procedures for TPP were developed for 3D systems (more specifically for rut depth, cross-slope, and edge drop off), and need to be evaluated for their applicability in faulting assessment. It is anticipated that the representative longitudinal profiles obtained using different technologies will differ in spacing, resolution, and quality. Furthermore, due to the different options proposed for calculating the fault magnitude, it is possible that different fault values may be obtained from the same joint. As such, the proposed certification procedure focuses on reducing the differences in faulting values obtained from various methodologies.

Average of Multiple Joints vs. Single Joint Standard

Averaging (or more specifically, taking the mean value of) multiple joints to arrive at single mean faulting measurement is a good way to improve the accuracy and precision of faulting data, assuming there is no systematic bias. The premise of averaging is that noise and any measurement errors are random, and therefore, by the Central Limit Theorem, the error will have a normal (Gaussian) distribution. Averaging multiple joints, provides a Gaussian distribution, the mean of which is statistically close to the actual value. The standard deviation is proportional to $1/\sqrt{n}$, where n is the number of samples in the average. Therefore, the more joints that are taken in the average, the smaller the standard deviation from the average. In other words, the more joints averaged, the more accurate is the data collected based on the definition of accuracy. However, having sections longer than 0.1 mile is not recommended because 0.1 mile resolution is typically needed for SHAs' network level decision making purposes. Consider if faulting averages were computed every 0.5 miles or 1.0 miles, then any variations within those segment lengths would not be captured by the faulting data.

Although averaging multiple joints improves accuracy and precision of faulting data, it does not have an impact on any systematic bias in the collection of the faulting data. For example, if a device was consistently measuring 0.02 inches higher on all joints due to an equipment issue, the mean of all joints would be 0.02 inches higher than the true mean. However, without performing a joint by joint analysis it would be difficult to ascertain whether the difference between the equipment mean and the reference mean is due to a systematic bias, or attribute the difference to normal variability / poor precision. To ensure that any systematic bias is captured properly and addressed, it is useful to specify accuracy and precision for faulting data collected at each joint rather than average of multiple joints (or a 0.1-mile section). This allows for addressing and resolving any systematic bias independent of the precision requirements.

Based on the above discussion, the faulting-specific certification process is proposed to be in 2 phases: (a) controlled faulting assessment and (b) field assessment.

Faulting Certification under Controlled Environment (for Accuracy)

The proposed test for faulting entails testing on a manufactured artifact designed to simulate the joint fault and the texture of PCC surfaces. Initially, it was envisioned that the goal of such controlled environment testing is to evaluate the systematic bias (i.e., accuracy) of the production

device at low speed (e.g., 5 mph) without the influence of other pavement factors that may affect faulting (e.g., curling).

It is proposed that the faulting calculated from the production device meet the requirement statements shown in Table 8. The faulting equipment should be accepted for accuracy if it meets the requirement shown in the above table. Then, the equipment may proceed to the precision requirement testing which will be evaluated through the repeatability measurements under the field environment (described in the following section). If there is a bias, the device is rejected and the cause of the bias (e.g., sampling interval, vertical resolution etc.) needs to be examined before another round of accuracy evaluation.

The preliminary designs and the features of the faulting artifact are described in the next chapter of the report.

Table 8. Controlled test requirement statements for faulting.

Output Test Statistic	Accuracy and Precision Defined as Bias and Confidence Intervals, inch				
	Lower Bounds (%-tiles)		Bias	Upper Bounds (%-tiles)	
	90% (5%)	50% (25%)		50% (75%)	90% (95%)
Faulting Error	-0.02	-0.01	0	0.01	0.02

Faulting Certification under Field Environment (for Precision and Joint Detection)

The purpose of the controlled test described above is to ensure that the production devices can produce faulting values that are comparable to the reference measurements from a single, idealized joint. In reality, however, the production devices collect data at speeds much higher than 5 mph and for multiple joints with different characteristics (opening, spalling, etc.). Furthermore, the joint detection algorithm is not tested under the controlled test.

Note that the accuracy test is not included in the field environment testing. This is primarily due to the other factors in the field that may affect the faulting measurements. As discussed previously, faulting (the distress) is affected by temperature-related curling and moisture related warping, which may vary within a few hours (Ytterberg 1987, Choubane and Tia 1992, Byrum 2001, Huang 2004, Rao and Roesler 2005, Chang et al. 2008). From a practical point of view, this means that by the time all reference measurements are taken (say 30 joints or so), the slabs may be under a completely different thermal gradient (and hence curling) and may not be valid when all repeat measurements are taken using the production device.

The purpose of the certification under field environment is to evaluate the production devices can produce under realistic conditions encountered by an SHA. As such, the proposed test statistics include not only precision of the measured fault but also the joint detection rate. The detailed process is described below.

Certification Section

AASHTO R 56 specifies that a minimum section length of 0.1 mile for IRI certification. It is proposed that this minimum length be also adopted for faulting certification section as it will provide approximately 35 joints (assuming joint spacing of 15 ft.) and consistency with the method for IRI certification. For sections with longer joint spacing, the agency may need to

increase the section length to ensure that at least 30 joints are included within the certification section. The selected sections need to have variety of conditions (faulting magnitude, pavement surface, joint configuration, etc.) that can be expected to be encountered during production testing. However, it is quite likely that many agencies do not have easy access to a certification section that meets a full range of conditions, in which case an agency may have to select multiple sections that meet the criteria cumulatively.

Joint and Crack Detection Requirements

It is proposed that a minimum of 3 repeat runs be made for joint/crack detection and repeatability testing. The equipment will need to meet a minimum detection rate of 70% from all repeat runs to be certified.

Note, however, that the joint/crack detection does not have to be carried out using the elevation data that is to be used for fault calculation. E.g., the joints and cracks can be detected from downward pavement images or other means of identifying joints and cracks, as long as the data for joint/crack detection is collected simultaneously and synchronized with the elevation data.

Repeatability Requirements

As described earlier, different agencies have established different repeatability thresholds, likely based on their past experience as repeatability levels that could reasonably be achieved for the equipment currently in use.

However, the necessary repeatability level for faulting measurements can also be assessed based on practical uses of faulting data. As an example, consider a SHA that has defined the low severity faulting as those having a magnitude less than 0.2 in. An engineer runs the AFM and calculates faulting for a given joint that is equal to 0.18 in. and categorizes the joint as low severity faulting. However, if the repeatability of the AFM method used was given as ± 0.08 in., it means that a second AFM run on the same joint has a 95 percent probability of resulting in a faulting magnitude that ranges from 0.10 in. to 0.26 in. In other words, there is a relatively good chance that the joint may have a medium severity faulting rather than low severity. On the other hand, if the repeatability of the AFM was given as ± 0.02 in. then a second AFM run has a high probability (95 percent) of yielding a fault value between 0.16 in. and 0.20 in. (i.e., low severity). As such, the SHA may feel more comfortable with the initial fault value of 0.18 in. and may decide not to make an additional AFM for the joint being considered.

As seen from the above example, improved repeatability means improved reliability level for the AFM data (provided that the bias does not exist). However, the repeatability level cannot be improved indefinitely. As documented earlier, many agencies are using a resolution of 0.01 in. for reporting the fault. This means that any AFM faulting values ranging from 0.045 in. to 0.054 in. will be reported as 0.05 in. It is believed that this level of resolution is reasonable for assessing the fault of a given joint and for categorizing the severity level based on different thresholds used by SHAs. However, this also means that a repeatability level below this resolution (0.01 in.) is practically impossible to achieve.

Considering the example above and the resolution used for AFM, we deem it reasonable to require a repeatability of 0.02 in. or 0.03 in.

To assess the repeatability for faulting certification, we recommend a minimum of three repeat measurements be made with the AFM. Then, the variance of the fault magnitude should be calculated for each joint and pooled together to yield an overall representation of the AFM variance, as shown below (Figure 51).

$$S_{Pool}{}^2 = \frac{\sum_{i=1}^{n}(m-1)S_i^2}{\sum_{i=1}^{n}(m-1)}$$

Figure 51. Equation. Pooled standard deviation.

Where:

S_{Pool} = pooled standard deviation.
S_i = standard deviation from the individual joints.
m = total number of repeat runs (minimum of 3).

The S_{Pool} represents the expected variability of a single AFM run and is also known as the one-sigma-limit according to ASTM C 670. The S_{Pool}, however, does not represent the repeatability of the AFM. If another AFM run is made by the same operator and same equipment, the second run also has a variability (or uncertainty) of S_{Pool}. The difference between the first and the second AFM run will then have a standard deviation (S_{Diff}) as calculated by the equation shown below (Figure 52).

$$S_{Diff}{}^2 = S_{Pool}{}^2 + S_{Pool}{}^2 = 2 \cdot S_{Pool}{}^2$$

Figure 52. Equation. Difference standard deviation.

Where:

S_{Diff} = difference standard deviation.

Assuming a normal distribution for the differences in two AFM measurements, the above indicates there is 95 percent probability that the absolute difference between the two AFM measurements will be less than 1.96 times the standard deviation of the difference, as shown in below (Figure 53).

$$|X_1 - X_2| < 1.96 \cdot S_{Diff} = 1.96\sqrt{2} \cdot S_{Pool}$$

Figure 53. Equation. Absolute difference between two measurements.

Where:

X_1, X_2 = individual AFM measurements.

The right side of the equation above is also referred to as the "difference two-sigma limit" in ASTM C 670 and represents the repeatability level achieved by the AFM. If the difference two-sigma limit is calculated to be less than the required repeatability level (i.e., 0.02 in. or 0.03 in.), then the AFM is accepted for repeatability certification. Otherwise, it should be rejected and the cause of poor repeatability should be examined.

SUMMARY

Under TPF-5(299) for TPP measurements, 5 standards have been developed for 3D systems. Although these standards are not developed specifically for AFM purposes, the generic requirements specified for the equipment are applicable to faulting measurements for 3D systems and may also be applicable and will be evaluated for 2D systems. In addition, both 2D and 3D systems should meet the certification requirements under controlled environment and under field environment as described.

Note that the proposed certification and verification procedures still need to be evaluated and finalized using real equipment and real field data, including non-filtered x, y, z data collected by the equipment.

PRELIMINARY DESIGN AND FEATURES OF FAULTING CERTIFICATION ARTIFACT

As discussed in previous chapter, the certification process for the newly developed faulting assessment methodology is proposed to be in 2 phases, namely (1) the controlled faulting evaluation and (2) field assessment. The goal of the controlled faulting evaluation is to evaluate the systematic bias (or accuracy) of the production device under the environment where the influence of other pavement factors that may affect faulting (e.g., curling) is negligible. As such, the controlled faulting evaluation involves testing the equipment on an artificially manufactured faulting artifact (or fixture). This chapter describes the preliminary design and features of the faulting fixture.

CONCEPTUAL DESIGN OF FAULTING ARTIFACT (PHASE I)

A schematic drawing of the faulting artifact that was developed during Phase I of this study is provided in Figure 54. It was envisioned that the artifact should be able to provide a range of fault values from zero to 0.5 in., in increments of 0.1 inch, while alternative combinations of thickness (e.g. 0, 0.01, 0.02, 0.05, 0.1, 0.15, 0.20, 0.25, and 0.5) may be considered.

The idea behind this artifact design was that the elevation of the entire artifact, including those of the 2 ramps, are to be measured using an accepted reference device described in the previous chapter. This design was to intended to allow for certification of not only the 3D equipment but also the 2D equipment with lasers located at the wheelpaths.

The reference faulting is to be obtained from this measurement. The production devices (2D or 3D) will be driven over this artifact multiple times at a speed of 5 mph, which was determined for safety reasons. However, further discussion between the research team and FHWA arrived at an agreement that testing at such a low speed is not representative of the field data collection. As such, a new design for the faulting artifact has been developed during Phase II of this study, as described in the following.

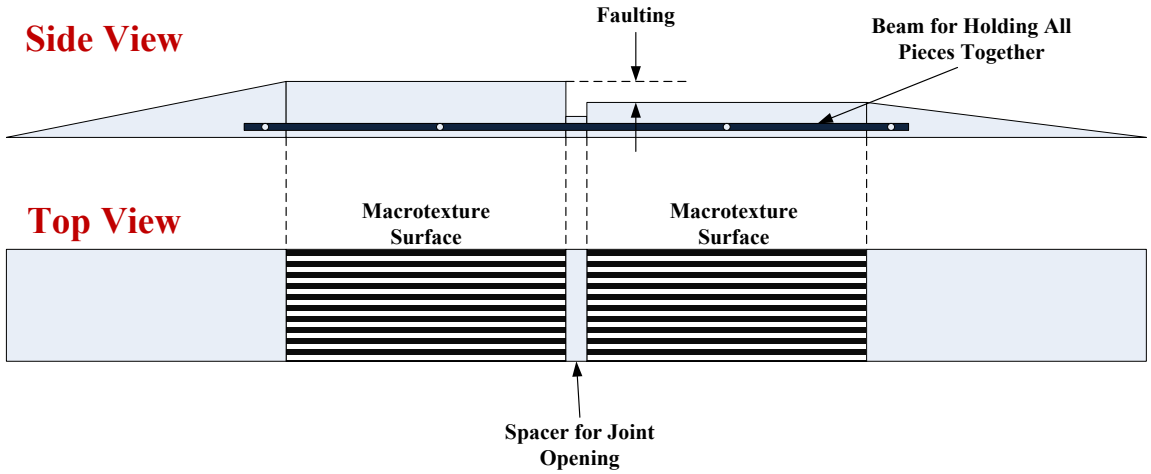

Source: FHWA

Figure 54. Diagram. Joint faulting artifact proposed in Phase I of this study.

PROPOSED FAULTING ARTIFACT (PHASE II)

Due to the ramps and the creeping speed needed for the Phase I design of the faulting artifact, a new design for the artifact was developed in Phase II. The new fixture was designed to be placed in between the wheelpaths such that the vehicle can drive at a speed that is greater than 5 mph. The limitation of this revised design is that for 2D equipment (whose lasers are mounted in the wheelpaths), the lasers will need to be moved to the center of the vehicle for the controlled faulting evaluation. The artifact placement should take into account the sensor system measurement area.

Based on the revised plan, the desired features of the faulting fixture are described as the following.

1. The fixture shall be placed in between the wheelpaths and shall not be in contact with the vehicle during testing.
    - As discussed above, this is to allow for a more realistic speed of the vehicle during the certification procedure.
    - This also eliminates the need for ramps before and after the fixture (which was present in Phase I design, to allow the vehicle tire to drive over the fixture).
2. The fixture should allow for simulating a wide variety of field conditions, including the following.
    - A range of positive and negative fault magnitudes.
    - A range of joint opening and joint depth.
    - Joints with and without spalling
    - Different rigid pavement textures (e.g., longitudinal vs. transverse grinding, etc.).
3. The fixture shall be easy to assemble and disassemble.

Components of Proposed Faulting Fixture

There are 4 major components to the proposed faulting fixture. These components are:

1. Base Plate
2. Connection Beam
3. Macrotexture Surface
4. Spacer(s) for Faulting Height

Figure 55 shows the base plate flipped upside down and the connection beam. As shown in the figure, the base plate is simply a hollow box with 8 holes (4 at the top plate and 2 in each of the side plates) for the shaft of the bolts (or fasteners) to pass through. The connection beams will be used for tying multiple base plates together with the gap in between the base plates representing the rigid pavement joint. Note that the connection beam also has 2 holes one of which is elongated for adjusting the joint width.

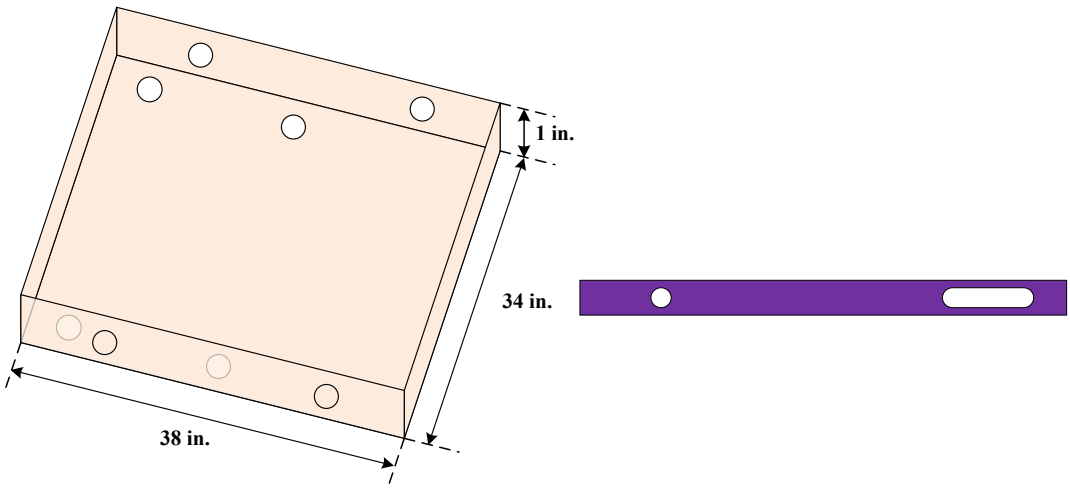

Source: FHWA

Figure 55. Diagram. Proposed base plate for (left, flipped upside down) and connection beam (right).

Figure 56 shows the other 2 major components, i.e., the macrotexture surface and the spacer for joint height simulation. The macrotexture surface has 4 holes that will be used for bolting it down to the base plate. In between the 4 holes, there is at least 30 in. of pure macrotexture area that simulates the PCC texture within a wheelpath.

Although the final decision has not been made, it is recommended that the macrotexture surface be 3D printed (rather than machined from a shop) with a surface texture that is used primarily by the local highway agency (e.g., transverse grooving, longitudinal tinning, etc.). The 3D model of the surface macrotexture can be obtained from typical, known configurations (e.g., known depth, width, and spacing of transverse grooves in accordance with an Agency's specification). However, it is also noted that the surface texture to be 3D printed can be obtained from a high-resolution laser texture scanner that can provide the detailed elevation data (x, y, and z) of the pavement texture.

The purpose of the height spacer (shown on the right hand side of Figure 56) is to elevate the macrotexture surface from the base plate, by placing one or more of them below the macrotexture surface and above the base plate. The thickness of the height spacer should be relatively thin (say 0.1 in.) so that the fault magnitude can be simulated at a consistent increment. It should also be noted that the height spacer is slightly longer than the macrotexture surface and has grooves rather than holes. The purpose of these grooves are (1) to allow for easy placement (or removal) and (2) to simulate different joint depths, as described in the following section.

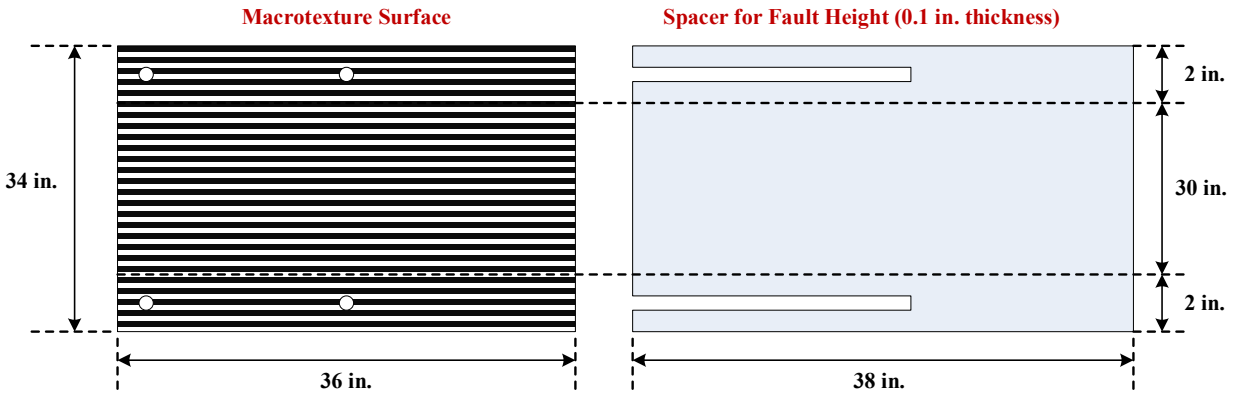

Source: FHWA

Figure 56. Diagram. Proposed macrotexture surface (left) and spacer for fault height (right).

Assembly of Faulting Fixture

Figure 57 shows the schematics of a slab being assembled (i.e., assembling the base plate, spacer, and the macrotexture surface). Essentially, the assembly simply requires inserting a bolt through the holes (of the base plate and macrotexture surface) and the grooves (of the height spacer) and tightening it with a nut. Note again that once this is assembled, the spacer(s) can easily be inserted or removed by loosening the bolt/nut connection and sliding it sideways (without having to take out the macrotexture surface completely).

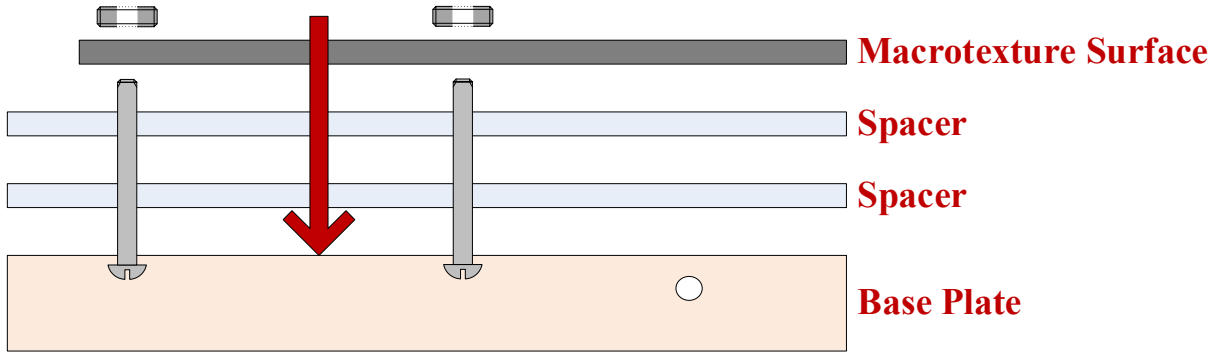

Source: FHWA

Figure 57. Diagram. Assembling the base plate, spacer, and macrotexture surface.

Figure 58 shows two of the above assembled slabs (Figure 57) connected using the connection beams, separated by the joint spacer. Note that the assembled fixture shown in Figure 58 is a specific example of 2 PCC slabs having a relatively deep joint depth and zero faulting.

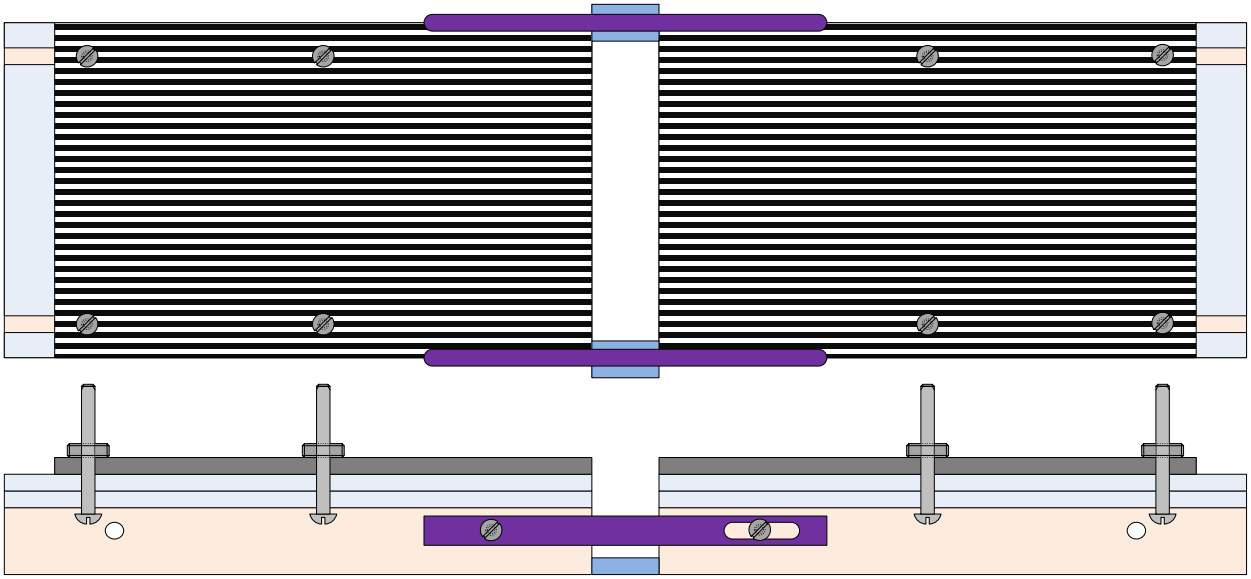

Source: FHWA

Figure 58. Diagram. Top view (top) and side view (bottom) of assembled fixture with no faulting.

Figure 59 shows another example of the assembled slabs. The only difference of this assembly and the one in Figure 58 is that one of the height spacers has been moved (by sliding) to the right to simulate a relatively shallow joint depth (i.e., presence of joint sealant, etc.).

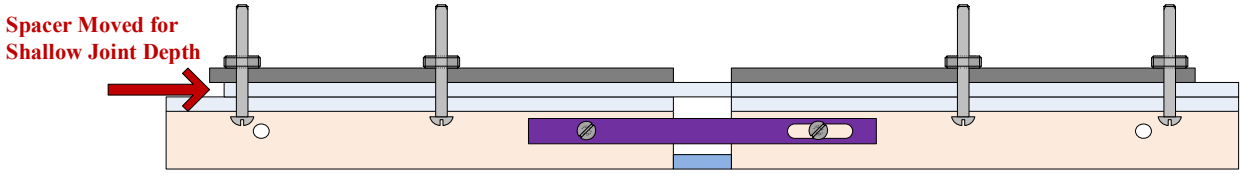

Source: FHWA

Figure 59. Diagram. Side view of assembled fixture with shallow joint depth and no faulting.

Figure 60 is an example of the assembled slabs with high positive faulting. Note again that the sliders can be easily installed or removed by loosening the bolt/nut connection and sliding them in and out as necessary.

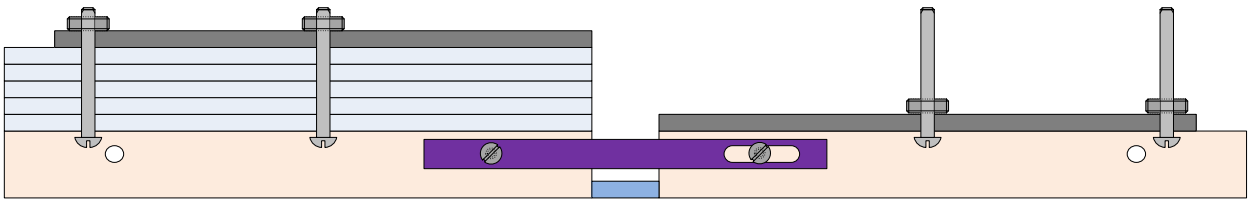

Source: FHWA

Figure 60. Diagram. Side view of assembled fixture with faulting.

Figure 61 shows another example of the assembled joint with positive faulting and minor, artificial spalling. Note that longer joint spacers were used for this example, and it would simply become a wider joint opening if the artificial spalling is removed (similar to Figure 58 bottom).

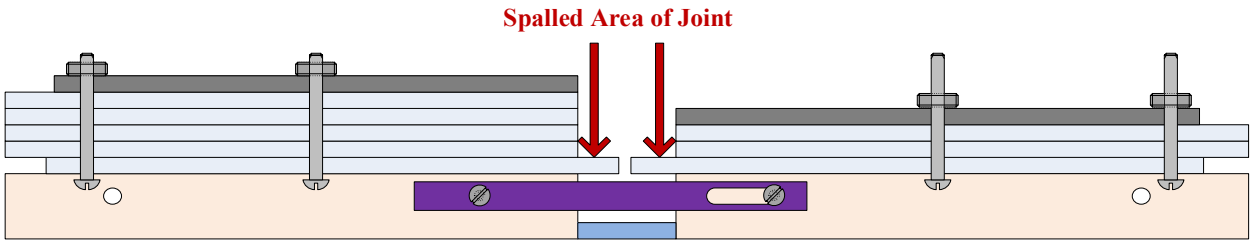

Source: FHWA

Figure 61. Diagram. Assembly of faulting fixture with positive faulting and spalling.

SUMMARY

The first part of the proposed faulting certification process involved a controlled environment testing (i.e., no grade or cross slope, etc.) using an artifact that can mimic a range of fault magnitudes under different conditions (e.g., with and without spalling, with and without joint sealant, etc.).

The faulting artifact developed during Phase I of this study for the purpose of controlled environment testing, involved a fixture with ramps so that the vehicle can be driven over at low speeds. The artificial faulting was intended to be located between the two ramps. Although this design was first proposed to allow for 3D systems as well as the 2D systems with laser sensors mounted within the wheelpaths, the low vehicle speed that was necessary due to the ramps made this design impractical. As such, the Phase II faulting fixture was designed such that it can be placed in between the wheelpaths, so that the vehicle could be driven over the fixture at more realistic speeds. Both the Phase I and Phase II designs were proposed such that a variety of joint and faulting scenarios can be simulated using realistic (i.e., 3D printed) rigid pavement surface textures.

EVALUATION OF NEW FAULTING DEFINITIONS AND PROCEDURES

During Phase I of this study, a more rigorous definition of faulting has been provided with the Enhanced Cumulative Difference Approach (ECDA) as a primary candidate method (Option 1) to calculate the joint faulting (as documented in the "Proposed Definition of Faulting" chapter of this report). The limited number of examples provided previously demonstrated that ECDA may have potential for calculating faulting while detecting and excluding other joint-related distresses (e.g., spalling). However, the Phase I examples were limited to those from 2D elevation measurements. Although it was hypothesized that ECDA, along with the new definition of faulting, can be used for calculating the sign and magnitude of joint faulting from both 2D and 3D elevation measurements in a consistent manner, this hypothesis has not been investigated through a robust evaluation.

SUMMARY OF PROPOSED WORK FOR PHASE II

The primary goal of the Phase II work involved further evaluation of the new definition and the ECDA method as a procedure for calculating faulting. More specifically, the Phase II work of this study was planned for the following subtasks:

- **Evaluation of the newly developed faulting procedures with 3D elevation data**: The purpose of this subtask was to build on the examples shown previously and further evaluate the ECDA procedure using additional 2D and 3D data that were readily available from (i.e., had already been gathered by) the SHAs. This evaluation was planned for a variety of PCC surface characteristics (i.e., textures) and joint conditions (e.g., skewed vs. perpendicular joints, with/without spalling, with/without sealants, narrow vs. wide joint opening, etc). The specific topics that were planned for investigation include the following (depending on the data availability):
  - Comparison of faulting calculated from 2D and 3D data.
  - Repeatability and reproducibility of ECDA faulting.
  - Effect of pavement cross-slope and grade on calculated faulting.
  - Detection of transverse cracks as well as calculation of faulting at the cracks.
  - Effect of wheelpath definition on the representative profile.
  - Effect of other inherent features of JCPs (e.g., PCC texture and curling) on the representative profiles obtained using different devices (2D systems with point vs. line lasers as well as 3D systems) as well as joint detection and faulting assessment.
  - Comparison of faulting results from the newly proposed methods (i.e., Options 1, 2, and 3) as well as those from the traditional AFM (e.g., ProVAL method).

- **Evaluation of the Ground Reference Equipment (GRE)**: The purpose of this subtask was to evaluate various devices (e.g., Creaform Metrascan 3DTM) to be used as a GRE for ground truth faulting measurements. The goal was to select one GRE that meets ground reference measurement quality needed to proceed with the pilot projects.
- **Pilot project (i.e., field) evaluation of new faulting definitions and procedures**: The pilot projects were intended for two main purposes: (1) development and refinement of certification and verification tests and standards, and (2) development, refinement, and validation of the proposed definitions and methods to quantify faulting at each

joint/transverse crack. More specifically, the goals of pilot projects were to achieve the following:

- Development and refinement of the artificial faulting fixture.
- Evaluation of proposed faulting certification procedure under controlled environment based on the faulting fixture test results gathered from various devices (GRE, 2D, and 3D).
- Evaluation of proposed faulting certification and verification procedure under field environment from a variety of field sections.
- Preliminary development of precision and accuracy assessments for the new faulting procedure.
- Refinement and recommendations for certification and verification procedures based on the lessons learned from the pilot project evaluations.

To state the bottom line up front, the above subtasks were not completed to meet the goals of this project. The primary reason was that based on the 3D data provided to the research team by four SHAs (and two different 3D devices) for the first subtask, it was determined the 3D data currently available to the SHAs are not "ready" for the proposed faulting calculation methods. As such, only the work conducted as part of the first subtask is presented in the following, along with the issues and challenges that the research study had faced.

ANALYSIS OF 2D DATA

One of the SHAs had provided the research team with a 2D pavement profile in *.ERD file format along with the 3D data from the same pavement, for the preliminary evaluation of faulting. The SHA also provided their results from the AFM analysis in ProVAL, along with the procedure used for running the ProVAL AFM module.

Using one of the ERD files provided by the SHA, the research team reproduced the results provided by the agency. The following is a brief summary of the results from ProVAL as well as the proposed faulting method (i.e., ECDA) that was developed during Phase I of this project.

Joint Detection from 2D Data

The 2D pavement profile was collected over a length of 5,485 ft. (i.e., there should be approximately 366 joints is the joint spacing was 15 ft., or approximately 274 joints if the spacing was 20 ft.). Figure 62 shows the pavement profile contained in the ERD file as well as the joints that were detected using the "Step" method built into ProVAL (note that the step method for joint detection was specified by the agency). Clearly, this method was not able to detect all joints.

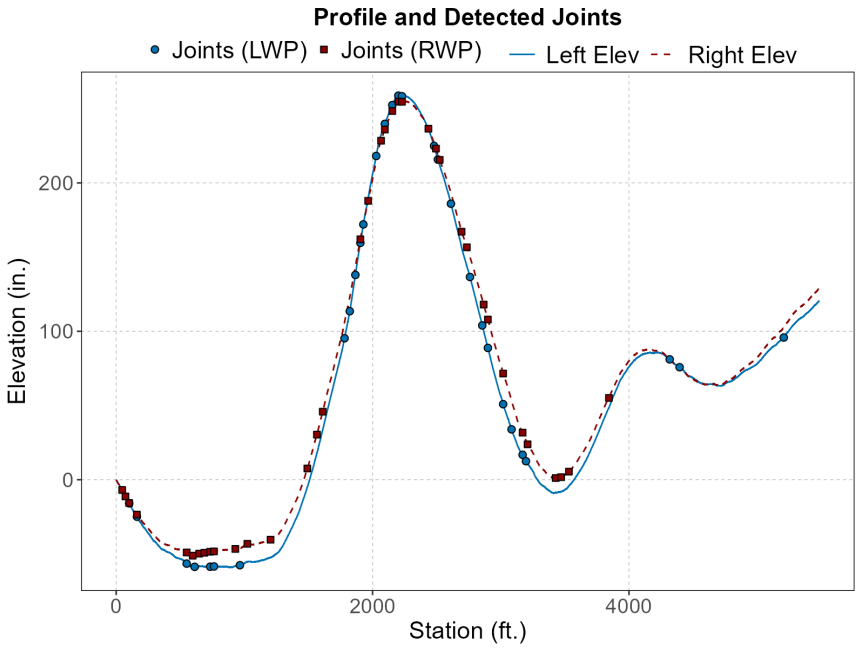

Source: FHWA

Figure 62. Chart. Joints detected from 2D data using ProVAL.

Figure 63 shows the joints detected using the Downward Spike Method implemented by the research team during Phase I. Although a lot of joints were detected along the first 2,500 ft. of the profile, this method was not capable of detecting the joints for the full length of the profile. Furthermore, it is also possible that the detected joints may include a lot of false alarms.

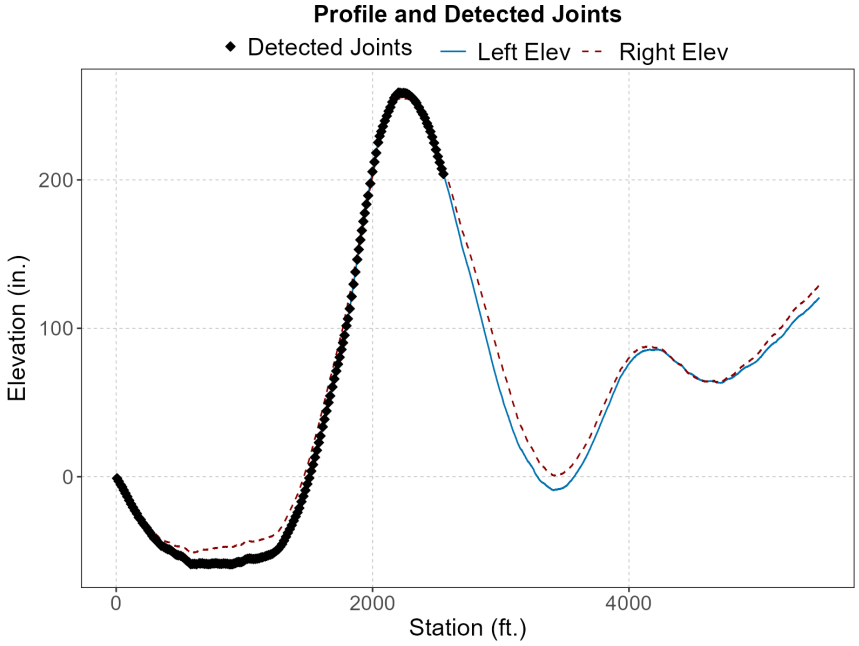

Source: FHWA

Figure 63. Chart. Joints detected from 2D data using downward spike method.

One of the issues seen from Figure 62 and Figure 63, is the long wavelength content included in the pavement profiles. As such, the pavement profile was processed through a high-pass filter using a base filter length of 300 ft. (i.e., the long wavelength content was removed). Figure 64 shows the filtered pavement profile, along with the joints detected using the Downward Spike Method.

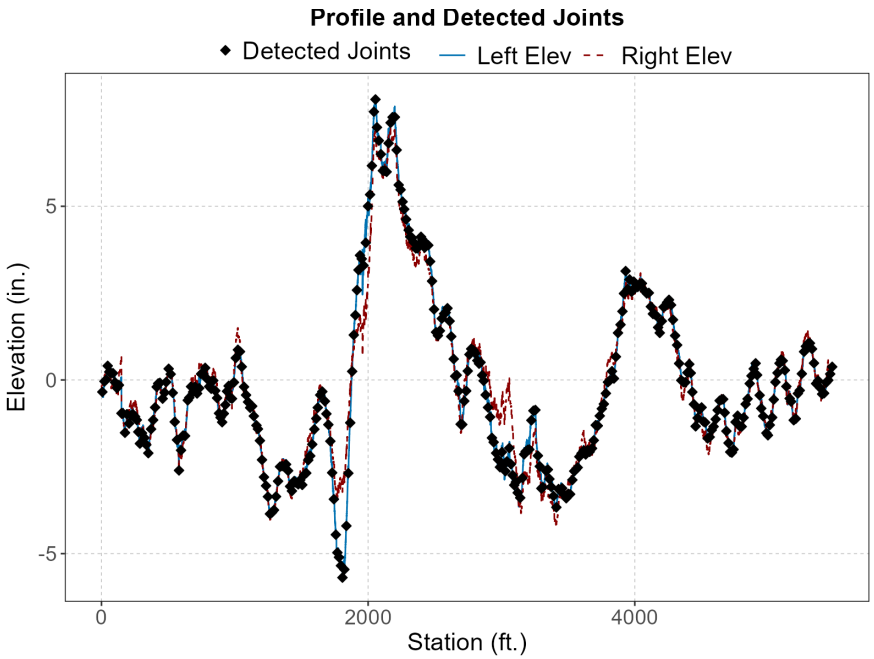

Source: FHWA

Figure 64. Chart. High-pass filtered 2D pavement profile and joints detected using downward spike method.

Table 9 provides a quick summary of the number of joints detected from the methods considered above. The table clearly shows that the joint detection algorithms were not successful using the original profile (i.e., without high-pass filtering). The table also shows that the Downward Spike method with high-pass filtering detected 377 joints in both wheelpaths, which is slightly more than the expected number of joints (i.e., 366) at a joint spacing of 15 ft. However, the nominal joint spacing for this section was unknown, and it is also possible that a few cracks may have been detected by the algorithm.

Table 9. Number of joints detected from different methods.

Wheelpath	Number of Joints Detected: Downward Spike with High-Pass Filtering	Number of Joints Detected: Downward Spike without High-Pass Filtering	Number of Joints Detected: Step Method in ProVAL
LWP	377	152	30
RWP	377	152	37

ECDA Example from 2D Data

As a preliminary exercise, the ECDA method was used to calculate faulting from the joints detected from the non-filtered profile (Figure 63) and the high-pass filtered profile (Figure 64). Figure 65 and Figure 66 show examples of the ECDA results from the same joint location detected from both profiles. The faulting calculated from the non-filtered (i.e., original) profile is much less than the faulting from the filtered profile. While a solid conclusion cannot be drawn at this time, it is possible that the long wavelength content may have an impact on fault magnitudes calculated using ECDA.

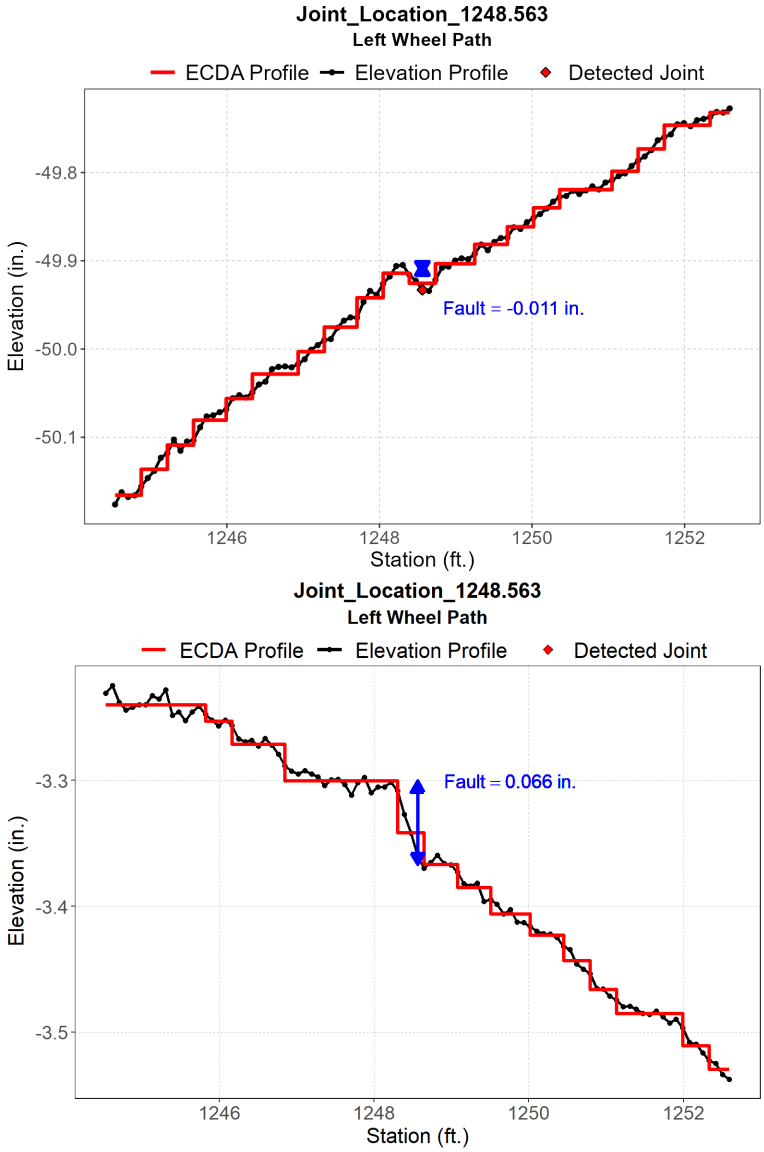

Source: FHWA

Figure 65. Charts. 2D ECDA faulting using (top) original profile and (bottom) high-pass filtered profile at joint location 1,248 ft.

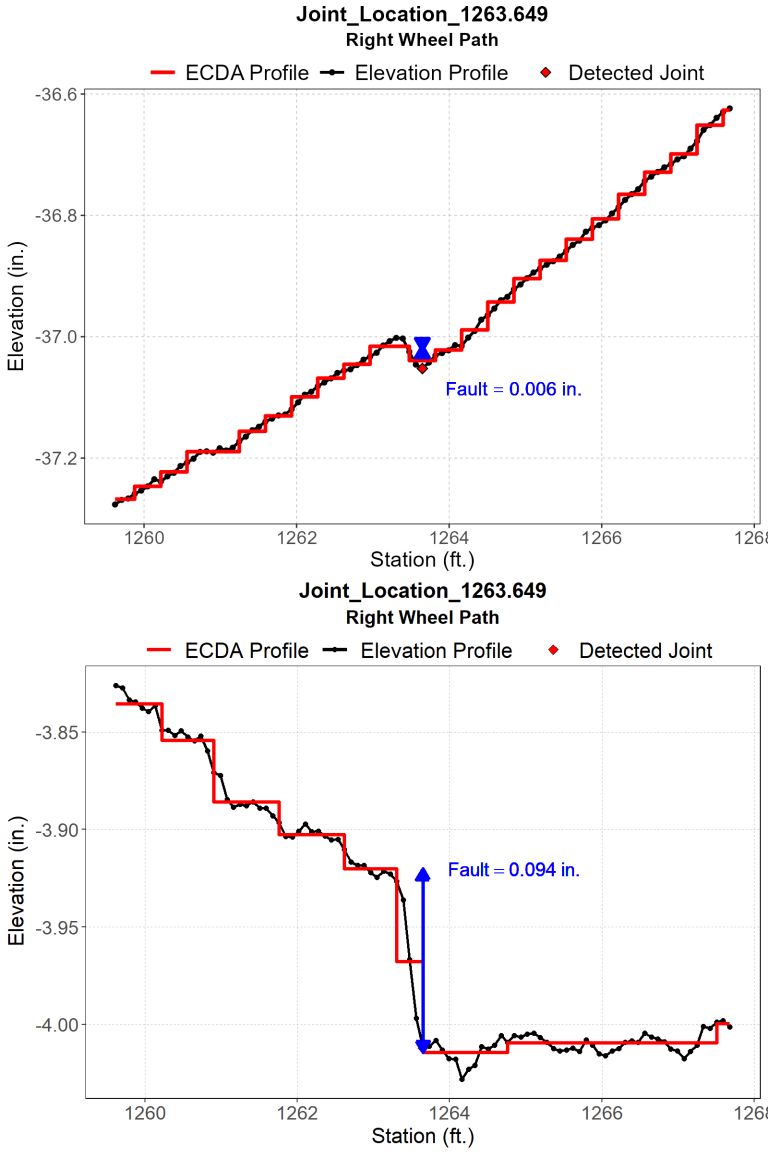

Source: FHWA

Figure 66. Charts. 2D ECDA faulting using (top) original profile and (bottom) high-pass filtered profile at joint location 1,263 ft.

Preliminary Faulting Comparison

Figure 67 shows a comparison of the faulting magnitudes obtained using ECDA from the high-pass filtered and non-filtered profiles. Note that only the joints that were found from both profiles were included in the figure. For both the left and the right wheelpaths, the correlation between the fault magnitudes were relatively poor, which may indicate the effect of long wavelength content on the ECDA calculation.

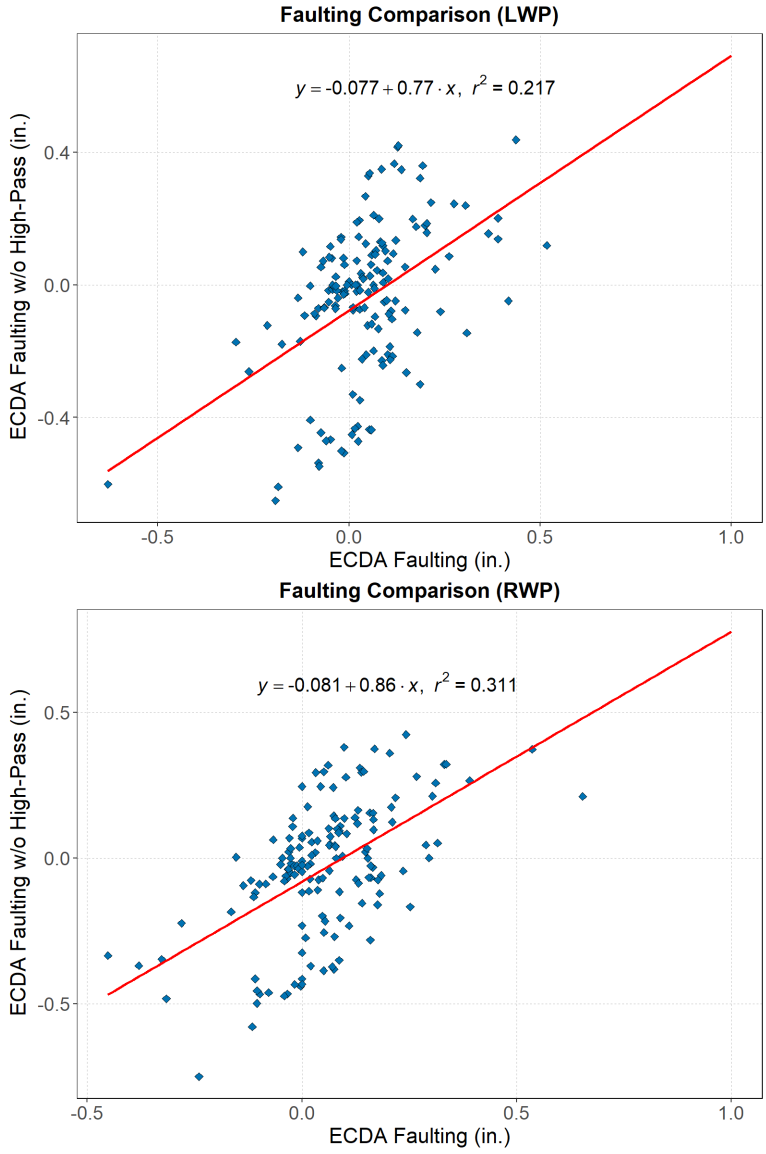

Source: FHWA

Figure 67. Charts. Comparison of 2D ECDA faulting magnitudes from non-filtered and high-pass filtered profiles for left wheelpath (top) and right wheelpath (bottom).

Similarly, Figure 68 shows a comparison between the fault magnitudes obtained using ECDA with high-pass filter and those from ProVAL AFM. Although the correlation (R^2) is slightly improved (compared to those in Figure 67), it is noted again that these were only based on less than 40 detected joints from ProVAL.

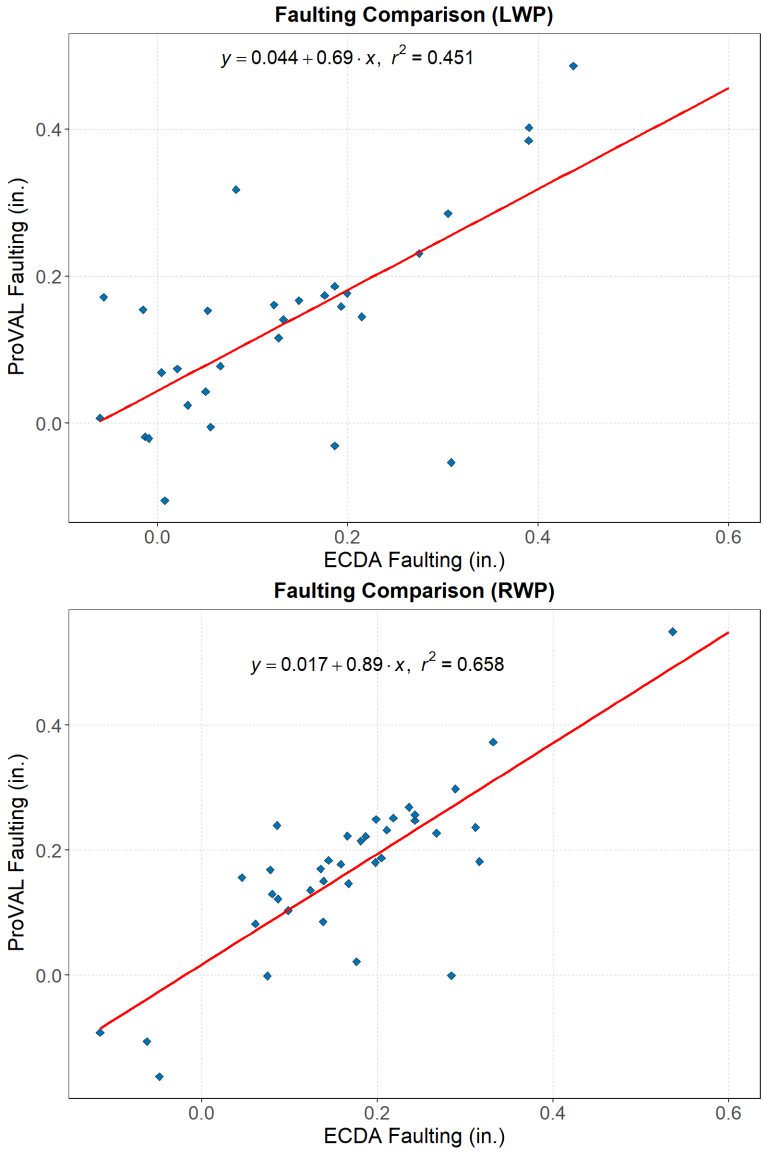

Source: FHWA

Figure 68. Charts. Comparison of faulting magnitudes from 2D ECDA with high-pass filter and ProVAL AFM for left wheelpath (top) and right wheelpath (bottom).

Summary and Recommendations for 2D Data

The following is a brief summary of the faulting exercise conducted herein, along with recommendations.

- For joint detection using 2D elevation data, it may be necessary that the profile be processed through a high-pass filter to remove the long wavelength content.
  - The threshold for the long wavelength content should be studied further from additional 2D and 3D data.
  - To the best of research team's knowledge, the high-pass filter cannot be applied directly within the ProVAL's AFM module. As such, it should be set up within

agency's protocol, prior to producing ERD file (if ProVAL is to be used for faulting assessment).

- The correlation between the fault magnitudes obtained from different processing methods were poor or fair (at best).
  - Although the high-pass filter improved the overall joint detection (from 2D), there is no evidence that the faulting calculated from the filtered profile is more accurate or appropriate.
  - It is recommended that these faulting magnitudes (especially those from 2D profiles) be compared to a reference measurement for accuracy and precision assessments.

ANALYSIS OF 3D DATA

One of the SHAs had provided a sample of 3D data collected from a rigid pavement section. The sample data was used to evaluate the "downward spike" method for joint detection from the representative profiles. The downward spike method involves the following:

1. Filter the profile using a high-pass, anti-smoothing moving average filter with a base length of 0.82 ft.
2. Normalize the filtered profile by its standard deviation.
3. Identify the potential joint location from the normalized profile. This is done by identifying the location of the negative spike whose value is less than a threshold (e.g., -2.5).
4. Identify the next joint by repeating Step 3 at a distance equal to the nominal joint spacing plus/minus some margin of error (e.g., 15 ft. ±2 ft.).

While the downward spike method worked well with 2D profiles collected from JCP sections with relatively uniform joint spacing (see Figure 64 for an example), the method did not return the expected joint locations from the representative profile constructed from the 3D data provided by the agency.

Figure 69 shows the representative profiles extracted from the 3D data as well as the joints detected by the downward spike method. Note that the joint detection method was terminated near station 2,100 ft., likely because the method did not detect a large enough spike at the next location where the joint was expected. Furthermore, there was a need to verify the joint locations detected from station 0 ft. to 2,100 ft.

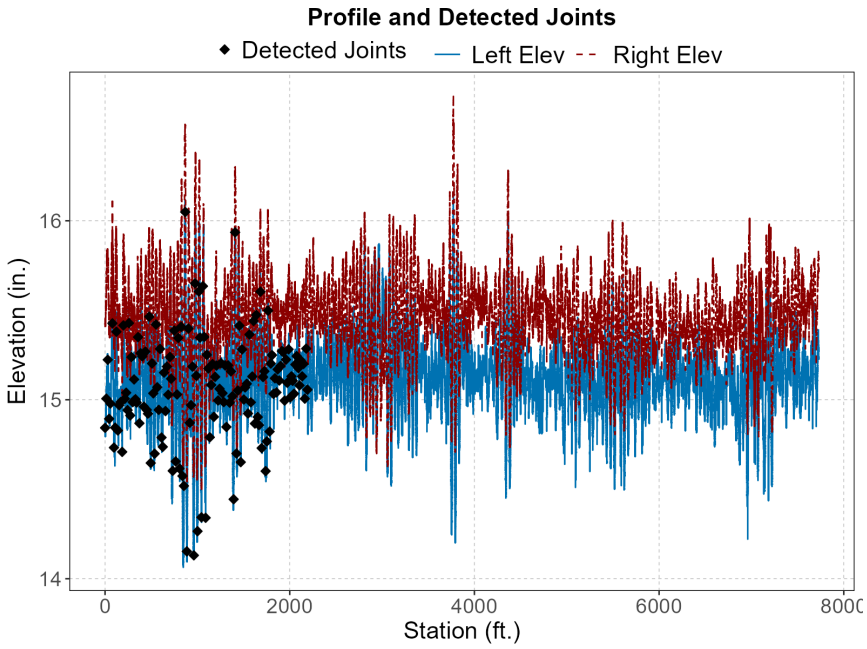

Source: FHWA

Figure 69. Chart. Joints detected using downward spike method from 3D data.

Joint Detection from 3D Images

Due to the limitations of the downward spike method in detecting the joints from the 3D representative profiles, a new method for joint detection has been developed and proposed herein. To demonstrate the new methodology for joint detection, the csv files provided by the agency were used to generate 3D elevation images of the pavement surface. An example of the 3D image is shown in Figure 70.

Source: FHWA

Figure 70. Image. Sample 3D elevation image.

The new joint detection algorithm involves 2 algorithms, namely the Canny Edge Detector and the Hough Transform. The Canny Edge Detector is an image processing algorithm that is widely used for detecting the "edges" within the input image. Figure 71 shows an example of the edges

of the detected by the algorithm from the input image shown in Figure 70. The edges of the joint are visible in the figure, along the center of the figure. However, the figure also shows many small and random edges detected from the pavement surface, likely due to the surface texture of the rigid pavement slabs.

Source: FHWA

Figure 71. Image. 3D image processed through Canny Edge Detector.

To eliminate the random edges detected from the Canny Edge algorithm, the Hough Transform was conducted on the images produced from the Canny Edge Detector. The purpose of the Hough Transform is to detect straight, continuous lines for the edges and to return a mathematical function for the line (in terms of pixel coordinates). An example of the line(s) detected from the Hough Transform is shown in Figure 72. The pixel coordinates for the detected joints were then converted to actual station distances.

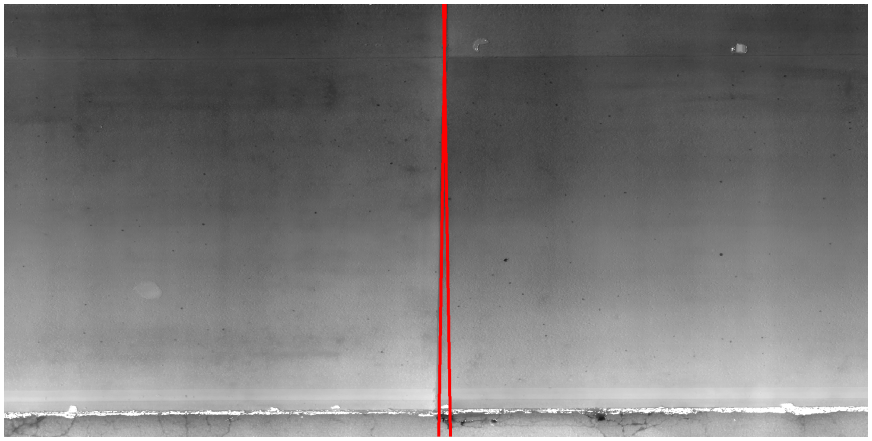

Source: FHWA

Figure 72. Image. Joint detected using Hough Transform.

Figure 73 shows the representative profile obtained from the image shown in Figure 72, as well as the joints detected using the new 3D method as well as the downward spike method. While the 3D method detected the joint properly, the downward spike method completely missed the joint. Instead, the downward spike method detected other "downward spikes" that were present in the representative profile.

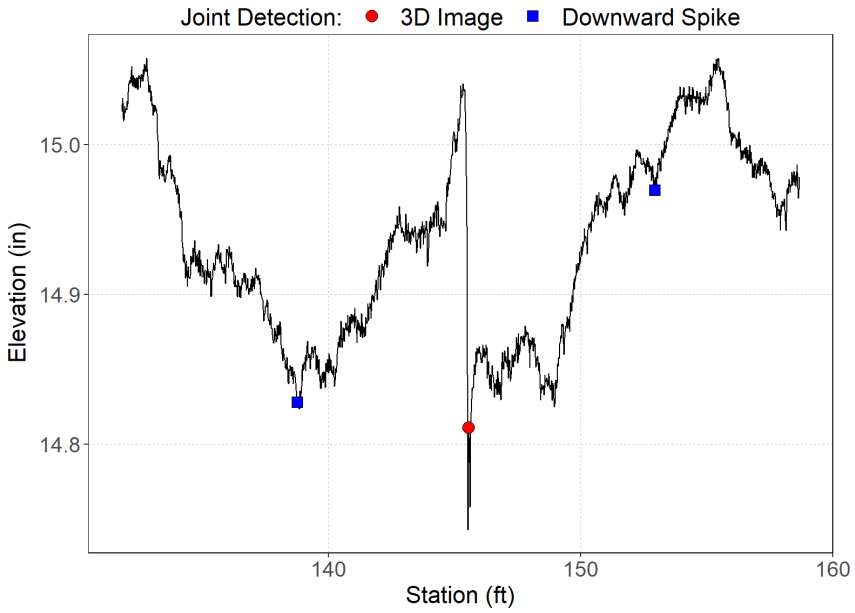

Source: FHWA

Figure 73. Chart. Joints detected from 3D image and downward spike methods.

Figure 74 shows the entire representative profiles of both wheelpaths as well as the joint locations detected using 3D images. For the subsequent analyses, the new joint detection method was used for detecting the joints from the 3D data.

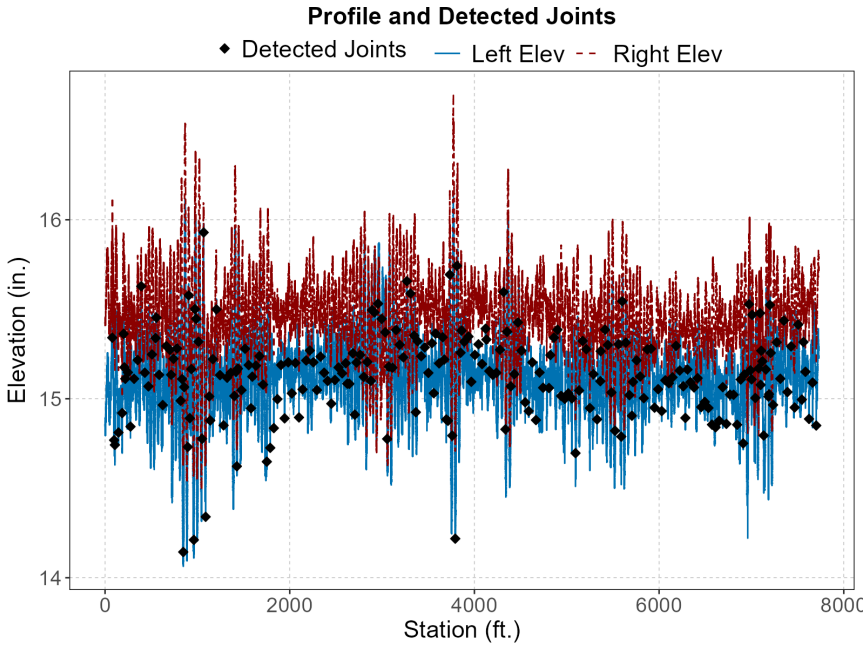

Source: FHWA

Figure 74. Chart. Joints detected from 3D image using the proposed method.

ECDA Example from 3D Data

Two SHAs (denoted as SHAs A and B herein) provided the research team with the 3D elevation data along with the corresponding 2D HSIP data from the same rigid pavement sections. It should be noted that these two agencies had used two completely different 3D devices for their data collection.

Figure 75 shows the comparison between the representative profiles obtained from 2D and 3D data. This figure clearly shows that the representative profiles obtained from the 3D data are "flatter" than those obtained from the 2D elevation data. Furthermore, the 3D data shows more spikes (both upward and downward) in the elevation. Follow up discussions between the research team, SHAs, and the 3D equipment manufacturer indicated that the 3D data sets provided to the research team were not "registered", i.e., the 3D elevation data were not corrected for vehicle motion in the longitudinal direction. This was either due to the equipment not having the capability to correct the 3D laser data for vehicle motion or the SHA not having the analysis option (in the equipment manufacturer's software) for extracting the registered elevation data.

Due to the above limitations, the representative profile obtained in the longitudinal direction for the purpose of faulting evaluation cannot be considered valid. This was a significant drawback in the 3D data that was not anticipated by the research team and is the primary reason the 3D data obtained for this project not being considered ready for evaluation of faulting using the methods proposed in this study. Additional efforts to obtain registered 3D data were unsuccessful.

In the following, the results from the proposed method of faulting analysis will be presented for both the 2D and 3D data. However, it is emphasized that because the 3D data is not registered, the associated results may not be valid. As such, the examples and results from 3D data are provided only for the purposes of demonstration and to highlight some additional challenges that the research team encountered.

Figure 76 and Figure 77 show examples of the faulting magnitudes obtained from the 2D elevation data from SHA A and B, respectively. Both these figures indicate that all three proposed options resulted in significantly different fault magnitudes. Recall that for Option 2, the average elevations before and after the joint are calculated using all elevation data points between the joint and 5 in. from the joint. The results in these figures generally indicate that the spacing of 5 in. for calculating the average elevation needs to be studied further. As for Option 3, the slopes of the projected elevations change signs before and after the joint (i.e., downward slope before the joint and upward slope after the joint). Referring back to Figure 36, the results shown in Figure 76 bottom and Figure 77 bottom generally indicate that the results may become problematic if faulting is evaluated at an offset location (i.e., the location at which one of the projected elevation is extended beyond the joint location).

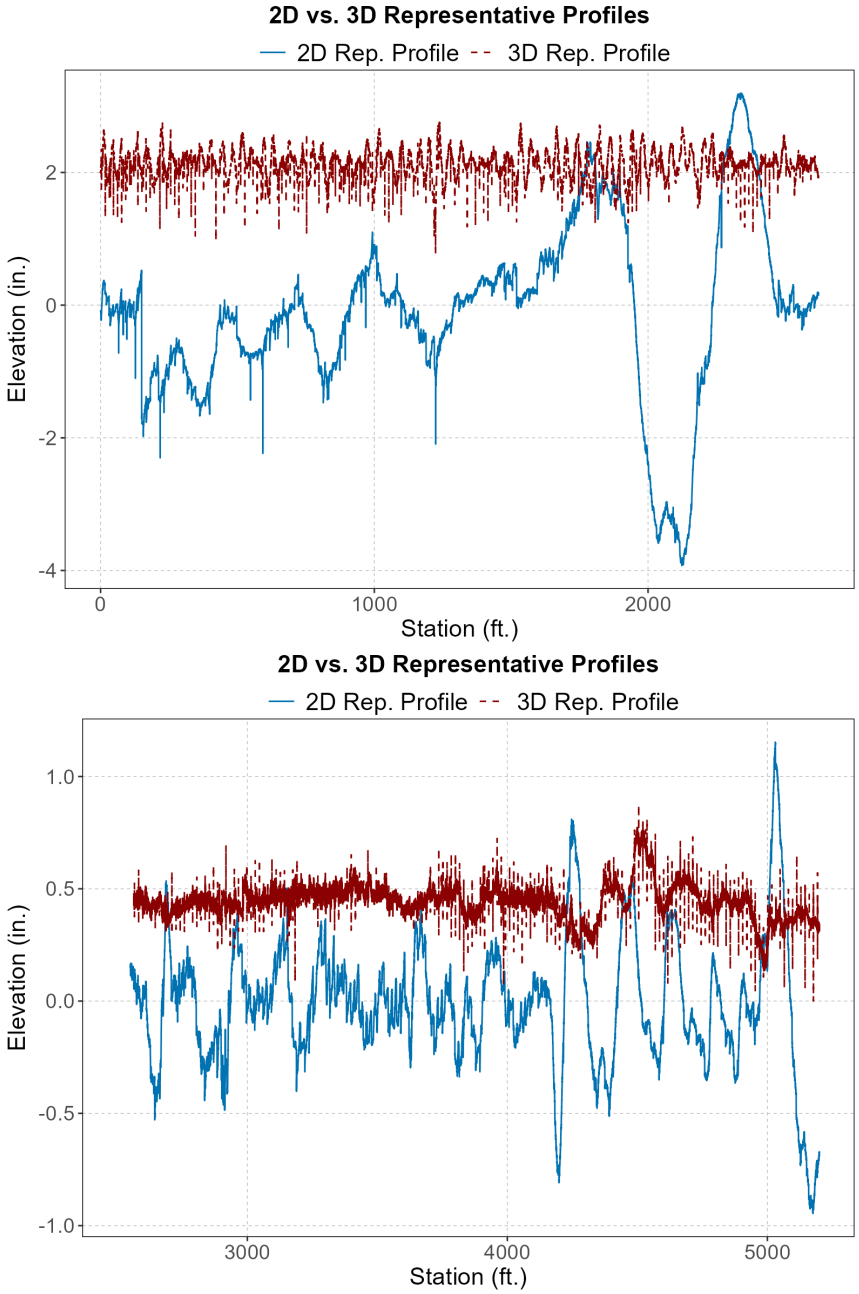

Source: FHWA

Figure 75. Charts. Comparison of 2D and 3D representative profiles from SHA A (top) and SHA B (bottom) data.

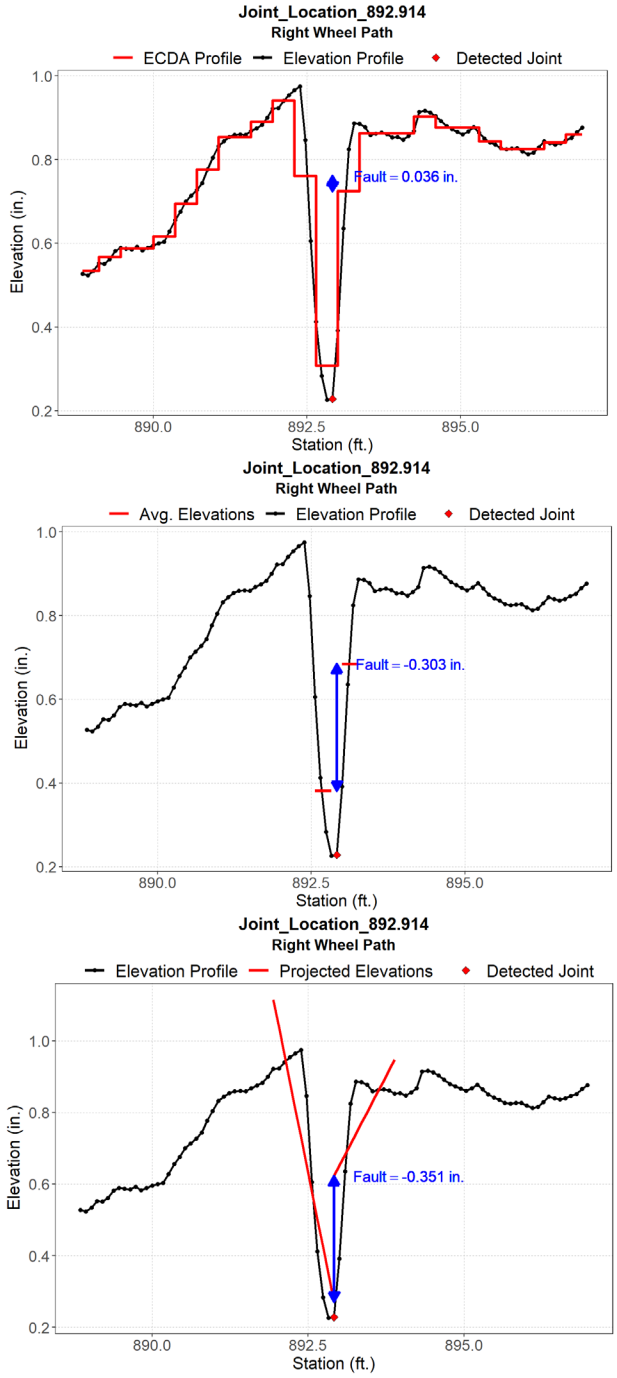

Source: FHWA

Figure 76. Charts. Example of faulting obtained from SHA A's 2D data using Option 1 (top), Option 2 (middle), and Option 3 (bottom).

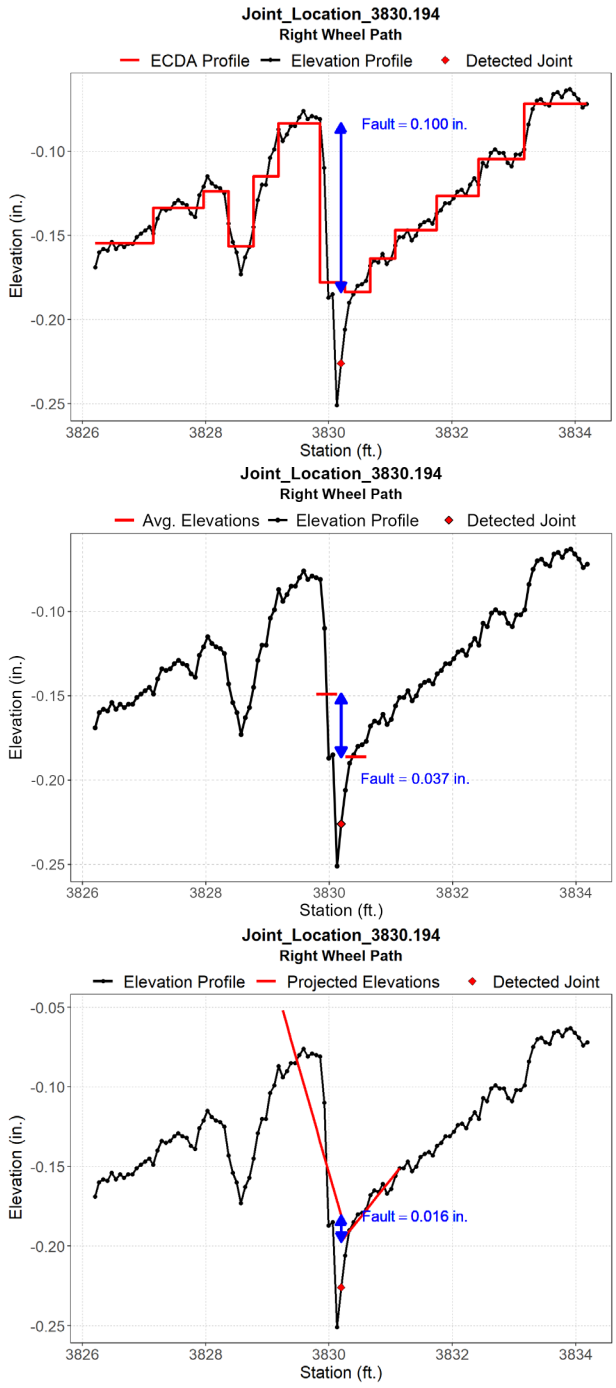

Source: FHWA

Figure 77. Charts. Example of faulting obtained from SHA B's 2D data using Option 1 (top), Option 2 (middle), and Option 3 (bottom).

Figure 78 shows the comparison of the fault magnitudes obtained from Option 1 and the other two options for SHA A's 2D data. Despite the scatter, a correlation can be observed between the results from these different options. Note that this pavement has a relatively good range of fault magnitudes, approximately from -0.25 in. to 0.5 in. (based on Option 1). On the other hand, Figure 79 shows the 2D faulting comparisons for the SHA B data. For this pavement, the

correlation is very poor, with a lot of joints showing no faulting based on Option 1, ECDA analysis. However, it should also be acknowledged that this pavement only showed minimal faulting, with magnitudes ranging from -0.02 in. to 0.03 in.

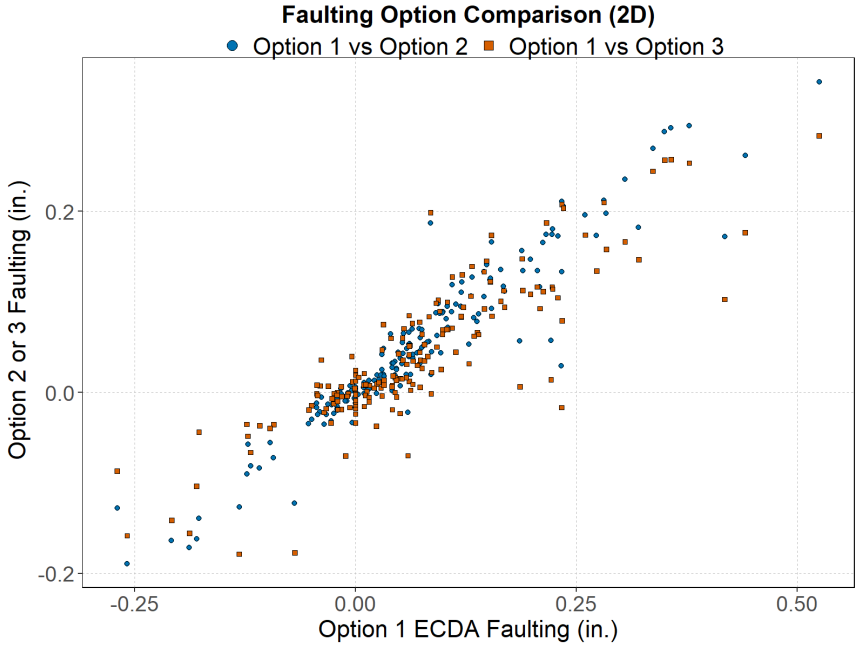

Source: FHWA

Figure 78. Chart. Comparison of faulting calculation options from SHA A's 2D data.

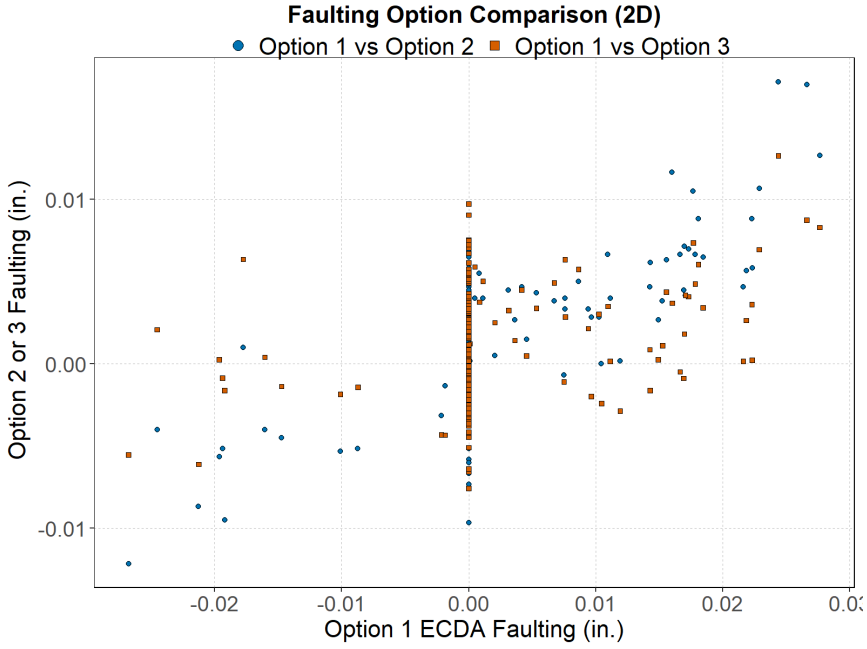

Source: FHWA

Figure 79. Chart. Comparison of faulting calculation options from SHA B's 2D data.

Figure 80 shows an example of the faulting magnitudes obtained from SHA A's 3D representative profile. Similar to those observed from the 2D data, this figure indicates that the faulting obtained from the three proposed options may differ significantly.

Figure 81 shows an example of the representative profile near a joint from SHA B's 3D data. The representative profile in this figure includes two positive peaks, one on each side of the joint. These positive peaks were observed on almost all of the joint locations identified in SHA B's 3D data. It is unclear if these positive peaks are real features of the PCC surface, or if they were caused by other data collection related issues (e.g., spikes in the laser data, unregistered elevation profile, or some other filtering that is occurring within the 3D equipment manufacturer's software).

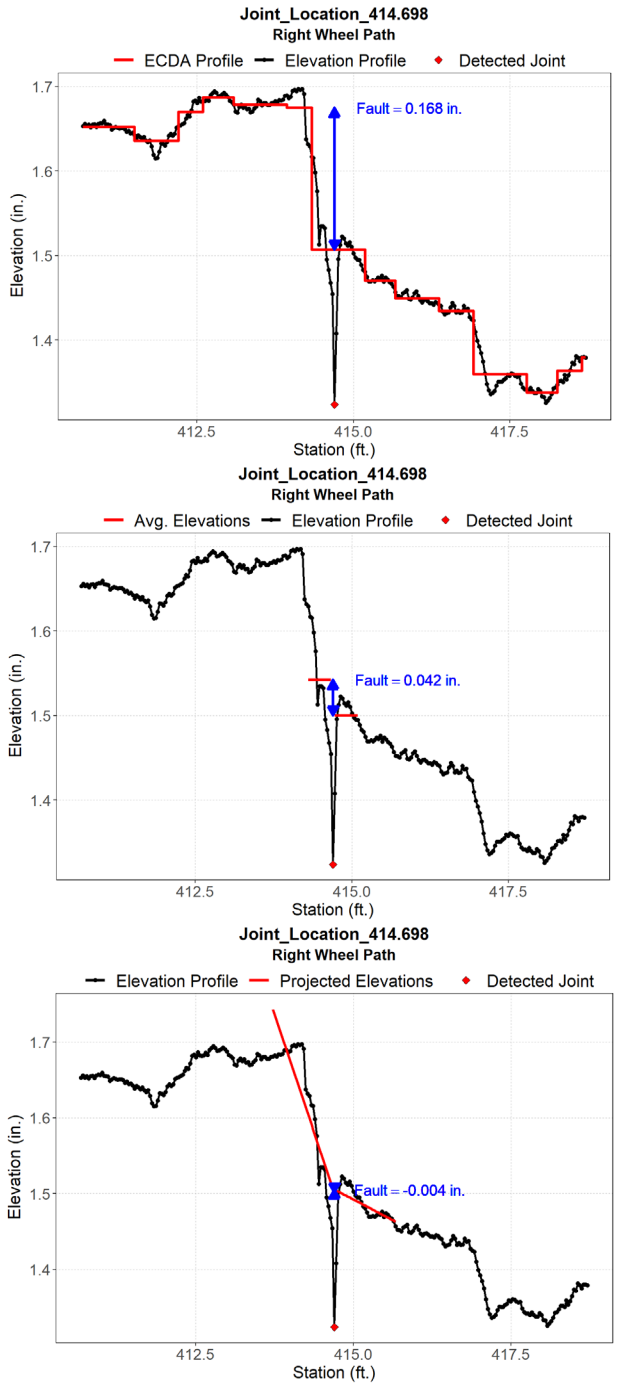

Source: FHWA

Figure 80. Charts. Example of faulting obtained from SHA A's 3D data using Option 1 (top), Option 2 (middle), and Option 3 (bottom).

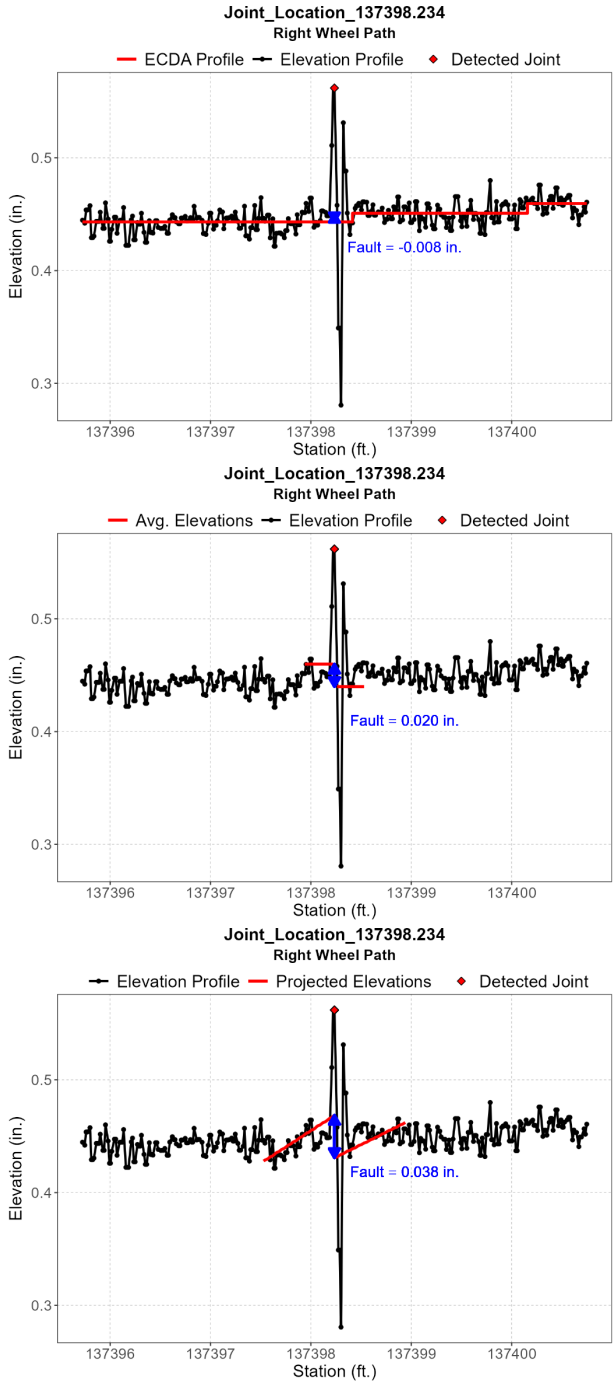

Source: FHWA

Figure 81. Charts. Example of faulting obtained from SHA B's 3D data using Option 1 (top), Option 2 (middle), and Option 3 (bottom).

Figure 82 shows the comparison of the fault magnitudes obtained from Option 1 and the other two options for SHA A's 3D data. Similar to its 2D counterpart (Figure 78) there is a correlation between the results from these different options for faulting calculation. Figure 83 shows the 3D faulting comparisons for the SHA B's data. Again, the correlation is very poor, with a lot of joints showing no faulting based on Option 1, ECDA analysis, likely due to the minimal faulting

present in the pavement. It is emphasized again that the faulting magnitudes shown in Figure 82 and Figure 83 were obtained from the 3D data that were not registered (or corrected for vehicle motion).

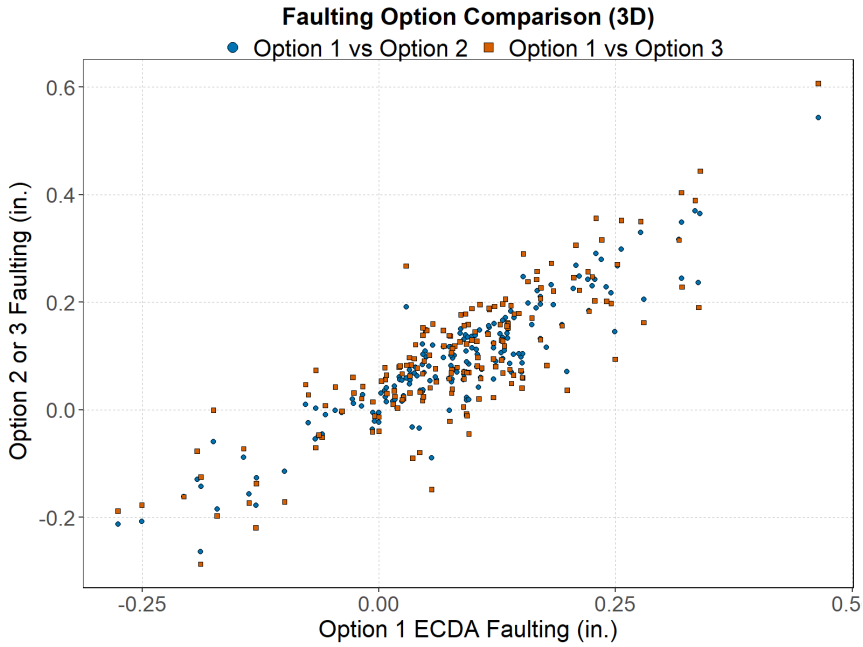

Source: FHWA

Figure 82. Chart. Comparison of faulting calculation options from SHA A's 3D data.

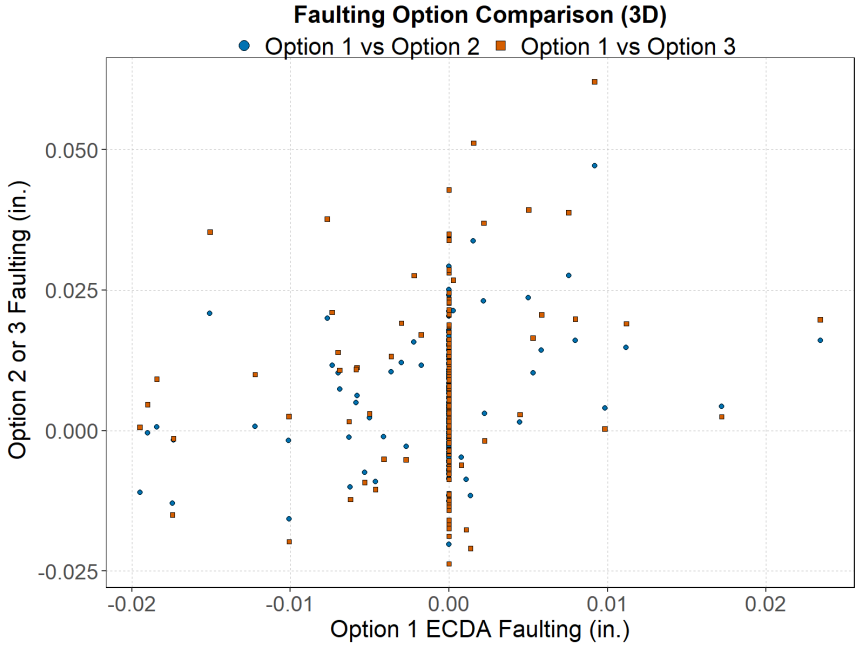

Source: FHWA

Figure 83. Chart. Comparison of faulting calculation options from SHA B's 3D data.

EFFECT OF OTHER JCP FEATURES ON JOINT DETECTION AND FAULTING ASSESSMENT

Unlike the texture of an asphalt surface which is mostly achieved by the placement of the surface layer without supplemental treatments, the macrotexture of a concrete surface is "manufactured" in the sense that it is mostly achieved by a supplemental treatment after material placement (e.g., burlap- or turf-drag, tining, grinding, grooving, etc.). Hence, the macrotexture of a concrete surface is affected not only by the mixture characteristics but also by any texturing done to the material after placement. As an example, Figure 84 shows a synthesized 3D surface of a longitudinally ground concrete pavement surface. Also shown in the figure are the 2D longitudinal and transverse profiles that are inherently different and will yield different elevation profiles, depending on the survey direction and other configurations of the laser sensors (especially 2D devices) used for the measurement. Therefore, it was anticipated that the representative profiles obtained from different laser devices may show different results when processed through various joint detection algorithms as well as the faulting calculation algorithms.

For illustration purposes, Figure 85 illustrates how the representative profile can be obtained from 2D and 3D data. As discussed previously, the 2D systems are prone to wander of the survey vehicle and may not yield the same representative profile as the 3D systems. Moreover, the 2D lasers with different configurations (i.e., point laser versus line lasers configured at different angles), combined with the effect of texture configuration (e.g., longitudinal or transverse grooving) and joint orientation (e.g., skewed joints), may pose additional challenges in obtaining reproduceable representative profiles from different devices.

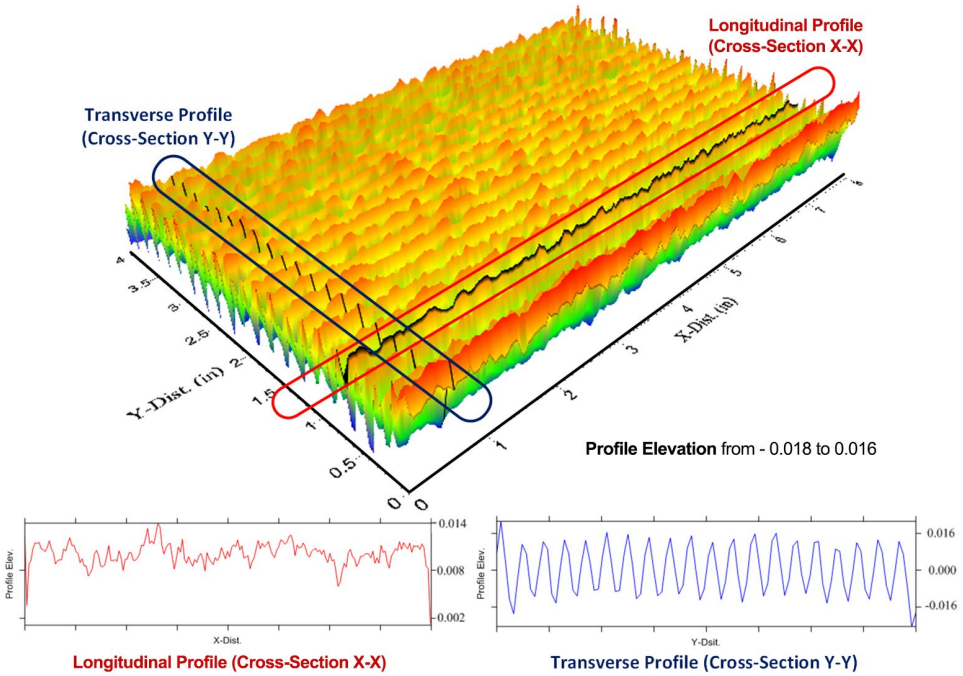

Source: FHWA

Figure 84. Illustration. 3-D surface and 2-D profiles (longitudinal and transverse).

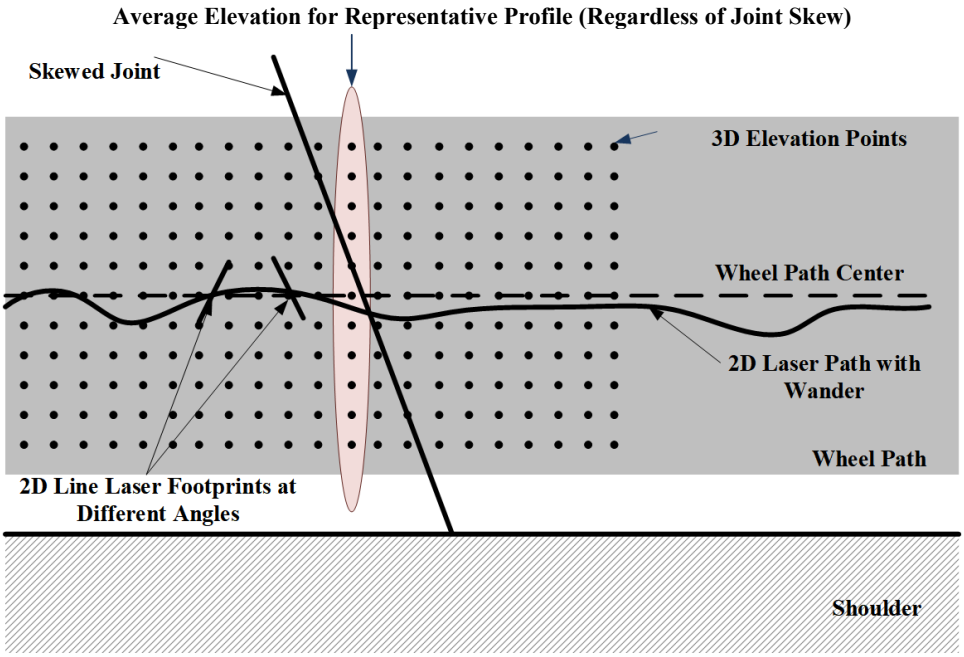

Source: FHWA

Figure 85. Illustration. Representative longitudinal profiles from different devices.

In addition to the PCC surface texture, curling and warping are inherent features of JCPs that significantly affect the surface elevation profiles due to seasonal, daily, and hourly variations in thermal gradient. However, one source of variability (or variation) that is not frequently mentioned in literature is the slab-by-slab curvature variability. In fact, Merritt et. al. (2015) showed that the JCP surface curvatures calculated on a slab-by-slab basis from a single profile may cover a range that is an order of magnitude greater than the median curvature. As schematically shown in Figure 86, it is believed that the curvature difference between two adjacent slabs (or differential curling) may result in an abrupt elevation change across the joint (i.e., faulting) due to differential curling. It is anticipated that this type of faulting would show seasonal, daily, and even hourly changes as much as slab curling does.

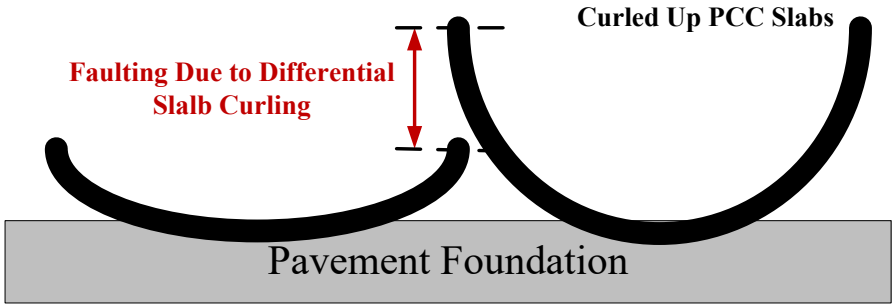

Source: FHWA

Figure 86. Schematic illustration of differential curling and consequent faulting.

Recently, Lee et al. (2020) introduced the Enhanced Second Generation Curvature Index (2GCI) method that can be used for extracting the curvature related profile and the non-curvature related profile from a single pavement profile (Lee et. al., 2020). The curvature related profile is

extracted by fitting Westergaard's curling equations (Westergaard, 1926 & 1927) to each slab within the pavement profile. The "curvature free" profile is obtained by subtracting the curvature related profile from the measured profile. Then, the curvature related IRI and the curvature free (i.e., non-curvature related) IRI values are calculated from the respective profiles extracted using this method. The schematic of the enhanced procedure is shown in Figure 87.

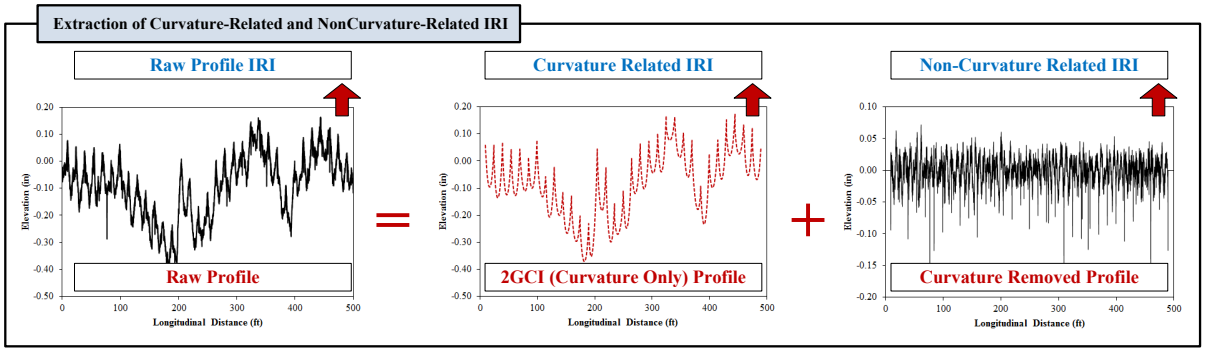

Source: Lee, Hyung.

Figure 87. Illustration. Schematics of enhanced 2GCI procedure.

As an example, Figure 88 shows a schematic example of the faulting that is observed due to the differential (i.e., non-uniform) curling that was obtained from an LTTP section in Arizona. The figure shows that the faulting due to non-uniform curling may range approximately from 0.02 in. to 0.05 in. over the 100-ft segment depicted in the figure.

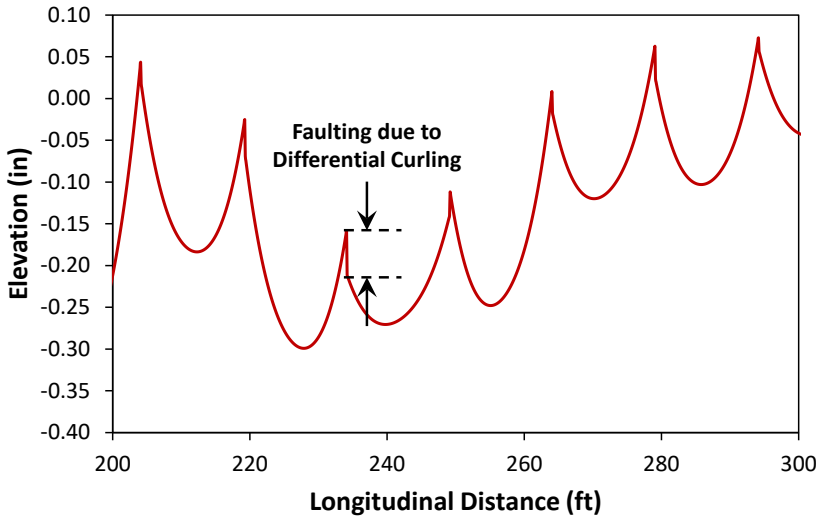

Source: FHWA

Figure 88. Illustration. Faulting due to differential curling.

Although the Phase II of the proposed work was planned to provide additional insight into the combined effect of PCC texture, curling, and laser configurations, the research team was not able to complete the planned subtasks due to the reasons mentioned previously. As such, it is recommended that a future study be conducted to look into these aspects in a more comprehensive manner.

SUMMARY AND RECOMMENDATIONS

In recent years, many SHAs have moved away from manual methods of faulting data collection and evaluation (e.g., Georgia fault meter), and have adopted high-speed, automated methods for that purpose. As a result, a variety of high-speed data collection equipment has been used which include not only the 2-Dimensional (2D) point or line lasers frequently used for roughness assessment, but also 3-Dimensional (3D) technologies that are becoming more popular for automated rut depth evaluation and crack assessment, etc. Accordingly, a variety of algorithms have been used for calculating the fault magnitude from these high-speed devices.

Due to the above diversity in technology for faulting data collection and analysis, quality assessment of measured faulting data has been difficult. Other surface distresses (e.g., joint and crack spalling) and pavement features (e.g., sealed vs unsealed joints) have caused additional challenges in obtaining harmonized, consistent results from different fault measuring technologies. Furthermore, although 3D technologies show potential for overcoming some of the limitations of 2D and manual devices, the newly developed 3D technologies have not been incorporated in the current standard for faulting assessment. As such, there was a need for developing a standard procedure for faulting that can be used with currently available technologies. It was envisioned that such standardized procedure may allow for consistent measurement and analysis of faulting data within a pavement section, between different pavement sections, and between different SHAs.

The primary objective of this study was to improve the faulting data collection and analysis methods and develop certification and verification procedures to evaluate the precision and accuracy. To meet the above objective, an extensive literature review and agency information gathering were conducted in this study. Then a new definition of faulting and three different analysis methodologies (i.e., Options 1, 2, and 3) were proposed and evaluated. As the focus of the study was to develop faulting algorithms that are “equipment neutral” (i.e., the algorithm(s) can be used with a variety of existing devices including 2D and 3D), all three proposed options utilize the concept of “representative profile” which essentially reduces the 3D data into a single, 2D-equivalent elevation profile for each wheelpath, which in turn, is used to evaluate faulting using one of the three proposed options. Option 1 utilizes the Enhanced Cumulative Difference Approach (ECDA) and is the preferred method. On the other hand, Option 2 is based on the average elevations of the pavement surface before and after a joint, while Option 3 is based on projected planes (i.e., regressed elevations) before and after a joint (similar to current AASHTO R 36, Method A).

In addition to the new definition and analysis methodologies, a procedure for faulting certification has been developed and proposed in this study. The proposed faulting certification procedure generally follows that of the Transverse Pavement Profile (TPP) measurement developed under TPF-5(299) and was designed to work for both 2D and 3D systems.

Building on the work conducted during Phase I of this study, the Phase II work was planned to further evaluation of the new definition and the ECDA method as a procedure for calculating faulting. The plan first called for the evaluation of ECDA using the data that was readily available from the SHAs before conducting a number of pilot projects with a variety of 2D and

3D devices as well as a Ground Reference Equipment (GRE). However, it was determined that the 3D data currently available to the SHAs are not "ready" for the proposed faulting calculation methods. The primary reason behind this is that the 3D data sets that SHAs can extract from the raw point cloud data were not "registered", i.e., the 3D elevation data were not corrected for vehicle motion in the longitudinal direction. This was either due to the equipment not having the capability to correct the 3D laser data for vehicle motion or the SHAs not having the analysis option (in the equipment manufacturer's software) for extracting the registered elevation data. Due to the above limitations, the representative profile obtained in the longitudinal direction for the purpose of faulting evaluation were not considered valid.

Owing to the above, it is recommended that the definition of faulting and the methodologies for the analysis be further evaluated in future research. In addition, the proposed methodologies for faulting equipment certification need to be evaluated along with the preliminary thresholds that were proposed in this report, to ensure that these procedures are achievable and practical while ensuring that the faulting evaluation assesses not only accuracy but does so in an equipment neutral and consistent manner.

REFERENCES

AASHTO. *AASHTO Guide for Design of Pavement Structures*. American Association of State Highway and Transportation Officials, Washington, D.C. 1993.

AASHTO. *Mechanistic-Empirical Pavement Design Guide: A Manual of Practice, 2nd Edition*, American Association of State Highway and Transportation Officials, Washington, DC. 2015.

AASHTO R 36, "Standard Practice for Estimating Faulting of Concrete Pavements", American Association of State Highway & Transportation Officials, Washington, D.C., 2017.

Alabama Department of Transportation (ALDOT). *Network-level pavement condition data collection procedure. ALDOT Bureau of Materials and Tests*. Montgomery, AL. 2015.

Agurla, M., and Lin, S. *Long-Term Pavement Performance Automated Faulting Measurement*. FHWA-HRT-14-092. Federal Highway Administration, Washington, D.C. 2015.

Bandini, P., Halter, S., B., Montoya, K., R., Pham, H., V., and Migliaccio, G., D. *Improving NMDOT's Pavement Distress Survey Methodology and Developing Correlations Between FHWA's HPMS Distress Data and PMS Data.* Final report No# NM10MNT-01, New Mexico Department of Transportation. New Mexico, NM. 2012.

Byrum, C. R. *A High Speed Profiler Based Slab Curvature Index for jointed Concrete Pavement Curling and Warping Analysis*. Doctoral Dissertation, University of Michigan. 2001.

Byrum, C.R., and Perera, R.W. "The Effect of Faulting on IRI Values for Jointed Concrete Pavements," *Proceedings of 8th International Conference on Concrete Pavements*, Colorado Springs, CO, August 2015.

California Department of Transportation. *Concrete Pavement Guide.* Division of Maintenance Pavement Program. Sacramento, CA. 2015.

Cebon, D. *Handbook of vehicle-road interaction. Swets and Zeitlinger Publishers*. Netherlands. 1999.

Chang, G., K., Karamihas, S., M., Rasmussen, R., O., Merritt, D., K., and Swanlund, M. "Quantifying the Impact of Jointed Concrete Pavement Curling and Warping on Pavement Uneveness," *Proceedings of 6th Symposium on Pavement Surface Characteristics (SURF).* Portoroz, Slovenia. 2008.

Chang, George K., et al. "Quantifying the Impact of jointed Concrete Pavement Curling and Warping on Pavement unevenness," *Presented at the 6th Symposium on Pavement Surface Characteristics: SuRF 2008*, Portoroz, Slovenia. 2008.

Chang, G.K., Rasmussen, R., Merritt, D., and Garber, S. *Impact of temperature curling and moisture warping on jointed concrete pavement performance*. Technical Brief, FHWA-HIF-10-010. Federal Highway Administration, Washington, D.C. 2010.

Chang, G., K., Watkins, J., and Orthmeyer, R. *Practical Implementation of Automated Fault Measurement Based on Pavement Profiles. Pavement Performance: Current Trends, Advances, and Challenges*. STP 1555. ASTM. 2012.

Chang, G. *Grade Effects and Other Issues Regarding JCP Joint-Fault Measurement*. Unpublished Report. 2012.

Choubane, B. and Tia, M. "Nonlinear Temperature Gradient Effect on Maximum Warping Stresses in Rigid Pavements," *Transportation Research Record*, No. 1370. pp. 11-19. 1992.

Florida Department of Transportation (FDOT). *Rigid Pavement Design Manual*. Florida Department of Transportation: Office of Design, Pavement Management Section. Tallahassee, FL. 2018.

FHWA. *Distress Identification Manual for the Long-Term Pavement Performance Program*. FHWA-HRT-13-092. Federal Highway Administration. Washington, D.C. 2014.

FHWA. *Highway Performance Monitoring System (HPMS).* Office of Highway Policy Information website. Federal Highway Administration, Washington, DC. 2014.

FHWA. *Highway Performance Monitoring System (HPMS) Field Manual.* Federal Highway Administration, Washington, DC. 2016.

FHWA. *Guidelines for Development and Approval of State Data Quality Management Programs*. 2018.

Geary, G., M., Tsai, Y., J., and Wu, Y. "An Area-Based Faulting Measurement Method Using Three-Dimensional Pavement Data," *Transportation Research Record*, No. 2672(40), pp. 41-49. 2018.

Guo, B. and Yuan, Y. "A Comparative Review of Methods for Comparing Means Using Partially Paired Data," *Statistical Methods in Medical Research*, Vol. 0, No. 0, pp. 1-18. 2015.

Haider, S.W. and Varma, S. "Another Look at Delineation of Uniform Pavement Sections based on Falling Weight Deflectometer Deflection Data," *Canadian Journal of Civil Engineering*. Vol. 43, pp. 40-50. 2015.

Haider, S.W., Chatti, K., Zaabar, I., and Eisma, R.J. *Impact of Diamond Grinding on Rigid Pavement Performance. Airfield and Highway Pavements*. American Society of Civil Engineers, 2015.

Huang, Y.H. *Pavement Analysis and Design*. 2nd Ed. Prentice Hall, New Jersey. 2004.

Gillespie, T. D., Sayers, M. W., and Segel, L. *Calibration of Response-Type Road Roughness Measuring Systems*. NCHRP Report 228. TRB, National Research Council, Washington, D.C., Dec. 1980.

Illinois Department of Transportation (IDOT). *Pavement Rehabilitation Chapter 53*. Illinois Department of Transportation: Bureau of Design and Environment Manual. Springfield, IL. 2014.

Karamihas, S. M., and Senn, K. *Curl and warp analysis of the LTPP SPS-2 site in Arizona*. FHWA-HRT-23-068. 2012.

Lee, H.S., S.W. Haider, K. Chatti, and N. Buch, "Effect PCC Slab Curling and Warping on Pavement Roughness," *presented at 12th International Conference on Concrete Pavements*, Minneapolis, Minnesota, 2020.

Merritt, D.K., Chang, G.K., Torres, H.N., Mohanraj, K., and Rasmussen, R.O. *Evaluating the Effects of Concrete Pavement Curling and Warping on Rde Quality*. Report No. CDOT-2015-07. Colorado Department of Transportation, Denver, CO. 2015.

Mraz, A., Nazef, A., Lee, H., Holzschuher, C., and Choubane, B. "Precision of Florida Methods for Automated and Manual Faulting Measurements," *Transportation Research Record*, No. 2306. pp. 131-137. 2012.

Nazef, A., Mraz, A., Iyer, S. and Choubane, B. "Semi-Automated Faulting Measurement for Rigid Pavements: Approach with High Speed Inertial Profiler Data" *Transportation Research Record*, No. 2094, pp. 121-127. 2009.

Nazef, A., Mraz, A., and Choubane, B. "Alternative Validation Practice of an Automated Faulting Measurement Method," *Transportation Research Record*, No. 2155. pp. 99-104. 2010.

Pierce, L., M., McGovern, G., and Zimmerman, K., A. *Practical Guide for Quality Management of Pavement Condition Data Collection*. 2013.

Rao, S., Yu, T., Khazanovich, L., and Darter, M. "Longevity of Diamond-Ground Concrete Pavements," *Transportation Research Record* 1684. Transportation Research Board, National Research Council, Washington, D.C. pp. 128-136. 1999.

Rao, S. and J. Roesler, "Characterizing Effective Built-In Curling from Concrete Pavement Field Measurements," *Journal of Transportation Engineering*, Vol. 131, No. 4, American Society of Civil Engineers, Reston, VA, pp. 320–327, 2005.

Selezneva O, Jane, J., and Shiraz, D., T. *Preliminary Evaluation and Analysis of LTPP Faulting Data.* Final Report No. FHWA-RD-00-076. Turner-Fairbank Highway Research Center, 2000.

Tsai, Y.J., Wu, Y., Ai, C., and Pitts, E. "Critical Assessment of Measuring Concrete Joint Faulting Using 3D Continuous Pavement Profile Data," *Journal of Transportation Engineering*, Vol. 138, No. 11, pp. 1291-1296. 2012.

Vavrik, W. R., L. D. Evans, J. A. Stefanski, and S. Sargand. *PCR Evaluation—Considering Transition from Manual to Semi-Automated Pavement Distress Collection and Analysis.* Final Report. Ohio Department of Transportation, Columbus, OH. 2013.

Wang, K., Li, L., and Li, J., Q. "Automated Joint Faulting Measurement Using 3D Pavement Texture Data at 1 mm Resolution," *Proceedings of 2nd Transportation & Development Congress*, pp. 498-510. 2014.

Westergaard, H.M. "Computation of Stresses in Concrete Roads," *Proceedings of 5th Annual Meeting of the Highway Research Board*, Washington, D.C. pp. 90–112. 1926.

Westergaard, H.M. "Analysis of Stresses in Concrete Pavements Due to Variations of Temperature," *Proceedings of 6th Annual Meeting of the Highway Research Board*, Washington, D.C. pp. 201–215. 1927.

Ytterberg, R. F. 1987. *Shrinkage and Curling of Slabs on Grade.* ACI Concrete International, April, May, and June 1987, American Concrete Institute. 1987.

Zhao, H. Wu, D., Ling, J., and Wu, S. "Study of Dynamic Load Generated by Aircrafts and Concrete Slab Joint Faults," *Transportation Research Board* 96th Annual Meeting Compendium of Papers, No. 17-01817. Washington, D.C., 2017.